

STELLINGEN

De Nod factor is een *vet* molecuul.

(hoofdstuk 3 van dit proefschrift)

De structuur van de vetzuurstaart van een Nod factor is belangrijk voor herkenning en niet voor "targeting".

(hoofdstuk 4 en hoofdstuk 5 van dit proefschrift)

In tegenstelling tot de bevindingen van Philip-Hollingsworth et al., blijkt uit de resultaten beschreven in dit proefschrift, dat Nod factoren in de wortelepidermis extracellulair herkend worden.

(dit proefschrift; Philip-Hollingsworth et al., 1997, *J. Lipid Res.*, **38**, 1229-1241)

In vitro bindingsstudies met intracellulaire moleculen, uitgevoerd in een oplossing die het extracellulaire medium nabootst, zouden door tijdschriften afgewezen moeten worden.

(Kavran et al., 1998, *J. Biol. Chem.*, **273**, 30497-30508)

In order to be an integral part of a thesis, the "stellingen" need to be in English.

Werd technologie-ontwikkeling in eerste instantie gedreven door de drang tot overleven, tegenwoordig zijn de voornaamste drijfveren luiheid en gemakzucht.

Iedereen zou op de vingers moeten leren tellen tot 1024, uitgaande van het binaire systeem, om tot een beter begrip van de huidige digitale omgeving te komen.

Fluorescentie onderzoek staat in een slecht daglicht.

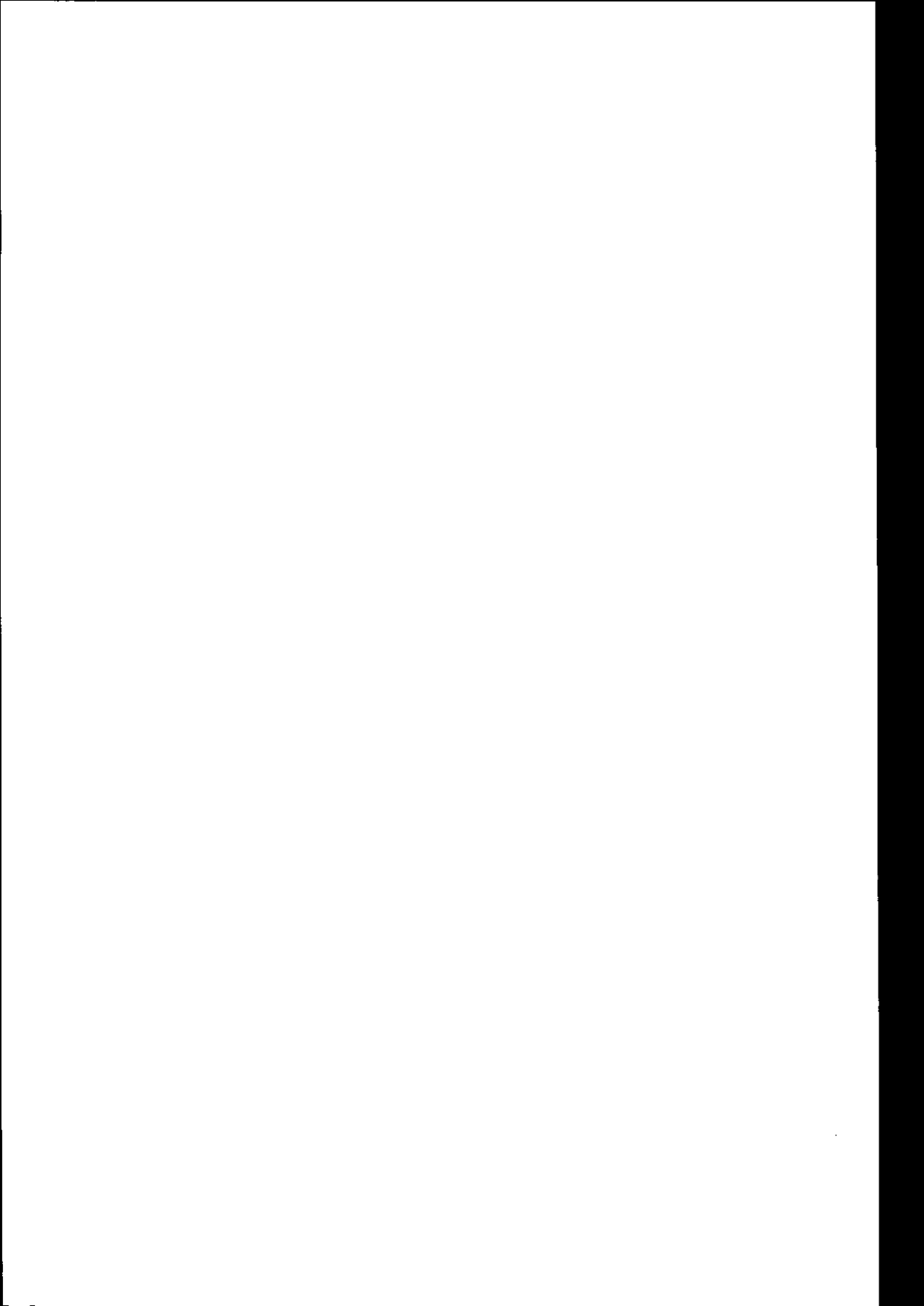
(Volkskrant, 9 juli 1997, pagina 3)

Naar aanleiding van de gevolgen van de privatisering van de Nederlandse Spoorwegen, zou de uitdrukking "het loopt als een trein" veranderd moeten worden in "het treint zoals het loopt".

Behorende bij het proefschrift

"Probing Nod Factor Perception in Legumes by Fluorescence Microspectroscopy"

door Joachim Goedhart, te verdedigen op 14 september te Wageningen.



**PROBING NOD FACTOR PERCEPTION IN LEGUMES
BY FLUORESCENCE MICROSPECTROSCOPY**

Joachim Goedhart

Promotoren: prof. dr. A.H.J. Bisseling
Hoogleraar in de Moleculaire Biologie
Wageningen Universiteit

prof. dr. T.W.J. Gadella Jr.
Hoogleraar in de Moleculaire Cytologie
Universiteit van Amsterdam

Samenstelling promotiecommissie:

dr. J.V. Cullimore (INRA-CNRS, Castanet-Tolosan, France)

dr. A. Musgrave (Universiteit van Amsterdam)

prof. dr. H.P. Spink (Leiden Universiteit)

prof. dr. ir. P.J.G.M. de Wit (Wageningen Universiteit)

nr 201, 3027

**PROBING NOD FACTOR PERCEPTION IN LEGUMES
BY FLUORESCENCE MICROSPECTROSCOPY**

Joachim Goedhart

Proefschrift
ter verkrijging van de graad van doctor
op gezag van de rector magnificus
van Wageningen Universiteit,
prof. dr. ir. L. Speelman
in het openbaar te verdedigen
op vrijdag 14 september 2001
des namiddags te half twee in de Aula.

Probing Nod Factor Perception in Legumes by Fluorescence Microspectroscopy

Goedhart, Joachim

Thesis Wageningen University, The Netherlands

With references - with summary in Dutch

ISBN 90-5808-481-7

aan mijn ouders

voor Monique

ABBREVIATIONS

BODIPY FL-C ₁₆	4,4 difluoro-5,7-dimethyl-4-bora-3a,4a-diaza-s-indacene-3-hexadecanoic acid
BODIPY 558/568-C ₁₂	4,4 difluoro-5-(2-thienyl)-4-bora-3a,4a-diaza-s-indacene-3-dodecanoic acid
BODIPY 581/591-C ₁₁	4,4 difluoro-5-(4-phenyl-1,3-butadienyl)-4-bora-3a,4a-diaza-s-indacene-3-undecanoic acid
BODIPY 581/591-C ₁₆	4,4 difluoro-5-(4-phenyl-1,3-butadienyl)-4-bora-3a,4a-diaza-s-indacene-3-hexadecanoic acid
DHPE	1,2-dihexadecanoyl- <i>sn</i> -glycero-3-phosphoethanolamine
DMAB	<i>p</i> -dimethylaminobenzaldehyde
DMAP	4-(dimethylamino)-pyridine
DMSO	dimethylsulfoxide
DOPC	1,2-dioleoyl- <i>sn</i> -glycero-3-phosphocholine
DPPA	1,2-dipalmitoyl- <i>sn</i> -glycero-3-phosphate
FCM	fluorescence correlation microscopy
FLIM	fluorescence lifetime imaging microscopy
FRET	fluorescence resonance energy transfer
FRIM	fluorescence ratio imaging microscopy
FSPIM	fluorescence spectral imaging microscopy
GFP	green fluorescent protein
GlcNAc	<i>N</i> -acetylglucosamine
(GlcNAc) ₄	tetra- <i>N</i> -acetyl-chitotetraose
LCO	lipo-chitooligosaccharide
NBD	7-nitrobenz-2-oxa-1,3-diazole
Nod factor	nodulation factor
NodR _{lo}	nodulation factors from <i>Rhizobium loti</i>
NodR _{lv}	nodulation factors from <i>Rhizobium leguminosarum</i> bv. <i>viciae</i>
NodR _m	nodulation factors from <i>Rhizobium meliloti</i>
NPE	1-(2-nitrophenyl)ethyl
PBS	phosphate buffered saline
PGM	plant growth medium
PLC	phospholipase C
PLD	phospholipase D
PtdCho	phosphatidylcholine
PtdOH	phosphatidic acid
RP-HPLC	reversed phase high performance liquid chromatography
SDS	sodium dodecylsulfate
TCSPC	time-correlated single photon counting

CONTENTS

Outline	1
Chapter 1 Advanced fluorescence microspectroscopic methods for the study of single living root hairs	5
Chapter 2 Rapid colorimetric quantification of lipo-chitooligosaccharides from <i>Rhizobium loti</i> and <i>Rhizobium meliloti</i>	31
Chapter 3 Nod factors integrate spontaneously in biomembranes and transfer rapidly between membranes and to root hairs, but transbilayer flip-flop does not occur	45
Chapter 4 <i>In vivo</i> fluorescence correlation microscopy (FCM) reveals accumulation and immobilization of Nod factors in root hair cell walls	63
Chapter 5 Localization, immobilization and cell wall accumulation of sulfated and non-sulfated Nod factors is identical in root hairs of host and non-host legumes	79
Chapter 6 Synthesis of photoreleasable phosphatidic acid to study lipid signaling	99
Chapter 7 Summarizing discussion	109
References	119
Nederlandse samenvatting	131
Dankwoord	137
Curriculum vitae	139
List of publications	141

OUTLINE

Plants of the family of legumes are capable of forming a symbiosis with *Rhizobium* bacteria. These Gram-negative bacteria invade the root system of a host legume and fix nitrogen in a specialized organ, the so-called root nodule. In exchange for sugars, the bacteria convert atmospheric nitrogen to ammonia which can be used by the plant. This remarkable alliance allows the plant to grow independently from nitrogen sources provided by the soil. Examples of leguminous plants are clover, pea, and soybean.

The symbiosis is initiated by a molecular dialogue. The plant produces flavonoid compounds which are recognized by the bacterial NodD protein. The signaling pathway which is activated leads to the synthesis and secretion of lipo-chitooligosaccharides which are also called Nod factors. The production of Nod factors by the *Rhizobium* bacteria is an essential step for accomplishing symbiosis and also determines host specificity. The general structure of Nod factors comprises a chitin backbone of three to five β -1,4-linked *N*-acetylglucosamine units. A fatty acid of 16-20 carbon atoms is *N*-linked to the terminal non-reducing sugar residue. The exact molecular structure can comprise different acyl chains and a variety of decorations on the chitin backbone depending on the *Rhizobium* species.

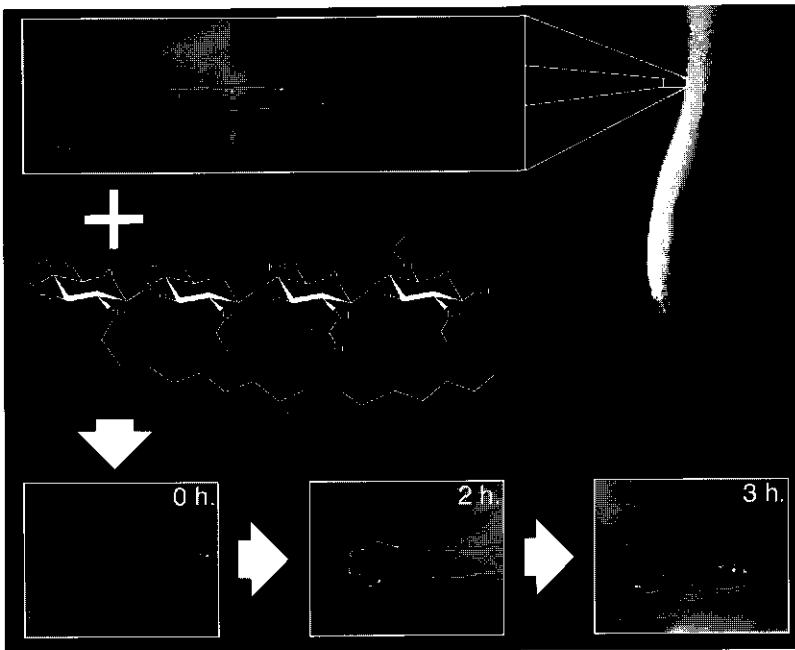


Figure 1: Nod factors can induce root hair deformation on a compatible host legume. When sulfated Nod factors are administered to the growth medium of a *Medicago truncatula* (barrelclover) root, swelling of the tip of root hairs can be observed with a microscope after two hours followed by re-initiation of tip growth in a random direction after three hours.

After successful recognition of the bacteria by the legume, a remarkable morphogenic process takes place, which is known as root hair curling. The root hair curls around the *Rhizobium* colony by which the bacteria are entrapped within the so-called shepherd's crook. Subsequently, the rhizobia enter the root hair through an infection thread, starting from the center of the curl. Via the infection thread several cell layers are crossed after which the bacteria are released in nodule primordium cells, where they differentiate into bacteroids that fix nitrogen.

Nod factors in the absence of bacteria, either purified from *Rhizobium* cultures or chemically synthesized can elicit a wide variety of responses on a compatible legume host. When Nod factors are applied to roots, the earliest visible response takes place in root hairs. Root hairs are single tip-growing cells that develop from the epidermis of a root and grow perpendicular from the longitudinal axis of the root. Generally, root hairs that are terminating growth are susceptible to Nod factors and respond by swelling of the tip of the root hairs, followed by the re-initiation of tip growth in a random direction (figure 1). This typical Nod factor response is referred to as root hair deformation and can be observed with a microscope 2-3 hours after addition of Nod factors.

The perception of Nod factors by the plant, and the downstream signaling cascades that are activated are major research topics in the *Rhizobium*-legume interaction. The low concentration (down to 10^{-12} M) at which Nod factors can still induce root hair deformation and the dependence of the bioactivity on specific decorations of the Nod factor suggest that these molecules are perceived by receptors at the root hair. However, to date no such receptors are characterized. Moreover, it is far from clear where Nod factor recognition by root hairs takes place. Therefore an approach was taken in which fluorescent Nod factor derivatives were synthesized, allowing to probe the ligand binding sites on legume root hairs.

The research described in this thesis focuses on the quantification, characterization and perception by legumes of Nod factors. In order to detect Nod factors at physiologically relevant concentrations sensitive techniques are required. A number of fluorescence spectroscopy and microscopy based techniques can be used to study fluorescent derivatives of signaling molecules. In **chapter 1**, the use of fluorescence microspectroscopic techniques available in the laboratory are discussed. Examples how these techniques can be used for the study of root hairs and other living cells are described.

In **chapter 2**, two methods to quantify purified Nod factors are described. An enzymatic step which is crucial for the first method was analyzed in detail. The second method was optimized and validated using fluorescent and radiolabeled Nod factor derivatives. The chapter describes in detail how the two optimized methods can be used for quantifying Nod factors as well as potential pitfalls.

In **chapter 3**, the spectral properties of three novel fluorescent Nod factor derivatives are described. It is checked whether these fluorescent Nod factors can still elicit root hair deformation on *Vicia sativa* roots. The properties of the amphiphilic signaling molecules were

characterized *in vitro* in the absence and presence of micelles and model membrane systems using fluorescence spectroscopy. Time-correlated single photon counting fluorescence spectroscopy was used to measure rotational mobility of the fluorophore. These experiments are complemented with fluorescence correlation spectroscopy to examine diffusional mobility of the Nod factors. A lipid transfer assay was used to measure the rate of intermembrane transfer and intramembrane flip-flop of Nod factors.

In **chapter 4**, a detailed study is reported describing the sites at which the fluorescent Nod factors accumulate. Fluorescence microscopy is used to examine the location of fluorescent Nod factors on root hairs during the initial perception and during root hair deformation. Subsequently, the diffusional mobility of the fluorescent Nod factors is measured *in vivo* using fluorescence correlation microscopy (FCM), allowing quantification of molecular mobility and concentration of fluorescent Nod factors in living root hairs at a molecular level. This study is continued in **chapter 5** in which also novel sulfated fluorescent Nod factors are used and characterized, enabling a direct comparison between sulfated and non-sulfated Nod factors on a host and non-host legume. Also, the origin of the molecular mobility of the Nod factors is studied in more detail.

In **chapter 6** a novel approach towards manipulating phospholipid second messengers in single cells with spatiotemporal control is presented. The synthesis of a fluorescent and caged derivative, NPE-phosphatidic acid, which releases phosphatidic acid upon exposure to UV is described. The release of phosphatidic acid from the caged compound is studied *in vitro* and *in vivo*. The use of photoreleasable phosphatidic acid for studying phospholipid signaling *in vivo* is evaluated.

Chapter 7 summarizes the conclusions that can be drawn from the results described in this thesis. The implications for Nod factor secretion by the bacterium and subsequent perception by legume root hairs are discussed.

**ADVANCED FLUORESCENCE MICROSPECTROSCOPIC METHODS FOR THE
STUDY OF SINGLE LIVING ROOT HAIRS**

Contents

1 Introduction

2 Fluorescence Ratio Imaging Microscopy (FRIM)

2.1 Principle

2.2 Implementation of FRIM onto a fluorescence microscope

2.3 Applications

3 Fluorescence SPECTral Imaging Microscopy (FSPIM)

3.1 Principle

3.2 Implementation of FSPIM onto a fluorescence microscope

3.3 Applications

4 Fluorescence Lifetime Imaging Microscopy (FLIM)

4.1 Principle

4.2 Implementation of fluorescence lifetime imaging capabilities in a
microscopy system

4.3 Applications

5 Fluorescence Correlation Microscopy (FCM)

5.1 Principle

5.2 Implementation of FCS

5.3 Applications

6. Concluding remarks

1 Introduction

Root hairs are very suitable for fluorescence microscopy, as they consist of a single cell, have low autofluorescence (because of the lack of chloroplasts) and are not covered by other cell layers. For many plants, transferring seedlings to liquid medium contained between a microscopy slide and a coverslip and growth for one or two days at room temperature is sufficient for microscopic observation of root hairs. Cytoplasmic streaming provides an easy check for viability.

Fluorescence microscopy has the advantage that it is sensitive, non-invasive, and can be used for the study of living cells. Moreover, it provides the possibility to monitor specifically fluorescently tagged molecules with very high spatial and temporal resolution. Fluorescence microscopy not only enables the study of localization and dynamics of fluorescent (bio)molecules but also enables probing of the local microenvironment of the fluorescent molecule. This can be achieved by carefully monitoring the spectral properties of the fluorophores in the microscopic object. The integration of spectroscopic modalities into fluorescence microscopes is referred to as fluorescence microspectroscopy. This chapter will highlight a number of such techniques and their use for studying biomolecular behavior in single living root hairs.

For each microspectroscopic technique, the principle, the implementation onto a fluorescence microscopy system, and an application to the study of root hairs will be described. We will show that in addition to localization in root hairs, we also can probe the local environment of fluorescent (bio)molecules, reporting on absolute concentration, diffusional mobility, local pH, hydrophobicity, and molecular proximity of (bio)molecules, all of which influence the spectroscopic properties of the probe fluorescence.

Some of the microspectroscopic techniques will be illustrated by showing the results obtained after application of fluorescent analogs of nodulation (Nod) factors. Nod factors are lipochito-oligosaccharides that are secreted by *Rhizobium* bacteria and are essential for accomplishing symbiosis between the bacteria and the root system of legumes. Nod factors consist of a tetra- or pentamer of *N*-acetylglucosamine residues and an acyl chain attached to the non-reducing sugar residue (Lerouge et al., 1990; Spaink et al., 1991). Purified Nod factors are active at subnanomolar concentrations, induce morphological changes on root hairs of legumes (Heidstra et al., 1994), and activate several signaling events in root hairs including membrane depolarization (Ehrhardt et al., 1992; Felle et al., 1995), calcium spiking (Ehrhardt et al., 1996), alkalization (Felle et al., 1996) and activation of genes possibly through the activation of G protein linked phospholipase C (Pingret et al., 1998). Fluorescent Nod factors (Gadella Jr. et al., 1997b) allow us to study the binding sites for these molecules on living root hairs. However, to obtain results at physiologically relevant concentrations of these factors, advanced microspectroscopic techniques are of vital importance, e.g. for discriminating root hair autofluorescence from Nod factor fluorescence. In this chapter we will discuss the Nod factor

studies only with respect to the microspectroscopic technology used for monitoring their in situ behavior on living root hairs. Although these studies have significant biological relevance in relation to the *Rhizobium*-legume interaction, these aspects are described elsewhere in this thesis. In this way we intend to stress the more general technological applicability of the microspectroscopic methodology for the study of root hairs. Of course, the microspectroscopic techniques have a wider applicability than the study of root hairs. So if appropriate, references will be made to studies of other (plant) systems.

2 Fluorescence Ratio Imaging Microscopy (FRIM)

2.1 Principle

Fluorescence ratio imaging microscopy (FRIM) employs the property of fluorescent probes that change their absorbance or fluorescence spectral properties in the presence of ions (Bright et al., 1989), voltage changes (Bullen and Saggau, 1999; Gross and Loew, 1989) or upon complexation to other molecules. By far most popular is the application of ratio imaging to the measurement of intracellular ion concentrations. Ratio probes can be divided into two groups, the so-called excitation ratio dyes and the emission ratio dyes. An example of a calcium sensitive excitation ratio dye is fura-2 which has an absorption maximum at 362 nm in the absence of calcium, whereas the calcium bound state has a maximum at 335 nm (Bullen and Saggau, 1999; Gross and Loew, 1989). Both forms of the molecule emit at green wavelengths (around 510 nm). Consequently, the ratio of the intensity obtained with 335 nm excitation to the intensity obtained with 362 nm is directly related to the calcium concentration.

An example of a calcium sensitive emission ratio dye is indo-1, which absorbs maximally around 340 nm. The fluorescence emission is maximal at 482 nm in the absence of calcium, whereas the emission maximum is at 398 nm for the calcium bound form (Bullen and Saggau, 1999; Gross and Loew, 1989). The use of ratiometric dyes can easily be combined with imaging microscopy, allowing studies of single cells. There are also non-ratiometric fluorescent indicators of which only the magnitude of fluorescence (or quantum yield) can be influenced by external factors such as ions or hydrophobicity. These probes can be used for fluorescence lifetime imaging applications (see section 4).

The great advantage of ratiometric over non-ratiometric dyes is that by the ratioing procedure (pixel-by-pixel division of the fluorescence intensities at the respective wavelengths), the local dye concentration, optical pathlength or spatial excitation light distribution divide out completely. In other words, the ratio-images only reflect the relative spectral state of the fluorophore and as a result can be directly related to the indicator function of the dye.

By performing a calibration procedure, it is possible to quantitatively relate the experimental ratio values to an ion concentration (or other parameter). The ratio, R , is measured at different (known) ion-concentrations, yielding a sigmoid curve of ratio versus ion concentration. The

calibration curve shows the spectral response of the dye to the ion concentration, $[\text{ion}]$, and can be described by:

$$[\text{ion}] = K' \cdot [(R - R_{\min}) / (R_{\max} - R)] \quad (1)$$

or logarithmic:

$$p[\text{ion}] = pK' - \log [(R - R_{\min}) / (R_{\max} - R)] \quad (2).$$

The three parameters are the maximal ratio R_{\max} , the minimal ratio R_{\min} and the K' (the ion concentration at which the ratio is exactly halfway R_{\min} and R_{\max}). This last value is usually close to the actual K of the indicator (being the ion concentration at which half of the indicator is free and the other half is ion-bound) but depends on instrumental factors. The sensitivity of the probe is highest around the $(p)K'$.

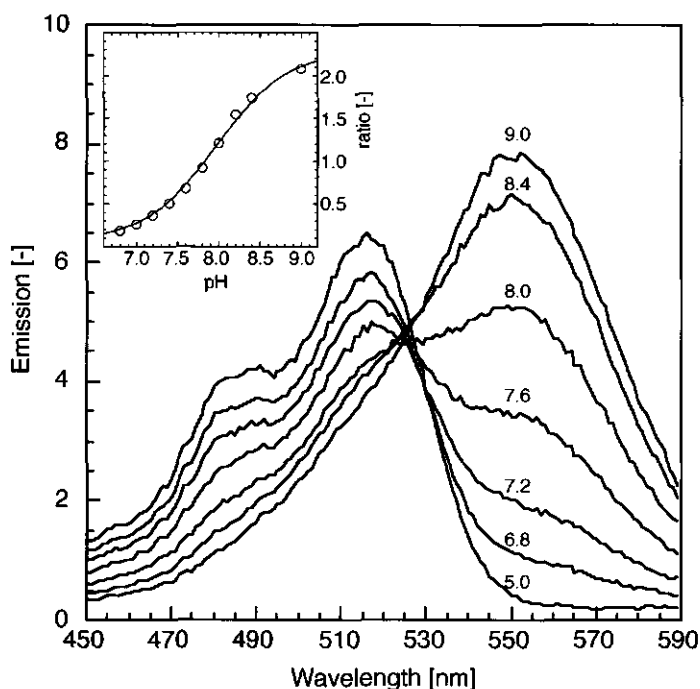


Figure 1: Excitation spectra of 0.1 μM of SNAFL-2 in 0.1 M phosphate buffer at different pH. The excitation spectra were acquired with a SPF 500 spectrofluorimeter (SLM Instruments, Urbana IL) by detecting fluorescence emission at 610 nm (slit 5 nm) and scanning the excitation from 450 to 590 nm (slit 1 nm). The inset shows the calibration curve obtained by calculating the ratios of the fluorescence intensities acquired upon excitation at 550 nm and 515 nm. The smooth curve represents the fit according to equation 2, yielding the parameters $R_{\max}=2.29$, $R_{\min}=0.064$, $pK'=7.97$, with regression $R=0.999$

For illustrating the basic principles of ratio measurements and the calibration procedure, we show the *in vitro* spectral properties of the pH sensitive dye, SNAFL-2 (Haugland, 1996; Whitaker et al., 1991) in figure 1. As can be inferred from this figure, the excitation spectra depend on the pH: at low pH the probe is most effectively excited at 515 nm, whereas the excitation maximum is shifted to 550 nm at alkaline pH. A calibration curve is constructed by calculating the ratio (emission observed at 620 nm after excitation at 550 nm divided by the emission observed at 620 nm after excitation at 515 nm) for every pH value. After fitting the calibration curve (inset of figure 1) according to equation 2, a pK' value of 8.0 was obtained. If however the detection wavelength is changed from 620 to 600 or to 640 nm, apparent pK s of 8.5 and 7.8 were obtained, respectively. On the one hand, this illustrates the dependence of the pK' on the instrumental settings, and the necessity to acquire new calibration curves when changing emission and excitation wavelengths (filters), or other optical components in the FRIM system (such as dichroic mirrors). On the other hand, it illustrates that by only changing some optical components in the (microscopy) system, the apparent pK can be adjusted to one's convenience. This can be very useful for optimizing the responsiveness of an indicator to a certain ion concentration.

2.2 Implementation of FRIM onto a fluorescence microscope

Excitation ratio-imaging can be easily implemented on wide-field fluorescence digital imaging microscopy (FDIM) systems by incorporating a filter wheel (with several different excitation bandpass filters) between the excitation source (Hg or Xe Arc lamps, or multiline laser) and the microscope. After implementation of an emission filter changer, emission ratio-imaging on an FDIM system can be done. However, this can be problematic due to registration aberrations (pixel shift) on the imaging detector (Bright, 1993). Emission ratio-imaging is more easily done with confocal laser scanning microscopy (CLSM), using dual channel detection of the fluorescence emission (Pawley, 1995). Alternatively, spectral imaging (discussed in section 3) can be used to monitor emission ratio dyes. The different implementation modes of FRIM and their (dis)advantages are reviewed by Bright (1993) and Fricker et al. (1999).

We have implemented excitation-FRIM by the incorporation of a Lep filter wheel (Ludl electronic products, München, Germany with 6 different bandpass filters) between a Leica DMR epifluorescence microscope (Leitz, Wetzlar, Germany) and its 100 W Hg excitation source. For FRIM of SNAFL-2, we used an Omega 520DF40 and an Omega 577DF10 bandpass filter (Omega, Brattleboro, VT, USA) in the filter wheel, and an Omega 595DRLP dichroic mirror with a longpass RG610 filter (Schott, Mainz, Germany) filter (both mounted into a filter cube of the microscope) for selecting the fluorescence emission. The images were captured using a Quantix CCD camera (Photometrics, with an Kodak KAF1400 grade 1 CCD sensor, Tucson, AZ, USA) which was mounted on the phototube exit (f-mount) port of the microscope. The CCD and the Lep filter wheel were controlled simultaneously using the IPLab

spectrum software package (Signal Analytics, Vienna VA, USA) on a Macintosh PowerPC 8500 (Apple computer Cupertino, CA, USA).

A complete ratio image acquisition (including exposures at the two excitation wavelengths and changing the excitation filter position) on the instrument described above can be achieved within 0.6 s, but usually takes about 2-3s depending on the integration/exposure time needed by the CCD to obtain satisfactory signal to noise values. The resulting two images, only differing in excitation wavelength, are used for the data processing/ratioing procedure. Data processing includes background subtraction (camera bias and background), calculation of the ratio image through pixel-by-pixel division of the fluorescence intensities of the two images, and the calculation of the in situ ion-concentration using equation 2. The procedures are implemented within the IPlab package using home-written macros, and within the SCILImage package (TPD, Delft, The Netherlands) on a Silicon Graphics Indy workstation (Silicon Graphics, Mountain View, CA, USA).

2.3 Applications

FRIM has found a wide application to measuring ion activities in single cells. The major application consists of measuring Ca^{2+} and pH (Gilroy, 1997; Read et al., 1992). Here we will focus on the measurement of pH in single living root hairs. Furthermore we will discuss a novel generation of indicators, which are based on fusion proteins containing the green fluorescent protein from *Aequoria victoria*.

2.3.1 Imaging root hair pH with SNAFL-2

In figure 2, we show the use of the ratiometric pH indicator SNAFL-2 for imaging the cytosolic pH in *Vicia sativa* (vetch) root hairs. The indicator (10 μM) is applied to the roots in an esterified, non-fluorescent form (SNAFL-2 diacetate from Molecular Probes, Eugene, OR, USA) for 30 min. Intracellular esterases cleave off the acetate groups and produce the fluorescent, negatively charged and membrane impermeable active form of the indicator. In this way, the indicator becomes highly concentrated in the root hair cytosol and the nucleus. Not all fluorescent indicators can be loaded as conveniently and efficiently as SNAFL-2. Some end up in the vacuole (e.g. BCECF (Brauer et al., 1995; Brauer et al., 1996)), while others are incompletely or not at all hydrolyzed (e.g. Calcium Green AM, Fluo-3 AM, J.Goedhart unpublished observations). Acid loading, microinjection or electroporation with or without dye-coupling to dextrans can be used under these circumstances. For a recent review on fluorescent dye loading strategies and protocols for living plant cells, we refer to (Fricker et al., 1999).

As shown in figure 2, the root hairs loaded with SNAFL-2 show an even distribution of the dye in the top left fluorescence image, which is acquired with an excitation bandpass filter of 520DF40 nm (fig. 2a). More fluorescence is visible in the cytosol in the top right image which is excited with the 557DF10 nm bandpass filter (fig. 2b), which preferentially excites the deprotonated form of SNAFL-2. Therefore in this image the more alkaline compartments will

show higher fluorescence intensities as compared to the other image. The excitation ratio at every pixel of the image is determined (fig. 2c), and can be converted into a pH image (fig. 2e) by using the parameters obtained from the calibration curve shown in figure 2d and equation 2. It is of note that in situ calibrations are generally more reliable than the *in vitro* calibration curves presented here (see Fricker et al. (1999) for extensive description of in situ calibration protocols).

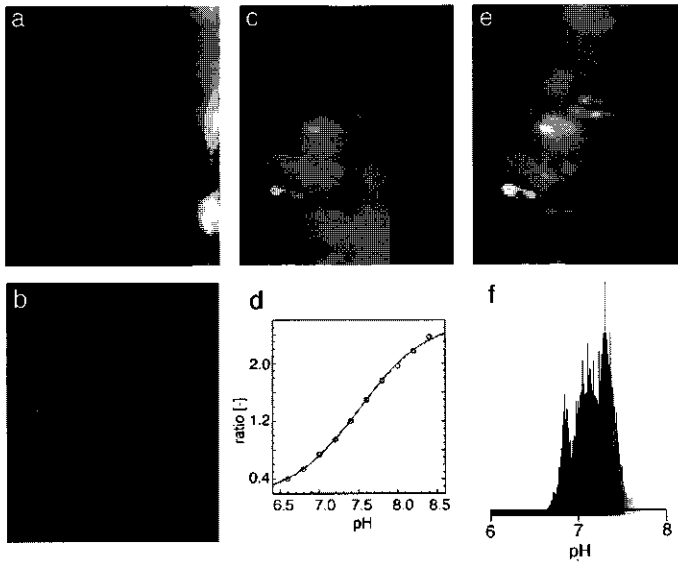


Figure 2: Root hair pH measurement by fluorescence ratio imaging microscopy (FRIM). The root system of *Vicia sativa* (vetch) grown in Fährus slides (Heidstra et al., 1994) was incubated with plant growth medium (Goedhart et al., 1999) containing 10 μM SNAFL-2 diacetate (esterified SNAFL-2, Molecular Probes, Eugene, OR) for half an hour. The individual images taken at the two excitation wavelengths: $\lambda_1=520\text{DF}40$ nm (a) and $\lambda_2=577\text{DF}10$ nm (b) are shown. After subtraction of background the ratio (c) was determined for every pixel by dividing the images (λ_2/λ_1). To translate the ratio image into a pH image (e), a calibration was performed by ratio-imaging of microcuvettes containing 5 μM SNAFL-2 in 0.1 M phosphate buffer set at various pH values, with identical microscope settings. The calibration curve (d) shows the response of the dye to pH. The smooth curve represents the fit ($R=0.9995$) according to equation 2 with $\text{pK}'=7.5$, $R_{\text{max}}=2.6$ and $R_{\text{min}}=0.14$. The pH in image (e) is represented by a grey-scale ranging from black (pH=6.0) to white (pH=8.0) as can also be inferred from the histogram (f) that is derived from the pH image

The pH distribution in a root hair shows a cytosolic pH of around 7.3, and is comparable to values measured in root hairs by others with either pH sensitive microelectrodes (Felle et al., 1996) or FRIM (Bibikova et al., 1998). The cytosolic pH value is close to the pK' of SNAFL-2 with these settings, which is the preferable situation. The pH in the vacuole region was much lower (around 6.8). It is of note that this value represents a mixed measurement of fluorescence arising from the acidic vacuole with the more alkaline cytosol in which the SNAFL-2 is more concentrated. With BCECF, which specifically sequesters into the vacuole of maize root hairs, Brauer et al. (1995) found a vacuolar pH of 5.8.

2.3.2 GFP-based ratio indicators

Recently, a new type of ion-sensitive probes has been developed, based on green fluorescent proteins (GFP) (Tsien, 1998). A fluorescent calcium sensitive chimeric protein, *cameleon*, based on calmodulin and GFP has been constructed by Miyawaki et al. (Miyawaki et al., 1999; Miyawaki et al., 1997). Two mutants of GFP, a cyan (CFP) and yellow fluorescing mutant (YFP) are attached to either side of a calmodulin and a calmodulin binding protein. The binding of calcium changes the relative orientation of the two fluorescent proteins, thereby causing an increased degree of intramolecular fluorescence resonance energy transfer (FRET, see also 4.3.3). Because of the increased FRET efficiency, the YFP/CFP fluorescence emission ratio is increased, allowing the use of the yellow *cameleon* as an emission ratio indicator (see also 3.3.2).

Additionally, pH-sensitive GFP mutants can provide an alternative way to measure pH. A pH-sensitive mutant of GFP is available which has similar spectral properties and pK as BCECF (Miesenböck et al., 1998). Hence, this so-called pHluorin, can also be used for excitation ratio-imaging of intracellular pH.

An important advantage of the gene-encoded indicators is that no dye loading or microinjection is required as the cells use their own biosynthesis machinery to produce the indicator. Furthermore, they can be specifically expressed in the cytosol or targeted to a variety of subcellular organelles. We anticipate many future applications of such indicators potentially unraveling detailed ionic activities in all plant cell organelles.

3 Fluorescence Spectral Imaging Microscopy (FSPIM)

3.1 Principle

Fluorescence spectral imaging microscopy (FSPIM) combines spatial resolution with spectral resolution. At every position across a line in a microscopic object a complete emission spectrum is obtained (Balaban et al., 1986). Consequently, this technique can be used to yield emission spectra of fluorescent molecules inside living cells (Martínez-Zaguilán et al., 1994). Hereby, the FSPIM measurement provides much more detail about the spectroscopic origin of the fluorescence than FRIM, which only employs two averaged regions of the spectra of fluorophores.

3.2 Implementation of FSPIM onto a fluorescence microscope

Spectral imaging (FSPIM) requires an imaging spectrograph mounted onto a fluorescence microscope. The basic elements of the spectrograph are an entrance slit and an astigmatic diffraction grating. The entrance slit, effectively reduces the spatial information of the microscopic object into one dimension (see figure 3). Imaging spectrographs are constructed in such way that the direction at which the photons are diffracted by the grating is perpendicular to

the orientation of the entrance slit. As a result, an image is produced at the exit port of the spectrograph with combined spatial and spectral resolution which is captured by a CCD camera. The photosensor of the camera is aligned to the spectrograph in such way that columns of pixels are parallel to the entrance slit and rows of pixels are parallel to the diffraction direction of the grating. Consequently, the image captured by the CCD camera contains spectral information in the horizontal direction and spatial information in the vertical direction.

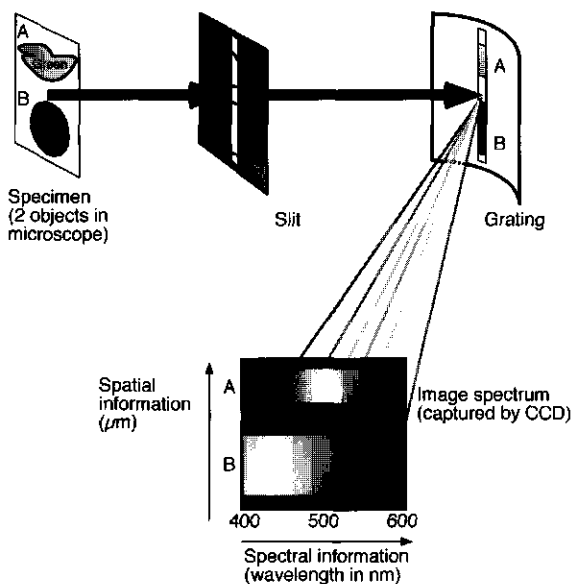


Figure 3: The principle of fluorescence spectral imaging microscopy (FSPIM). For explanation see section 3.2. Note that both the position (vertical axis) and the emission maximum (horizontal axis) of the green (a) and a blue (b) fluorescing objects can be discerned from the image spectrum

Our FSPIM instrument is built around a Leica DMR epifluorescence microscope and uses a laser (see section 4.2) or a 100 W Hg lamp/ filter wheel system (see section 2.2) as excitation source. The detector unit consists of i) a Chromex 250is (Chromex Inc., Albuquerque, NM, USA) f/4 image spectrograph mounted at the phototube exit (c-mount) of the microscope with ii) a slow scan series 200 (CH250) CCD camera (Photometrics, Tucson, AZ, USA) mounted at the exit port using a home-built f-mount adapter. The spectrograph has a remote-controlled slit width (adjustable from 20–2000 μm), 3 user selectable gratings with 150, 300 or 600 grooves/mm, all with a central wavelength of 500 nm. The spectrograph settings can be conveniently adjusted using the Chromex manual control unit. The CCD-camera is interfaced onto the Nubus slot of a Macintosh PowerPC 7100 computer and controlled using the IPlab Spectrum image processing software (Signal Analytics, Vienna VA, USA). Alternatively, the CCD camera and the spectrograph can be interfaced to a PC using an ISA slot and RS232 serial link, respectively. The CCD and spectrograph control are then integrated using the MAPS 2.0

software package (Photometrics, Tucson, AZ, USA) running under Microsoft Windows 95. The spectral dimension is conveniently calibrated using monochromatic laser lines, or mercury arc lamp lines.

The actual FSPIM measurement is not more complicated than any conventional fluorescence imaging measurement. Normal fluorescence filter cubes can be employed, however for the acquisition of full emission spectra, longpass emission filters should be used instead of bandpass filters. A typical experimental procedure includes i) setting the entrance slit and grating position to the required position, ii) aligning the cell of interest with the entrance slit of the spectrograph, iii) opening the excitation shutter (manually or TTL-controlled), iv) taking an exposure with the CCD (typically 1s-10s exposures), v) saving and processing of the acquired image spectrum. Usually only steps ii-v need to be performed if the instrument settings are identical for different microscopic objects. In a time-series an image stack can be acquired by repeating steps iii) and iv) several times with an optional user controlled delay between the exposures. This procedure provides spatial, temporal and spectral information in one data set.

3.3 Applications

3.3.1 *Decomposing multicomponent fluorescence emission and autofluorescence subtraction*

Spectral imaging is especially useful when more than one type of fluorophore is present in the specimen, yielding multicomponent fluorescence emission spectra (Martínez-Zaguilán et al., 1994). A component which is always present when studying living cells is autofluorescence. Especially at low fluorescent probe concentrations, where the probe fluorescence intensity approaches the autofluorescence levels, spectral imaging is a very useful tool to decompose the dual component spectra.

Growing plant root hairs display relatively low levels of autofluorescence. However, when fluorophores are studied at nanomolar or even lower concentrations (e.g. Nod factors) the fluorescence intensity is close to the intensity of autofluorescence. A unique feature of root hairs is their elongated shape allowing optimal alignment of the total cell with the entrance slit of the imaging spectrograph. Therefore, root hairs are the most ideal cell type for spectrographic studies. Gadella et al. described the use of FSPIM to be able to detect BODIPY FL labeled fluorescent Nod factors on *Vicia sativa* roots (Gadella Jr. et al., 1997b). A procedure was developed to decompose the dual component spectra into autofluorescence and a BODIPY component spectrum. In this way, it was possible to locate the presence of Nod factor on *Vicia sativa* root hairs when applied at a concentration of 1 μM and using an excitation wavelength of 475 nm.

The autofluorescence of *Vicia sativa* root hairs is significantly lower if the excitation is shifted from blue (475 nm, necessary for excitation of BODIPY FL) to green or yellow (510-580 nm) which is optimal for exciting recently developed red-shifted fluorescent Nod factors (Goedhart

et al., 1999). Upon application of plant growth medium containing 1 nM of the red-shifted BODIPY 581/591 tagged fluorescent Nod factor to *Vicia sativa* plant roots grown in a Fährus slide (Heidstra et al., 1994), the fluorescence signal of the probe is comparable to autofluorescence.

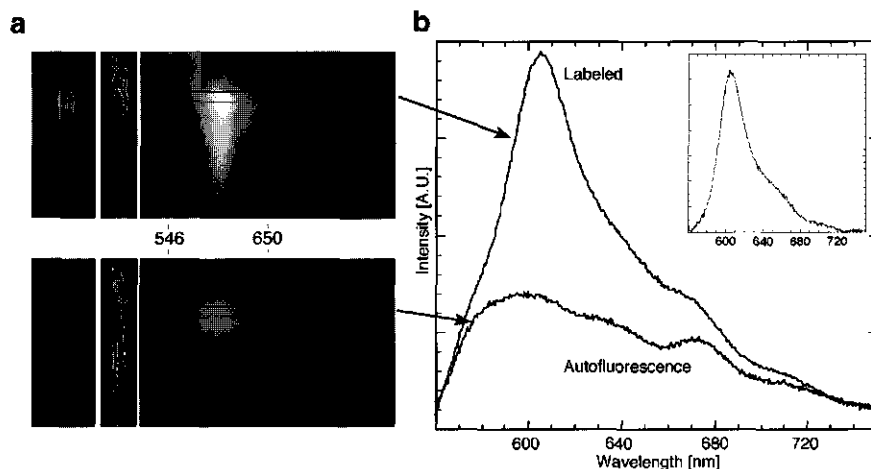


Figure 4: Spectral images (a) of a *Vicia sativa* root hair labeled with 1 nM NodRlv-IV (BODIPY 581/591-C16) (upper) and an unlabeled control (lower). A 10× PL fluotar NA 0.3 objective in combination with an Omega (Brattleboro, VT) 546DF10 nm bandpass excitation filter, an Omega 555DRLP dichroic mirror and a Schott (Mainz, Germany) OG570 longpass emission filter were used. The slit width of the imaging spectrograph was 200 μm and the central wavelength was 650 nm. The acquisition time was 10 s. Averaged fluorescence emission spectra of the tip region (indicated by the box) of labeled and unlabeled root hairs are shown (b). The difference spectrum representing net BODIPY 581/591 fluorescence is shown in the inset

In figure 4a, an FSPIM analysis of both a labeled and unlabeled root hair is shown. Left, a fluorescence image and a phase contrast image of both hairs is shown, indicating the width of the entrance slit. Both images are captured using the spectrograph with the diffraction grating set at zero-order position. In this position, the grating functions as a mirror enabling conventional fluorescence imaging. The spectral images are shown on the right side of the phase contrast images. In the vertical (spatial) dimension of the spectral image of the labeled root hair, clearly the most intensely labeled region of the root hair can be identified. In the horizontal (spectral) direction of the image spectrum the maximal fluorescence intensity is observed between 546 and 650 nm. Also some excitation light is detected with the spectrograph as can be seen from the band with the width of the entrance slit centered around 546 nm (a Hg-line). The analysis of the unlabeled root hair shows a reduced fluorescence intensity, but also no clear maximum in the horizontal direction of the image spectrum can be identified. This "flatness" is typical for autofluorescence spectra. In figure 4b average emission spectra of the tips of both root hairs are shown. From the figure it can be inferred that the BODIPY- and autofluorescence contribute equally to the total fluorescence. The spectrum acquired from the unlabeled root hair

shows a broad spectrum without any sharp peaks. The bump around 670 nm was also observed by Gadella et al. as a large peak, and corresponds to porphyrin fluorescence emission, which is excited less effectively at the wavelength used here (546 nm). Contrarily, the emission spectrum of the labeled root hair does show a clear peak, but also the autofluorescence spectrum can be discerned. Indeed, the difference spectrum of the labeled and unlabeled root hair, shown as an inset of figure 4b, represents a typical BODIPY emission spectrum. The emission maximum of the probe observed on root hairs is around 605 nm instead of the true maximum at 591 nm. The shift of the maximum from 591 to 605 nm is mainly caused by the reduced transmission of the dichroic mirrors and emission filters of the blue edge of the spectrum and by the increased sensitivity of the CCD camera in the red to near-infrared part of the spectrum. All these parameters contribute to the so called spectral instrument response curve. This curve can be considered as a multiplication of the transmission spectra of the microscope optics (lens, dichroic mirror and emission filter) with that of the spectrograph and the spectral response curve of the CCD sensor. With standard spectra, the instrument response can be determined and the spectra can be corrected. Correction is not necessary if different measurements are performed with the same instrument settings and if only relative spectral changes are important.

3.3.2 Usage of FSPIM for monitoring fluorescence emission ratio indicators

As mentioned before, FSPIM can also provide an alternative to emission ratio-imaging, as changes in emission spectra are easily detected by FSPIM. This even allows the simultaneous determination of Ca^{2+} and pH in single cells (Martínez-Zaguilán et al., 1996; Martínez-Zaguilán et al., 1994). Here, we will explain the principle of determining pH by FSPIM using SNAFL-2. In figure 5, the pH dependent emission spectra of SNAFL-2 as measured by FSPIM are shown. The deprotonated state (fig. 5a) shows an emission maximum above 580 nm, whereas the emission maximum of the protonated dye (fig. 5b) is below 580 nm. When a spectral image at intermediate pH is acquired (fig. 5c), it can be inferred that this is a mixture of the spectrum at low pH representing the protonated probe with that at high pH representing the deprotonated probe spectrum. By fitting these intermediate spectra, using the spectra of the pure protonated and deprotonated probe, the contributions of both species can be determined very accurately. In this way, a calibration curve can be constructed which describes the contribution of the protonated and deprotonated state for different pH values. These calibration values can be used to exactly measure pH in living plant cells after the decomposition of the in situ spectra in the deprotonated and protonated component spectra. When a third fluorescent species (i.e. autofluorescence) also contributes to the total emission spectrum the fit procedure (Gadella Jr. et al., 1997b) should be extended to three or more components. Especially under those conditions, the FSPIM method is superior to FRIM which would produce aberrant ratios in the presence of a significant amount of autofluorescence.

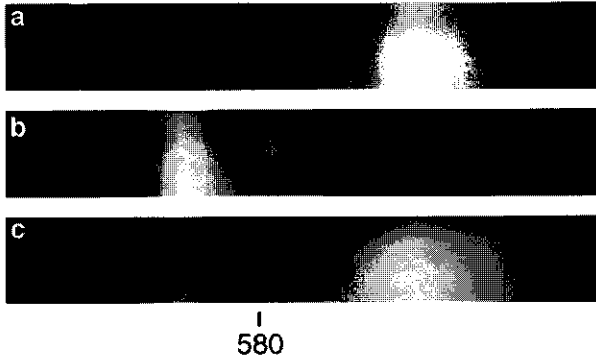


Figure 5: FSPIM of microcuvettes filled with 5 μM SNAFL-2 in an alkaline (pH=9.5) (a), acidic (pH=4.5) (b), or neutral (pH=7.0) (c) buffer. A 20 \times HC PL fluotar NA 0.5 objective in combination with an Omega 500RDF25 nm bandpass excitation filter, an Omega 525DRLP dichroic mirror and a Schott GG530 longpass emission filter were used. The slit width of the spectrograph was 200 μm and the central wavelength was 580 nm. Acquisition time was 10 seconds and 4 \times binning in the spatial direction was used on the CCD camera

Recently we successfully applied the FSPIM method for monitoring Ca^{2+} in living Lotus root hairs that were stably transformed with the yellow-cameleon calcium indicator (Miyawaki et al., 1999; Miyawaki et al., 1997), see also section 2.3.2. The CFP and YFP contributions from the yellowameleon fluorescence emission spectrum could be fitted and indicated a clear positive cytosolic calcium gradient towards the root hair tip. In addition to the CFP and YFP components, it is essential to fit an autofluorescence component and a background fluorescence component in order to obtain reliable data. The results and the four-component fit procedure are described in detail elsewhere (Gadella Jr. et al. 1999; Gadella Jr., manuscript in preparation).

A clear advantage of FSPIM over FRIM is that all spectral components are acquired in one measurement. FRIM usually employs two consecutive images acquired with different filter combinations. Consequently, the FRIM method is dependent on the stability of the excitation source, and in case of emission ratio imaging also registration errors can occur. FSPIM does not suffer from registration problems. However, the superior accuracy obtained by FSPIM is obtained at the sacrifice of one spatial dimension. Given their elongated shape, this may be tolerable for root hairs. In this respect, it should be noted that by scanning the microscope stage it is possible to obtain two-dimensional spatial information with FSPIM.

4 Fluorescence Lifetime Imaging Microscopy (FLIM)

4.1 Principle

Fluorescence lifetime imaging microscopy (FLIM) is a technique for imaging excited state lifetimes of fluorophores by means of a fluorescence microscope. Lifetime images produced by these instruments are digital images in which each pixel value represents the fluorescence lifetime (τ). As opposed to conventional steady-state fluorescence microscopy, FLIM reports on

a kinetic parameter (τ) which, unlike fluorescence intensity, is independent of probe concentration, excitation light intensity, moderate levels of photobleaching, direct absorption (or filtering) of fluorescence or on the optical path length in the microscope.

The fluorescence lifetime of a fluorophore is the average time that passes between absorption of an excitation photon by the fluorophore, and the release of the absorbed energy in the form of a red-shifted emission photon. Generally, excited state lifetimes are in the nanosecond (10^{-9} s) time range. The fluorescence lifetime is linearly proportional to the quantum yield Q of the fluorophore (the average number of photons produced by a fluorophore per absorbed photon, $0 < Q < 1$). The quantum yield of fluorophores is highly dependent on their direct chemical microenvironment. Parameters that change the fluorescence lifetime are local hydrophobicity, local pH, the availability of fluorescence quenchers, ions (e.g. Ca^{2+}) or the proximity of energy transfer acceptors. With steady-state fluorescence microscopy, quantum yields cannot be studied independent from probe concentration, because the local fluorescence intensity is a product of local probe concentration and the local fluorescence quantum yield (and several other parameters such as excitation light intensity, absorption cross-section, detector efficiency, and optical path length (Jovin and Arndt-Jovin, 1989b; Jovin et al., 1990)). Consequently, with conventional steady-state fluorescence microscopy, one cannot distinguish between a high fluorophore concentration with a low quantum yield and a low fluorophore concentration with a high quantum yield. FLIM, however, enables to generate separate images of fluorescence intensity and fluorescence lifetimes and thereby provides the capability to image both the local fluorophore concentration and the local fluorophore microenvironment.

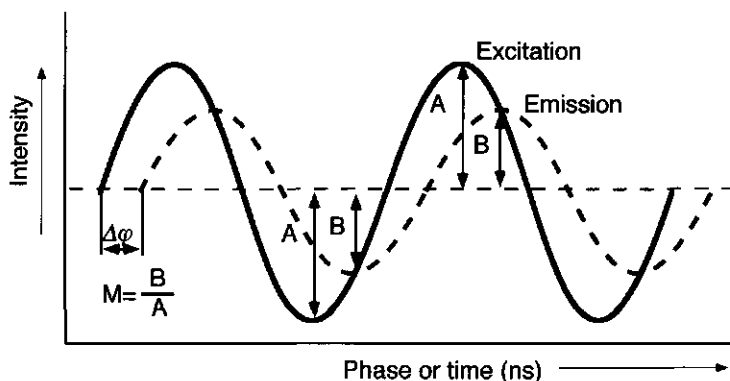


Figure 6: Principle of fluorescence lifetime determination with the frequency-domain approach. The excitation light is sinusoidally intensity-modulated. The resulting fluorescence emission is also sinusoidally intensity-modulated but phase shifted (by $\Delta\phi$ degrees, $0^\circ < \Delta\phi < 90^\circ$) and demodulated (by a factor M , $0 < M < 1$) with respect to the excitation light

Fluorescence lifetime imaging microscopes can be implemented in many different ways, for a recent review see (Gadella Jr., 1999). The two most widely used modes of implementation are the frequency domain (Gadella Jr. et al., 1993; Gadella Jr. et al., 1997a; Lakowicz and Berndt,

1991; So et al., 1994) and time domain approaches (Oida et al., 1993; Periasamy et al., 1996; Sytsma et al., 1998; Wang et al., 1992). In the time domain, a very short pulse (fs-ps time duration) of light excites the sample, and time-correlated detection of the fluorescence emission provides the lifetime information. In the frequency domain (used in our laboratory), the specimen is continuously excited with intensity-modulated light. The intensity-modulation occurs at a radio frequency (typically in the tens of MHz region) in a sinusoid or other shaped way. As a result, also the induced fluorescence emission of the microscopic object will be intensity-modulated. However, due to the time difference between excitation and emission (i.e. lifetime of the probe), the emitted light will be demodulated and phase shifted with respect to the excitation light. The frequency domain principle of fluorescence lifetime estimation is explained in figure 6. The two observables (phase shift $\Delta\phi$ and demodulation M) can be related to the fluorescence lifetime via two straightforward equations (Gadella Jr. et al., 1994; Jameson et al., 1984):

$$\tau_{\phi} = \frac{1}{2\pi f} \tan(\Delta\phi) \quad (3)$$

$$\tau_M = \frac{1}{2\pi f} \sqrt{(1/M^2) - 1} \quad (4)$$

where f is the frequency of modulation. When there is more than one way of radiative deactivation of one (or multiple) excited state(s), the fluorescence emission process can be described by more than one fluorescence lifetime and can be considered as multicomponent emission. The formulas relating the observables $\Delta\phi$ and M to these different lifetimes are more complicated in this case (see also Gadella Jr. et al. (1994b) and Gadella Jr. (1999)), but a multicomponent emission can be easily identified by the fact that the lifetimes determined from the phase (τ_{ϕ}) and from the modulation (τ_M) are different ($\tau_{\phi} < \tau_M$).

4.2 Implementation of fluorescence lifetime imaging capabilities in a microscopy system

The implementation of the frequency-domain method of fluorescence lifetime estimation in a microscope, requires the inclusion of specific components allowing fast modulation of the excitation light, an imaging detector capable of measuring fast changes in fluorescence intensities, and several electronics to control the modulation and phase settings. The set-up used in our laboratory has been described in detail by Gadella et al. (1997a), therefore only a basic description of the equipment will be given here, following the light path. The first component is a laser source (CW Ar/Kr laser) which puts out a single (user selectable) line which is passed through an acousto-optic modulator (AOM). The AOM modulates the laser light intensity up and down in MHz frequency range somewhere between 10-150 MHz. One of the diffraction

spots produced by the AOM is selected by a diaphragm, and after expanding the beam it is incorporated into a Leica DMR/BE epifluorescence microscope. A dichroic mirror reflects the excitation light onto the sample. The fluorescence emission is transmitted through the dichroic mirror and an emission filter. The filtered fluorescence emission is focused onto the photocathode of the rf-frequency gain-modulated image intensifier (Hamamatsu, model C5825). The light emitted from the phosphor screen of the image intensifier is focused onto the chip of a CCD camera (Photometrics model Quantix with an Kodak KAF1400 grade 1 CCD sensor, Tucson, AZ, USA) by means of a relay lens system. Two computer-controlled frequency synthesizers (Programmed Test Sources model 310, Littleton, MA, USA) drive the modulation on AOM and the image intensifier gain respectively. Phase image acquisition by the CCD, excitation shutter control and phase settings on the frequency synthesizers are computer controlled and integrated within the IPLab spectrum image acquisition/processing software package (Signal Analytics, Vienna VA, USA). Image analysis for constructing lifetime images from the phase images is done on an Silicon Graphics Indy workstation using self-written software (Gadella Jr. et al., 1994).

We use a homodyne detection scheme in which the fluorescence signal and the detector (image intensifier) gain-modulation occurs at exactly the same frequency. When the gain-modulation of the image intensifier happens to be exactly in phase with the fluorescence intensity-modulation, a maximal signal will be integrated on the CCD. If the phase difference is 180° (exactly out of phase), a minimum signal will be integrated on the CCD. In a typical experiment, the phase between the image intensifier gain-modulation and the excitation light-modulation is varied from 0 to 360° , and at each phase difference an image is captured by the CCD. Typically, 4 to 10 of such phase images (0.1-2 s exposure time each) are acquired by the CCD camera. The spatially resolved lifetime information is extracted from the phase image stack by fitting a sinusoid for every single pixel and determining the phase shift $\Delta\phi$ and demodulation M with an image analysis procedure (Gadella Jr. et al., 1994; Gadella Jr. et al., 1993).

4.3 Applications

The fluorescence lifetime is a fundamental spectroscopic parameter, like wavelength or intensity, and hence, lifetime-resolved images can be used for many applications, for a review see Gadella Jr. (1999).

4.3.1 Imaging of ion and oxygen concentrations

Several reports have appeared showing novel ways of detecting ion concentrations by employing non-ratiometric fluorescent indicators that change their lifetime rather than their fluorescence spectrum. For ratiometric determination of Ca^{2+} concentrations, using fura or indo (Haugland, 1996), UV excitation has to be employed. UV, however, is generally hazardous to living cells. UV excitation can be avoided by using non-ratiometric lifetime-based fluorescent Ca^{2+} indicators absorbing at longer wavelengths such as Ca-Green (blue excitation) (Lakowicz

et al., 1992; Sanders et al., 1994; So et al., 1995) or Ca-Crimson (orange excitation) (Periasamy et al., 1996).

Also the pH sensitive dye SNAFL-2 shows a change in the fluorescence lifetime upon altering the pH. By using FLIM, we determined that the lifetime (τ_{F}) of SNAFL-2 was 2.3 ns in alkaline solution (pH=9) and 4.0 ns in acidic solution (pH=5) upon excitation at 514 nm and detection with a 610DF20 nm emission bandpass filter. Similar experiments using 568 nm excitation, showed a relatively constant fluorescence lifetime around 1.0 ns both in alkaline and acidic solution, which is comparable to the value reported by others (Szmackinski and Lakowicz, 1993). Most likely, only the protonated probe is excited at 568 nm, which has a lifetime of 1.0 ns.

Many other lifetime-based fluorescence indicators which can be ester-loaded into living cells are available, e.g. for detecting Mg^{2+} (Magnesium-Green), Na^+ (Sodium-Green) Cl^- (N-ethoxycarbonylmethyl-6-methoxyquinolinium bromide (MQAE) and heavy metals (bis-BTC), but still await application in lifetime resolved imaging (Haugland, 1996; Szmackinski et al., 1994). By employing the ability of oxygen to decrease fluorescence lifetimes by collisional quenching, FLIM has also been successfully applied in imaging oxygen concentrations in living cells (Gerritsen et al., 1997).

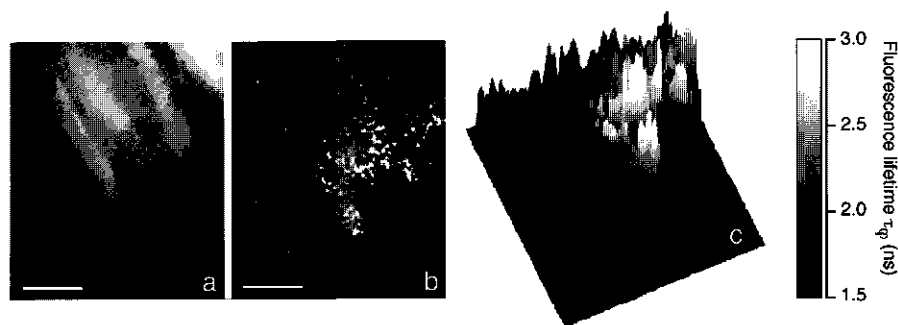


Figure 7: FLIM analysis of *Vicia sativa* root hairs labeled with a Nod factor containing a fatty acid tail with a BODIPY FL moiety. a: (steady-state) fluorescence intensity image, b: fluorescence lifetime image, c: pseudo three dimensional representation of the fluorescence lifetime image. The lifetime values are indicated in a grey-scale ranging from black (1.5 ns) to white (3 ns) as indicated next to figure c. The white distance bar represents 50 μm in the object plane. For labeling conditions and the Nod factor structure see ref. (Gadella Jr. et al., 1997b). The specimen was excited at 488 nm modulated at 51.204 MHz; a 40 \times PL Fluotar oil immersion objective (NA 0.5-1.0, set at 1.0), an Omega 505DRLP dichroic mirror and an Omega 525DF20 nm bandpass emission filter were used. Other conditions are similar to those described in (Gadella Jr. et al., 1997a)

4.3.2 Contrast enhancement

In a situation where autofluorescence and probe fluorescence intensities and spectra are comparable, it is very difficult to distinguish between probe fluorescence and autofluorescence using steady-state FDIM. However, if the fluorescence lifetime of the probe is different from that of the autofluorescing environment, the lifetime image can specifically enhance the contrast for that specific probe. Such a situation occurs upon labeling *Vicia sativa* roots with fluorescent Nod factors containing a BODIPY FL moiety (Gadella Jr. et al., 1997b). Upon excitation with

the 488 nm laser line, the green fluorescence produced by the Nod factor is very comparable with the root autofluorescence both in color and in intensity. Because the fluorescence lifetime of the autofluorescence is only about 1 ns, and the fluorescence of the BODIPY FL is about 5.5 ns, FLIM enables to study the localization of this Nod factor on living root hairs. In figure 7, the result of such an experiment is shown. The lifetime image shows that the fluorescence lifetimes vary between 1.5 and 3.0 ns, clearly representing a mixture of the two fluorescent components. Interestingly, the fluorescence lifetime increases when going towards the tips of the root hairs. This is due to the increased ratio of BODIPY FL fluorescence to autofluorescence. Hence this Nod factor has a preference to bind at the root hair tips.

4.3.3 FRET and GFP: probing molecular proximity

FLIM is also a very valuable tool for studying fluorescence resonance energy transfer (FRET). FRET is the process by which an excited donor fluorophore transmits its energy (radiationless) to a neighboring acceptor chromophore. FRET only occurs over a very short distance range: generally shorter than 8 nm. Hereby FRET provides an excellent way to monitor molecular interactions in complex environments (e.g. living cells) with a high spatial resolution. FRET is manifested by a decrease in donor fluorescence intensity and fluorescence lifetime and by an increased (sensitized) emission by the acceptor (if the acceptor is a fluorophore). For a detailed description of FRET, the reader is referred to (Clegg, 1995; Clegg, 1996; Förster, 1948; Stryer, 1978; Tsien et al., 1993; Wu and Brand, 1994).

Because quantitative measurements of fluorescence intensities are difficult in a steady-state fluorescence microscope, FRET measurements using FDIM are complex and sensitive to experimental errors (Gordon et al., 1998; Jovin and Arndt-Jovin, 1989a). FLIM, on the other hand, is a reliable and convenient method to quantify FRET in single living cells because it directly measures the decrease in donor-fluorescence lifetime upon the transfer of energy to a FRET acceptor. FRET-FLIM has been successfully applied to monitor proteolytic processing of protein kinase C (PKC) in intact cells (Bastiaens and Jovin, 1996), for monitoring membrane fusion in cells (Oida et al., 1993) and to monitor oligomerization of cell surface receptors (Gadella Jr. and Jovin, 1995). For each of these studies, alterations in the fluorescence lifetime reported on a change in proximity (on the nm distance scale) of two interacting molecules in single cells.

The green fluorescent protein (GFP) from the jellyfish *Aequoria victoria* is a very good probe for FLIM. The enhanced version (EGFP, S65T) has a lifetime of 2.67 ns and can be imaged in single living plant cells with a very high accuracy (coefficient of variation < 3.5%) (Gadella Jr., 1999). The availability of chromophore mutants of GFP with blue (BFP), cyan (CFP) and yellowish (YFP) colors enables to perform colocalization and FRET studies in single living cells (for reviews see (Ellenberg et al., 1999; Pollok and Heim, 1999; Tsien, 1998)). A review on GFP-based FRET applications in plant cells is published elsewhere (Gadella Jr. et al., 1999).

Recently, we could show that the GFP/FRET based calcium indicator yellow-cameleon2 (Miyawaki et al., 1999; Miyawaki et al., 1997) can be expressed in the cytosol of root hairs of *Lotus japonicus*, using the RH2 root epidermis specific promoter (Gadella Jr. et al., 1999). We could detect an increased FRET efficiency in yellow-cameleon2 at the tips of growing root hairs which indicates a local positive calcium concentration gradient at the root hair tip (Gadella Jr. et al., 1999). Because of the relative ease of plant transformation, many GFP-based (FRET-) FLIM applications are possible for the near future. The plant root hair seems to be an almost ideal cell type for such studies. Hence, it is likely that there will be an important role for FLIM in the detection of molecular interactions in single living root hair cells using GFP fusion proteins, which undoubtedly will shed new light on subcellular signaling, trafficking and communication mechanisms.

5 Fluorescence Correlation Microscopy (FCM)

5.1 Principle

Fluorescence correlation spectroscopy (FCS) is a fluorescence microscopic technique that gives information on diffusion and concentration of fluorescent molecules (Rigler, 1995; Schwille et al., 1997a).

FCS is based on the confocal fluorescence microscopic technique, but unlike confocal laser scanning microscopy (Pawley, 1995), the position of the confocal excited volume is fixed throughout the measurement. FCS measures fluorescence intensity fluctuations due to movement of single fluorescent molecules in and out a small (1 fL) open confocal volume element (Maiti et al., 1997), schematically illustrated in figure 8a. When slowly diffusing molecules enter the confocal volume, the rise in fluorescence will be longer as compared to fast diffusing molecules (figure 8b). Therefore, the dynamics of the intensity fluctuations contain information on the diffusional speed of the molecules. The diffusion constant for translational movement can be determined from the autocorrelation function $G(\tau)$, which relates the fluorescence intensity, I , at a time t to that τ seconds later:

$$G(\tau) = \frac{\langle I(t) \cdot I(t + \tau) \rangle}{\langle I \rangle^2} = \frac{\langle I \rangle^2 + \langle \delta I(t) \cdot \delta I(t + \tau) \rangle}{\langle I \rangle^2} \quad (5)$$

Here δI denotes the fluctuation of the fluorescence intensity around the mean value $\langle I \rangle$. In order to measure fluctuations in fluorescence intensity, it is essential that the number of fluorescent molecules inside the confocal volume element changes significantly over time. If there are more than 100 molecules on average in the volume element at any time, the change in fluorescence intensity due to the movement of a single molecule in or out of the detection volume will be very insignificant. Hence the number of molecules in the volume element must be *low* enough, determining the *upper* concentration limit at which FCS can be used (around 100 nM). The

lower concentration limit is confined by background or the time that can be spent in order to obtain enough intensity fluctuations and can be as low as 10^{-12} M (Rigler, 1995). Assuming a Gaussian shaped laser focus in three dimensions, the autocorrelation function can be written as:

$$G(\tau) = 1 + \frac{(1 - F + F \cdot e^{-\lambda\tau})}{N_m \left(1 + \frac{4D_{\text{tran}} \cdot \tau}{\omega_{xy}^2}\right) \left(1 + \frac{4D_{\text{tran}} \cdot \tau}{\omega_z^2}\right)^{1/2}} \quad (6)$$

where D_{tran} denotes the translational diffusion constant in $\text{m}^2 \cdot \text{s}^{-1}$ and N_m indicates the average number of fluorescent particles in the detection volume. Figure 8c shows the shape of the autocorrelation function. Equation 6 also contains a term F , describing the fraction of molecules in the triplet state and the characteristic triplet decay rate λ . The constants ω_{xy} and ω_z describe the dimensions of the volume element. These are defined as the distance from the center of the laser focus in the radial, ω_{xy} , and axial direction, ω_z , where the fluorescence intensity has dropped to e^{-2} ($\approx 13.5\%$) of its peak value. The laser radii can be resolved by calibration using reference compounds with known diffusion constants. The autocorrelation function can easily be extended for multiple contributions (Brock et al., 1998). However, quantum yields of different species contributing to the autocorrelation should be taken into account (Meseth et al., 1999).

The volume, V , of the confocal element (m^3) can be approached by a cylinder with radius ω_{xy} and height $2\omega_z$ in both directions from the center and hence equals:

$$V = \pi \omega_{xy}^2 \cdot 2\omega_z \quad (7)$$

The hydrodynamic radius, r , of the fluorescent particles is related to the diffusion constant via the Stokes-Einstein equation (Edward, 1970):

$$r = \frac{kT}{6\pi\eta D_{\text{tran}}} \quad (8)$$

in which η is the viscosity, T is the absolute temperature and k the Boltzmann constant.

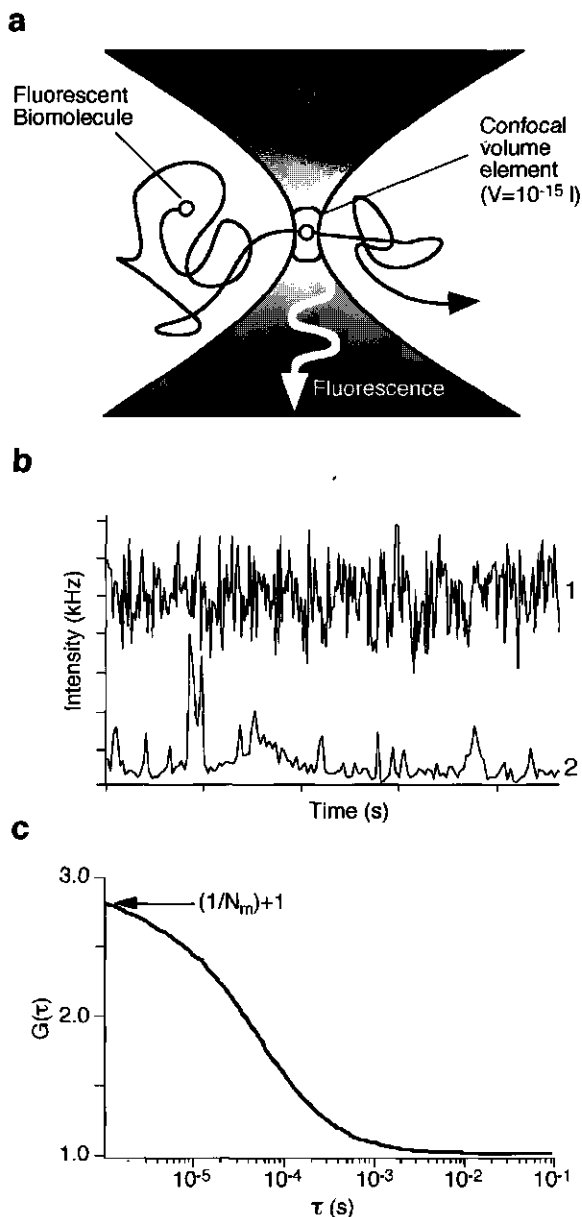


Figure 8: Principle of fluorescence correlation spectroscopy (FCS). A fixed confocal volume is continuously illuminated by a focused laser beam (a). Fluorescent molecules entering the confocal volume will give rise to a burst of fluorescence emission (b), of which the duration is dependent on the time they spend in the confocal volume. This is illustrated by curve 1 and 2, representing intensity fluctuations caused by diffusion of small organic fluorophores (Rhodamine green in H_2O) or large multilamellar vesicles labeled with fluorescent lipids, respectively. Autocorrelation of the intensity-fluctuations gives the autocorrelation curve (c) which can be analyzed to yield the average number of particles N_m in the confocal volume, and the diffusion constant D (see equation 5)

5.2 Implementation of FCS

FCS measurements were performed on a commercially available system: the Zeiss-Evotec ConfoCor (Carl-Zeiss, Jena, Germany and Evotec Biosystems, Hamburg, Germany). The system consists of a Zeiss Axiovert inverted microscope with standard confocal epifluorescence microscope optics. An argon ion laser (488/514 nm) and a helium-neon laser (543 nm) are used as excitation sources. Zeiss dichroic mirrors (we used the 560 nm dichroic), and Zeiss emission filters (we used the 565-610 nm bandpass filter) mounted in a Zeiss filter slider are employed to separate fluorescence from excitation light. The light is focused in the sample using a high grade Zeiss water immersion objective (40 \times , 1.2 NA) with a adjustable ring for matching slight differences in refractive index (e.g. caused by variation in coverglass thickness). Confocal detection is achieved by a motor-controlled pinhole (diameter usually 40 μ m). The detector behind the pinhole consists of an avalanche photodiode coupled to a fast digital correlator, which supplies a real-time display of the autocorrelation curve. The setup is described in detail elsewhere (Hink et al., 1999; Hink and Visser, 1998).

Calibration, to obtain the dimensions of the confocal volume (ω_{xy} and ω_z in equation 7), is done by acquiring autocorrelation curves of fluorophores with a known diffusion constant such as rhodamine 6G or tetramethylrhodamine in H₂O (both have diffusion constants of 2.8 \cdot 10⁻¹⁰ m² s⁻¹) (Rigler et al., 1992).

5.3 Applications

FCS has been applied mainly to study molecular diffusion in solution. Applications of FCS include measuring diffusion constants (Magde et al., 1974), aggregation states (Berland et al., 1995) hybridization of oligonucleotides (Kinjo and Rigler, 1995; Oehlenschläger et al., 1996) and receptor-ligand interactions (Rauer et al., 1996). So far the use of FCS in combination with digital microscopy (FCM) (Brock et al., 1998; Brock and Jovin, 1998) to study molecular diffusion and concentration in living cells has been limited. Still, FCM can be applied successfully to obtain quantitative information on concentration and diffusional behavior of fluorescent molecules in root hairs, as will be described below.

5.3.1 Study of Nod factor diffusional behavior on living root hairs by FCM

In figure 9, we show the results of an FCM analysis of a growing *Vicia sativa* root hair in the presence of 10 nM initially extracellularly applied fluorescent Nod factor. We used an orange fluorescing BODIPY 558/568 tagged Nod factor in combination with the 543 nm He/Ne laser line. If the 488 nm or 514 nm laser line were used for excitation, the autofluorescence of the root hairs was too high. However, at 543 nm excitation the autofluorescence, was low enough to allow FCM experiments with orange or red fluorescing dyes. By moving the microscopy stage, the FCM confocal volume element can be positioned anywhere in the slide. We positioned the confocal volume just before the tip of a growing root hair after which several autocorrelation curves (60 s each) were acquired sequentially. The first three correlation curves (see figure 9),

taken extracellularly, show fast Nod factor diffusion ($D=2.3 \cdot 10^{-10} \text{ m}^2 \cdot \text{s}^{-1}$), but then suddenly a shift of the autocorrelation curves to slower diffusion is observed upon entering (growth) of the root hair into the confocal volume element. Also the fluorescence intensity is markedly increased when the cell wall enters the confocal volume. As soon as the cell wall exits and the cytosol moves into the volume element the fluorescence intensity drops, and autocorrelation curves of faster diffusing particles are obtained. From analysis of the correlation curve 5 in figure 9 (representing diffusion monitored in the cell wall) an average diffusion constant of approximately $2.3 \cdot 10^{-13} \text{ m}^2 \cdot \text{s}^{-1}$ is calculated, indicating a 1000-fold decreased diffusional mobility as compared to Nod factor diffusion in water. Under the employed labeling conditions, the average number of fluorescing particles inside the confocal volume element is usually around 50. Given the confocal volume of approximately 1.4 femtoliter ($1.4 \cdot 10^{-15} \text{ L}$) this implies a concentration of 60 nM. The actual concentration of Nod factors in the cell wall will be several fold higher because the thickness of the cell wall is less than the diameter of the excited volume element. Considering the initial extracellularly applied concentration of Nod factor of 10 nM, these results demonstrate a marked accumulation of the Nod factor at the root hair cell wall, and a large reduction in mobility.

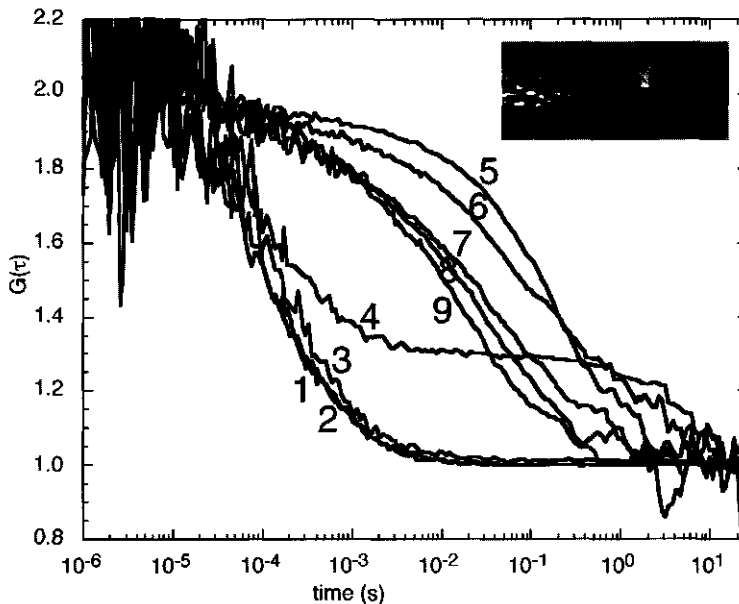


Figure 9: Autocorrelation curves acquired with FCM after addition of 10 nM of NodRlv-IV (BODIPY 558/568- C_{12}) to the root system of *Vicia sativa*. Seedlings were grown a Fåhrens slide (Heidstra et al., 1994), which was inverted in such way that the coverglass was facing the microscope objective. The confocal volume element was positioned just before the tip of a growing root hair. The resulting autocorrelation curves of the fluorescent Nod factor in medium (1-4), cell wall (4-6) and cytosol (7-9) of a root hair are shown. The inset shows a mixed fluorescence/phase contrast image of a root hair. The bright spot at the tip of the root hair is fluorescence originating from the excited confocal volume. For a detailed description of the experiment we refer to (Goedhart et al., 2000)

Even inside the root hair, fluorescent particles could be detected in the confocal volume above the autofluorescence background. It is remarkable that on average as few as ten fluorescent particles could be detected upon positioning the confocal volume element inside a *living* root hair and that the diffusional behavior of these particles could be studied quantitatively. These measurements clearly demonstrate that FCS provides close to single molecule-detection sensitivity even in living root hairs. Hence, FCM is a promising technique to obtain detailed information on biomolecular diffusion and quantity at very low probe concentrations with subcellular resolution.

6. Concluding remarks

Implementation of spectroscopic modalities into a fluorescence microscope allows the study of detailed *in vivo* behavior of fluorescent molecules with high spatial and temporal resolution. In this chapter we have described how various spectroscopic parameters of fluorescent molecules, including excitation- (FRIM) or emission spectral properties (FSPIM), fluorescence lifetimes (FLIM) and molecular diffusion (FCM), can be monitored inside single living root hairs. There are a number of microspectroscopic methods which have been described elsewhere but still await their application for the study of root hairs. Examples are i) photobleaching microscopy, to measure the photochemical stability of fluorophores thereby reporting on their (subcellular) microenvironment (Arndt-Jovin et al., 1979; Gadella Jr. and Jovin, 1995; Gadella Jr. and Jovin, 1997), ii) fluorescence anisotropy microscopy to measure rotational mobility of molecules in cells (Dix and Verkman, 1990) and iii) fluorescence polarization microscopy to measure orientational distributions of molecules in cells (Axelrod, 1989). Furthermore, two or more spectroscopic modalities can be integrated (e.g. combined temporally and spectrally resolved imaging (Vereb et al., 1998)) to obtain more detailed spectroscopic information in a single measurement.

A potentially interesting new development is the combination of two-photon excitation (TPE) with microspectroscopic methods, e.g. two-photon FLIM (So et al., 1995) and two-photon FCS (Berland et al., 1995). The main advantage of TPE is that the excitation is restricted to the focal point, which minimizes photobleaching and produces data lacking out-of-focus fluorescence, avoiding the need for insertion of a pinhole in the detection light path of the microscope. However, for thin samples such as root hairs, TPE might not provide significant improvement in signal-to-noise ratio over conventional confocal microscopy (Piston, 1999). Still, TPE could be advantageous for exciting blue or UV-absorbing probes that are less compatible with common single photon CW laser systems.

The FCM experiments demonstrate that it is possible to attain close to single molecule-detection sensitivity even in the cytosol of living root hair cells. This is not only because of the high sensitivity of this technique but also because of the very low autofluorescence levels of growing root hairs upon excitation at wavelengths higher than 540 nm. The background fluorescence can

be effectively reduced by yet another new microspectroscopic technique: cross-correlation FCS, which cross-correlates intensity fluctuations of molecules carrying two different fluorophores. As a result, only molecules emitting at the two corresponding wavelengths are observed (dual color fluorescence cross-correlation spectroscopy see (Rigler et al., 1998; Schwille et al., 1997b)). By this technical advancement, *in vivo* detection of dual labeled single molecules might be accomplished, possibly revealing *in vivo* molecular conformation fluctuations, on- and off-rates for molecular association and single molecule enzyme kinetics (Weiss, 1999). All of these potential and novel applications demonstrate that advanced microspectroscopy applied to the study of single plant cells (e.g. root hairs) is a rapidly emerging scientific field, and undoubtedly will shed new light on a variety of molecular processes inside living root hairs.

Acknowledgments

We are grateful to Mark Hink for his contribution to the experiments shown in figure 9. J.G. is supported by the Netherlands Council of Earth- and Life Sciences (ALW) and T.W.J.G. by the Royal Netherlands Academy of Arts and Sciences (KNAW).

RAPID COLORIMETRIC QUANTIFICATION OF LIPO-CHITOLIGO-SACCHARIDES FROM *RHIZOBIUM LOTI* AND *RHIZOBIUM MELILOTI***Abstract**

Nod factors are lipids with a chitin-like headgroup produced by gram-negative *Rhizobium* bacteria. These lipo-chitooligosaccharides (LCOs) are essential signaling molecules for accomplishing symbiosis between the bacteria and roots of legume plants. Despite their important role in the *Rhizobium*-legume interaction, no fast and sensitive Nod factor quantification methods exist. Here we report two different quantification methods. The first is based on the enzymatic hydrolysis of Nod factors to release N-acetylglucosamine (GlcNAc) which can subsequently be quantified. It is shown that the degrading enzyme, glusulase, releases exactly two GlcNAc units per pentameric NodR1o factor, allowing quantification of LCOs from *Rhizobium loti*. The second method is based on a specific type of Nod factors that are sulfated on the reducing GlcNAc, allowing quantification analogous to the quantification of sulfolipids. Here, a two-phase extraction method is used in the presence of methylene blue, which specifically forms an ion-pair with sulfated lipids. The blue ion-pair partitions into the organic phase, after which the methylene blue signal can be quantified. To enable Nod factor quantification with this method, the organic phase was modified and the partitioning was evaluated using fluorescent and radiolabeled sulfated Nod factors. It is shown that sulfated LCOs can be quantified with this method using SDS for calibration. Both methods allow Nod factor quantification in semi-high throughput enabling a fast and easy detection of nanomole quantities of Nod factors.

Joachim Goedhart, Jean-Jacques Bono[§] and Theodorus W.J. Gadella Jr.

[§]Laboratoire de Biologie Moléculaire des Relations Plantes-Microorganismes, UMR 215 INRA-CNRS, BP 27 31326 Castanet-Tolosan, France.

Introduction

Nod factors are lipo-chitooligosaccharides (LCOs) secreted by Rhizobia and are essential to accomplish symbiosis with legumes (Long, 1996). The exact structure of the Nod factor differs for each *Rhizobium* species, but the basic structure comprises a chitin backbone of 3 to 5 β -1,4-linked GlcNAc residues to which a fatty acyl chain is attached at the non-reducing terminal sugar (see figure 1). Nod factors produced by Rhizobia or chemically synthesized can elicit responses at picomolar concentrations on a compatible host plant (Gadella Jr. et al., 1997b; Heidstra et al., 1994; Lerouge et al., 1990; Spaink et al., 1991).

Quantification of Nod factors is usually done by measuring absorbance of the unsaturated acyl chain (Etzler et al., 1999) or by comparison to standards on RP-HPLC, see e.g. (Gressent et al., 1999). However, purified Nod factors generally consist of a mixture of differently absorbing compounds due to different unsaturations of the acyl chain, each requiring an individual standard. Furthermore, potential UV absorbing impurities can overestimate the real amount of Nod factors whose extinction coefficient is very low ($\epsilon_{210} = 3,000 \text{ M}^{-1} \text{ cm}^{-1}$). Reliable and fast methods to quantify both purified or synthesized LCOs will be of great help for basic research and biotechnological applications. For example, the precise knowledge of the concentration of Nod factors is important in experiments aiming to determine the affinity constants of Nod factor binding proteins (Etzler et al., 1999; Gressent et al., 1999), the measurement of dose-response curves using different bioassays (Felle et al., 1995; Staehelin et al., 1994a) or the preparation of Nod factor solutions deliverable to plants in agronomic trials. A promising approach to quantify Nod factors is reported by Staehelin et al. (1994). First, Nod factors are treated with hydrolyzing enzymes from snail gut, releasing GlcNAc monomers (Boller and Mauch, 1988). The GlcNAc monomers are subsequently quantified colorimetrically by the method of Reissig (Reissig et al., 1955).

Unfortunately, no Nod factor-independent standard was used for calibrating the method since known amounts of Nod factors from *Rhizobium* sp. NGR (pA28) were used as a standard. In this study, we used the method described by Staehelin et al. but (GlcNAc)₄ was used as a reference compound for calibration. In addition we analyzed the breakdown products of the *Rhizobium loti* Nod factors after treatment with snail gut enzyme, showing that the enzyme quantitatively digests these Nod factors.

Subsequently, a novel approach is described for quantification of sulfated Nod factors, based on the quantification of sulfated lipids by a method originally developed by Kean (Kean, 1968) which was improved by Radin (Radin, 1984). In this assay, comprising a biphasic liquid system with an aqueous layer and an apolar organic layer, sulfated lipids form an ion-pair with a cationic dye after which the complex enters the organic phase. The sulfolipid can be quantified by measuring the absorbance of the cationic dye in the organic phase. Using a novel sulfated green fluorescent Nod factor derivative, we optimized the partitioning of Nod factors into the organic phase. Determination of the partitioning efficiency and the color yield of the ion-pair

allow the quantification of Nod factors from *Rhizobium meliloti* which have a sulfate group on the reducing end of the chitin backbone (Lerouge et al., 1990).

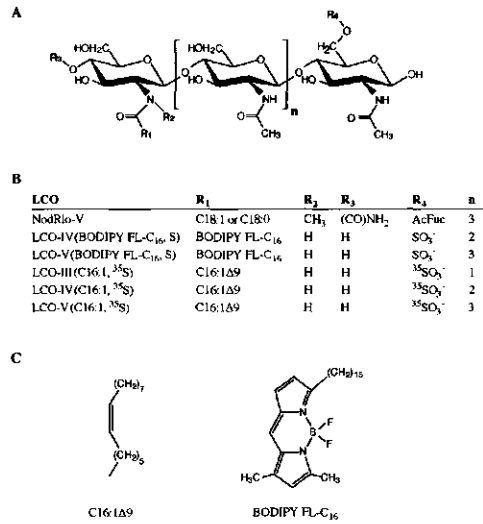


Figure 1: Structures of the LCOs used in this study. The chitin-like headgroup (A) with decorations R1-R4 and different degrees of GlcNAc polymerization referred to as trimers (n=1), tetramers (n=2) and pentamers (n=3). (B) The NodRlo factors are a mixture of Nod factors having either a cis-vaccenic acid (C18:1) or stearic acid acyl chain (C18:0) and various substitutions among which a 4-O-acetylucose (AcFuc) residue on the terminal reducing sugar. Sulfated Nod factors carry a ³⁵S radiolabeled sulfate group at R4 and have the natural occurring C16:1Δ9Z acyl chain (C) at R1, or carry a non-labeled sulfate group at R4 and a fluorescent BODIPY FL-C₁₆ fatty acid at position R1.

Results

Hydrolysis of (lipo-)chitooligosaccharides by snail gut enzyme

The first method to quantify Nod factors is based on the quantification of GlcNAc monomers enzymatically released from the chitin backbone of the Nod factors by treatment of glusulase. To investigate conditions under which the glusulase completely hydrolyses chitooligosaccharides, we measured the release of GlcNAc from (GlcNAc)₄ or NodRlo during incubation with snail juice containing this enzyme. When 10-25 μl of snail juice was used, (GlcNAc)₄ was completely hydrolyzed to GlcNAc monomers within one hour (data not shown), which agrees with a previous observation (Boller and Mauch, 1988). Subsequently, (GlcNAc)₄ was used to prepare a calibration standard, by incubation with enzyme and subsequently measuring the amount of released GlcNAc by the Reissig method. The OD at 585 nm was linearly dependent on the amount of (GlcNAc)₄ indicating that this approach can be used for calibration (inset of fig. 2). The calibration curve was characterized by a slope of 44 OD units per μmol of (GlcNAc)₄.

Identical conditions were used to check whether the enzyme was also able to release GlcNAc units from the Nod factors. The release of GlcNAc from NodRlo was measured at different time points to ensure complete digestion by the enzyme (see figure 2). At time point zero almost no absorbance was measured. Apparently, LCOs, like GlcNAc polymers (Domard and Vasseur, 1991), are hardly detected by the method of Reissig. After a rapid increase of free GlcNAc within the first half hour, the amount of GlcNAc reaches a constant level. The results indicate that GlcNAc can be released from NodRlo and that all accessible GlcNAc monomers are released enzymatically from the Nod factor within one hour.

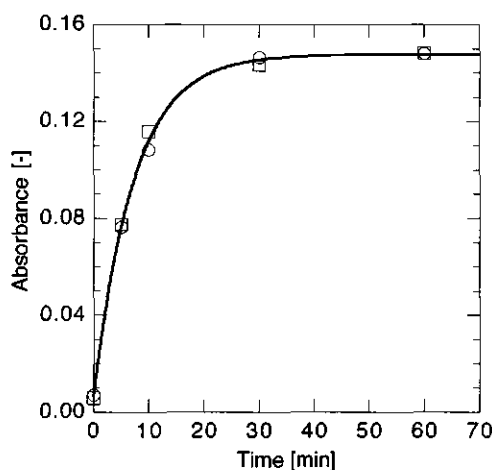


Figure 2: Quantification of NodRlo-V with snail gut enzyme. After digestion, the amount of GlcNAc was determined by the method of Reissig. The data shown are the results of two experiments. A monoexponential curve is fit to the average of the two experiments, yielding a half-time of 5 minutes. The inset shows a calibration curve with a slope of 46 OD/ μ mol prepared by glusulase hydrolysis of known amount of (GlcNAc)₄. The data shown is the average of two measurements

Analysis of the products produced by snail gut enzyme

It is well established that enzymes from snail gut hydrolyze chitooligosaccharides completely into GlcNAc monomers (Boller and Mauch, 1988; Cabib and Bowers, 1971). On the other hand, plant chitinases break Nod factors down to tri- or dimers but not to monomers (Staelin et al., 1994a). For our assay it was essential to correlate the amount of GlcNAc removed from NodRlo by the snail enzyme to the amount of unreacted NodRlo and the breakdown products containing the fatty acyl chain and the non-reducing end. Therefore we analyzed Nod factor breakdown products produced by the action of the snail juice by RP-HPLC.

RP-HPLC profiles of NodRlo incubated with glusulase for 0, 5 and 60 minutes are shown in figure 3. At time point zero, the major component in the HPLC profile has a retention time (Rt) of approximately 6 minutes and represents intact NodRlo, which is a mixture of NodRlo-V(C18:1, NMe, Carb, AcFuc) and NodRlo-V(C18:0, NMe, Carb, AcFuc) (Lopez-Lara et al.,

1995). After 5 minutes incubation with snail juice the peak at $R_t=6$ min. decreases and two new peaks at $R_t=2.3$ min. and $R_t=8.9$ min. arise. The peak at $R_t=2.3$ min. is due to a component of the enzyme preparation (data not shown), whereas the peak at $R_t=8.9$ min. represents a NodRlo breakdown product. After 60 minutes incubation, the peak corresponding to the intact Nod factors is almost completely absent, whereas the peak at $R_t=8.9$ min. is still present and increased. The time scale of NodRlo breakdown is compatible with the kinetics of the release of GlcNAc monomers, and shows that the saturation of the curve after 30 minutes (fig. 2) indeed reflects complete digestion of NodRlo.

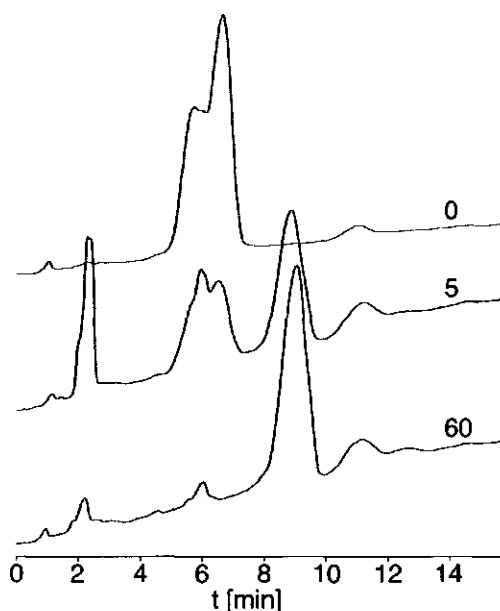


Figure 3: RP-HPLC analysis of NodRlo-V breakdown products after hydrolysis with snail gut enzyme for 0, 5 and 60 minutes. Due to the treatment with glusulase, the peak at 6 minutes representing intact NodRlo-V decreases, whereas a new more hydrophobic breakdown product accumulates with a retention time of 9 minutes.

To obtain data on the exact composition of the more hydrophobic breakdown product ($R_t=8.9$ min.), we performed a mass spectrometric analysis. The spectrum contains a main pseudomolecular ion at m/z 907.3. Calculation of the molecular weight of expected products, i.e. a shorter LCO, carrying four, three or two GlcNAc units, gives 1110, 907 and 703 respectively. Thus, the main pseudomolecular ion at m/z 907.3 is consistent with a Nod factor with three GlcNAc units: NodRlo-III(C18:1/C18:0, NMe, Carb), implicating that glusulase removes two GlcNAc units per NodRlo. The calibration standard prepared by hydrolysis of $(\text{GlcNAc})_4$ (inset of fig. 2) is characterized by a slope of 46 OD units per μmol $(\text{GlcNAc})_4$ from which the absorbance of hydrolyzed NodRlo is derived: 23 OD units per μmol . Now, the amount of the NodRlo can be quantified after hydrolysis with snail gut enzyme and subsequent determination

of GlcNAc. For example, the final absorbance of the hydrolyzed NodR1o sample shown in figure 2 minus background was 0.14 which is 6.1 nmol NodR1o.

Partitioning of sulfated LCOs in a two-phase solvent system

The second method to quantify Nod factors colorimetrically is based on the specific decoration of Nod factors produced by *Rhizobium meliloti* which have a sulfate group. Sulfated lipids can be quantified by a method developed by Kean (1968) which was improved by Radin (1984). In this method a two-phase solvent system is used. An aqueous phase in which a cationic dye is dissolved (methylene blue or azure A) and an apolar phase consisting of organic solvents which excludes the cationic dye. The principle of the assay is that the sulfated lipid forms an ion-pair with the cationic dye, after which the resulting complex partitions into the organic phase. Hence, the staining of the organic upper phase with the cationic dye is proportional to the amount of sulfated lipid. This amount can be easily quantified by measuring the absorbance of the cationic dye.

We started to use the conditions published by Radin (1984) which uses a relative apolar upper phase (isooctane/chloroform/isoamylalcohol/isopropanol (v/v/v/v) 3:1:1:1). Unfortunately under these conditions, no sulfated Nod factors could be detected in the upper phase, probably because the solvent polarity of the upper phase was too low (data not shown). Hence, we tried to increase the polarity of the upper organic phase in order to accomplish partitioning of Nod factors to this phase. However, the organic upper phase can not be too polar as it should exclude uncomplexed methylene blue. As butanol is used to isolate Nod factors from aqueous medium (Lerouge et al., 1990; Spaink et al., 1991), our first effort was to try butanol as the organic phase. Unfortunately, even in the absence of sulfated lipids methylene blue partitioned extensively into the butanol layer (data not shown). To achieve intermediate polarity of the upper phase, heptane was included at different percentages and partitioning of methylene blue was examined in the absence of sulfated lipids. As shown in figure 4, increasing the amount of heptane reduced the amount of methylene blue in the organic phase. From this figure it can be inferred that the methylene blue background in the organic phase is sufficiently low when at least 60% of heptane is included in the upper phase, whereas the presence of 50% heptane is still usable but gives rise to a relative high background absorbance (around 0.1).

To investigate whether under these new conditions Nod factors could partition into the upper phase, we used green fluorescent sulfated LCOs and quantified their partitioning efficiencies. As expected, increasing percentages of heptane reduced the amount of LCO in the organic phase (fig. 4). With 40% heptane in the upper phase all LCOs were present in the organic phase, whereas less than half of the fluorescence was observed when the heptane percentage was increased to 60%. Hence, the most favorable situation (50% heptane present in the upper phase) is still far from optimal: the background is significant (around 0.1) and only 75% of the LCOs are in the upper phase.

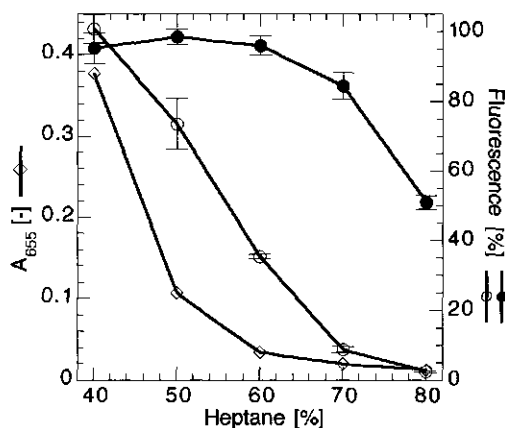


Figure 4: Effect of the organic upper phase composition on background absorbance and LCO partitioning. The volume percentage of heptane is increased at the expense of butanol.

(◇) Absorbance of methylene blue in the upper phase in the absence of sulfated lipid.

(○,●) Recovery of fluorescence in the upper phase using non-acetylated (○) or acetylated (●) LCO-IV(BODIPY FL-C16, S).

In order to increase the partitioning of Nod factor into the upper phase we attempted to increase the hydrophobicity of the LCOs by peracetylation with acetic anhydride. TLC analysis on silica coated plates with chloroform/methanol (4:1 v/v) as the mobile phase showed a single spot with $R_f=0.45$ for the peracetylated LCO-IV(BODIPY FL-C16, S) and $R_f=0.0$ for the unreacted LCO (data not shown), clearly indicating the increased hydrophobicity of the LCO after peracetylation.

The partitioning experiments at different percentages of heptane were repeated with the acetylated LCO. As can be inferred from figure 4 the peracetylated LCO-IV partitioned well into the organic upper phase up to a heptane percentage of 60%. Hence, peracetylation clearly improved the partitioning conditions since it allows the assay to be performed at a heptane percentage of 60%, yielding a low background (<0.05) and substantially improved partitioning of $>90\%$.

Calibration with SDS as a standard

To evaluate whether the upper phase consisting of butanol/heptane 2:3 is compatible with quantification of sulfated lipids by the Kean assay, a calibration curve was prepared by using different amounts of SDS. The absorbance of methylene blue in the organic phase shows a linear dependence on the amount of SDS present (figure 5), clearly demonstrating that SDS has a good partitioning and can be used as standard.

Based on the slope of the curve we calculated that our upper phase had an OD of $51/\mu\text{mol}$ sulfated lipid, which corresponds to an absorbance coefficient of the SDS-methylene blue complex of $51,000 \text{ M}^{-1} \text{ cm}^{-1}$, assuming complete partitioning of SDS into the upper phase.

Using the same volumes but the upper phase composition as described by Radin (1984) we obtained an OD of $65/\mu\text{mol}$ sulfated lipid at 655 nm (data not shown). Hence, the color yield of the methylene blue-SDS complex is lower in case of the more polar organic upper phase.

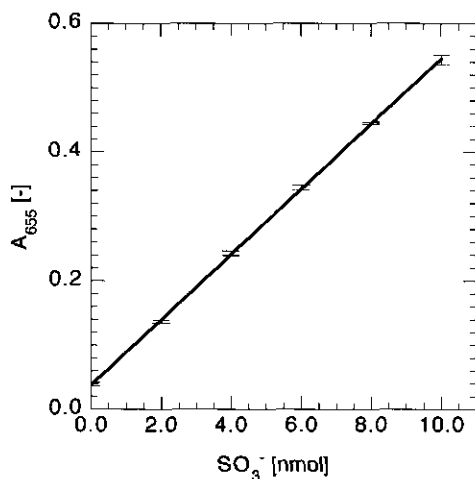


Figure 5: Calibration of the partitioning assay using SDS. After partitioning between the aqueous methylene blue containing phase and the upper phase consisting of 40% butanol and 60% heptane, the upper phase was isolated, the absorbance at 655 nm was measured (average and standard deviation of three measurements), and plotted as a function of the initially added amount of SDS. The slope of the calibration curve is 51 OD/ μmol .

Determination of the color yield of the LCO-methylene blue complex

As the color yield of a LCO-methylene blue complex is unknown we took advantage of the availability of a fluorescent derivative of Nod factors to correlate the amount of LCO based on the absorbance of the fluorescent acyl chain with the amount of methylene blue that partitioned into the organic phase. The concentration of acetylated LCO-IV(BODIPY FL-C₁₆, S) and acetylated LCO-V(BODIPY FL-C₁₆, S) was measured by absorbance in methanol, $\epsilon_{505}=90,000 \text{ cm}^{-1} \text{ M}^{-1}$ (Haugland, 1996).

Table 1: Quantification of sulfated LCOs with fluorescent acyl chains.

LCO	Recovery sulfate ^a [%]	Recovery LCO ^b [%]	LCO-MB ^c [OD/ μmol]
LCO-IV(BODIPY FL-C ₁₆ , S)	89.5	95.9 ± 2.8	47.6
LCO-V(BODIPY FL-C ₁₆ , S)	91	95.2 ± 4.4	48.8

^aRecovery of sulfate in the upper phase using the SDS calibration curve and assuming identical color yield.

^bRecovery of Nod factor (average and standard deviation of three measurements) in the upper organic phase as measured by fluorescence.

^cColor yield of the LCO-methylene blue complex calculated by (recovery sulfate / recovery LCO) * 51 OD/ μmol .

Subsequently, a known amount was used in the assay, and the sulfate concentration was determined by absorbance of methylene blue using SDS as a standard. Based on the SDS calibration about 90% of the total amount of LCO added was detected in the upper phase for both species (see table 1), which corresponds to a color yield of 45.9 OD units per μmol LCO. This measured color yield is the product of the partitioning efficiency and the true color yield of the LCO-methylene blue complex. Since the recovery of fluorescent LCOs in the upper phase is known (see also figure 4), it is possible to calculate the true color yield of the complex. According to this quantitative comparison, we could determine the average color yield of the LCO-methylene blue complex in the upper phase which is 48.1 OD/ μmol (table 1). This value is slightly lower than that of the SDS-methylene blue complex (about 94 %).

Partitioning of natural sulfated Nod factors

The partitioning experiments with the fluorescent Nod factor show that this method can be used to quantify LCO-IV(BODIPY FL-C₁₆, S). However, our aim was to quantify sulfated Nod factors with natural acyl chains. Hence, the partitioning of natural Nod factors into the upper phase containing 60% heptane was determined by using ³⁵S radiolabeled LCOs. The partitioning efficiency of the radiolabeled Nod factors was determined by counting the radioactivity associated with the upper phase and the lower phase in three separate experiments. The recovery of acetylated radiolabeled LCO in the upper phase listed in table 2 shows that natural Nod factors partition less well into the upper phase as compared to the fluorescent LCOs. Furthermore, the partitioning into the upper phase decreases in the order LCO-III(C₁₆:1, ³⁵S) > LCO-IV(C₁₆:1, ³⁵S) > LCO-V(C₁₆:1, ³⁵S), as the overall hydrophobicity of the Nod factors decreases due to the increased contribution of the polar oligosaccharidic moiety. Assuming a similar color yield of the LCO-methylene blue complex for fluorescent and natural acyl chain substituted Nod factors we calculated the effective optical density of the upper phase per μmol added LCO (see table 2). Because of the lower partitioning efficiencies these numbers are slightly lower than for the fluorescent acyl chain labeled compounds.

Table 2: Quantification of radiolabeled LCOs with natural acyl chains.

LCO	Recovery LCO [%] ^a	LCO-MB ^c [OD/ μmol]
LCO-III(C ₁₆ :1, ³⁵ S)	92.0 ^b	44.3
LCO-IV(C ₁₆ :1, ³⁵ S)	83.7 \pm 4.2	40.3
LCO-V(C ₁₆ :1, ³⁵ S)	77.0 \pm 5.3	37.1

^aThe recovery of Nod factor (average and standard deviation of three measurements) in the upper organic phase as measured by liquid scintillation counting.

^bOnly one measurement was performed due to the limited amount of material.

^cThe color yield of the LCO-methylene blue complex by correcting the average value (48.1) obtained in table 1 for the recovery.

Effect of Contaminants

Although the method is developed to quantify HPLC purified Nod factors, it is relevant to examine the effect of contaminants in the Nod factors sample. In the original article by Kean, a number of contaminants have been checked (Kean, 1968). Here we describe only the effect of a few contaminants that could be relevant for Nod factors quantification. The methylene blue absorbance of 0 nmol and 10 nmol SDS was evaluated in the presence of 10 nmol non-sulfated NodR10 factors, 40 μg stearic acid and 10 μg lipopolysaccharide, which were all subjected to acetylation before the partitioning. As can be inferred from figure 6, a minor increase in absorbance is observed when non-sulfated Nod factors are included, whereas no effect of the acyl chains is observed. In contrast, a strong increase in both background, i.e. 0 nmol SDS, and the sulfate containing sample is observed when LPS is present. Thus, LPS interferes with the methylene blue partitioning method, indicating that the method can only be applied to purified samples when Nod factors are obtained from a biological source.

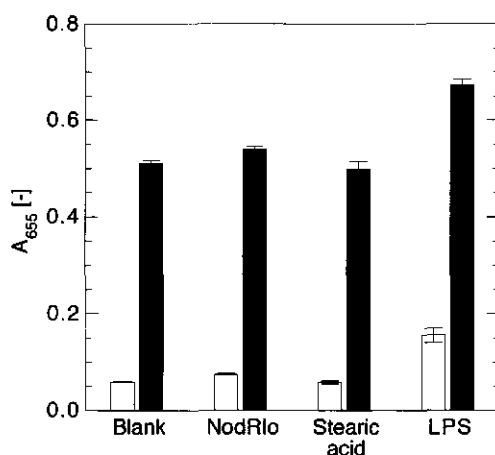


Figure 6: Influence of contaminants on sulfate quantification. Samples without (open bar) and with 10 nmol SDS (closed bar) were taken to which 10 nmol NodR10, 40 μg stearic acid or 10 μg LPS was added as a contaminant before partitioning. The absorbance of the upper phase was measured at 655 nm (average and standard deviation of three measurements).

Discussion*Quantification by enzymatically released GlcNAc*

Under the conditions described, complete enzymatic degradation of pentameric to trimeric Nod factors has been obtained, allowing reliable quantification of NodR10 by the release of GlcNAc monomers. The assay is completed within 2 hours and can be calibrated with GlcNAc monomers. However, the use of (GlcNAc)₄, which is completely hydrolyzed to GlcNAc

monomers by the snail juice, can also be used and appears more convenient because it can act as a positive control for glucosylase activity.

The absence of tetramers generated from the hydrolysis of NodRlo-V strongly suggests that the enzyme mixture does not remove single GlcNAc units. In agreement with this observation, the enzyme mixture was unable to degrade fluorescent LCO-IV(BODIPY FL-C₁₆) (data not shown). Therefore, the enzyme preparation from snail intestinal juice most likely releases a GlcNAc dimer from NodRlo which is subsequently hydrolyzed to GlcNAc units that can be quantified. The RP-HPLC analysis shows that the enzyme is not able to hydrolyze NodRlo-III. The release of two GlcNAc units per Nod factor give rise to increased sensitivity of the assay. Possibly, Nod factors tetramers can be quantified by this assay after including chitinase from *Streptomyces griseus* which has been shown to degrade fluorescent and natural Nod factor tetramers to dimers (Heidstra et al., 1994; J. Goedhart, unpublished observation).

Quantification based on the sulfate group

Detection based on the sulfate has the advantage that it is very sensitive and quick. A minor drawback is that this method can only be applied to sulfated Nod factors which have to be further modified (peracetylated) to determine concentrations quantitatively. However, when presence of sulfated Nod factors is to be detected qualitatively, the method can still be applied, using an upper with 50% heptane which has the advantage that the LCOs can be recovered.

The fact that approximately 92% - 77% of acetylated natural sulfated Nod factors is found in the upper phase depending on the size of the chitin backbone, is due to incomplete partitioning into the upper phase. Despite the incomplete partitioning, Nod factors can be quantified using SDS as a standard when both the partitioning percentage and color yield of the complex is taken into account (table 2).

For sulfated Nod factors with other acyl chains the partitioning efficiencies of the LCO-methylene blue complexes are unknown. Based on our results, we hypothesize that in case of a higher hydrophobicity of an unknown sulfated LCO as compared to LCO-IV(C₁₆:1, S) one can assume a partitioning efficiency of >84% yielding an error in the determination of maximally 16%. The presence of large amounts of contaminants can interfere with this assay, indicating that the quantification should be preferentially used on purified Nod factors rather than on crude preparations.

Conclusion

Accurate quantification of Nod factors is indispensable when one is interested in Nod factor production by chemical or biological processes or when dose dependence response experiments are carried out either *in vitro* (e.g. for the calculation of the binding thermodynamic constants) or *in vivo* (for biological activity tests or crops treatments). We have described two methods that allow a fast, sensitive, accurate and parallel quantification of Nod factor samples. These assays

can be used routinely for quantifying Nod factor fractions during purification of natural or synthetic Nod factors. Furthermore, these approaches can be used as a starting point for developing quantification assays for other Nod factors.

Materials and Methods

Materials

Tetra-*N*-acetyl-chitotetraose ((GlcNAc)₄) was obtained from Seikagaku (Tokyo, Japan), LPS (serotype 055:B55), stearic acid, GlcNAc, DMAB and snail intestinal juice (β -glucuronidase EC 3.2.1.31, catalog number G 7017) were from Sigma (Zwijndrecht, The Netherlands). Heptane (99%) was from Acros ('s-Hertogenbosch, The Netherlands), DMAP, 1-butanol p.a. and methylene blue (for microscopy) from Merck (Darmstadt, Germany). SDS was either from Life Technologies (Breda, The Netherlands) or from Biorad (Hercules, CA, USA). GlcNAc, (GlcNAc)₄, phosphate and borate stock solutions were stored at -20 °C. A DMAB stock solution was prepared as reported (Reissig et al., 1955) and could be stored at 4 °C for at least three months without deterioration. Before use, 0.5 ml snail juice was mixed with 0.5 ml 20 mM KCl and applied to a Biorad biogel P-6 column. Pre-equilibration and elution was done at 4 °C with 10 mM KCl containing 1 mM EDTA. The first 1.5 ml after the void volume was collected and stored at 4 °C. This fraction was used in all experiments.

Nod factors

The structures of the LCOs used in this study are shown in figure 1. NodRlo was purified according to (Lopez-Lara et al., 1995) with a slight modification. Pre-purification on the octadecyl extraction column was done by eluting with 40% (v/v) and 60% (v/v) acetonitril. Both fractions were further purified by reversed phase HPLC on a Pharmacia Superpac spherisorb ODS 2 column (5 μ m, 4x250 mm). Samples were applied at 20% (v/v) acetonitril and eluted with 40% (v/v) acetonitril and 60% (v/v) H₂O. The elution flow rate was 1 ml/min, and the eluent was monitored at 206 nm. Nod factors radiolabeled with ³⁵S were prepared as described (Gressent et al., 1999). Synthesis of LCO-IV(BODIPY FL-C₁₆, S) and LCO-V(BODIPY FL-C₁₆, S) will be described elsewhere (De Medina et al, manuscript in preparation).

Degradation of chitooligosaccharides by glusulase

To 1-20 μ l of Nod factor or (GlcNAc)₄ stock solution was added 5 μ l 1 M phosphate buffer (pH=7.1), 25 μ l snail juice and H₂O to a final volume of 125 μ l. This was incubated for 1 hr. at 37° C unless indicated otherwise.

Identification of breakdown products

Samples from the incubation mixture were taken and extracted with an equal amount of butanol at indicated time points. The butanol layer was isolated after centrifugation, evaporated and the residue was dissolved in 20% (v/v) acetonitril/H₂O and analyzed by reversed phase HPLC on a Pharmacia Superpac spherisorb ODS 2 column (5 μ m, 4x250 mm). Elution was done with a linear gradient of acetonitril in H₂O from 40% to 80% (v/v) in 30 minutes. Other conditions were as described above. To determine the release of GlcNAc, samples were taken at indicated time points and quickly frozen in liquid nitrogen. Time point zero was obtained by omitting glucosylase.

Reissig method for determination of GlcNAc

The method of Reissig (1955) was used to quantify the amount of GlcNAc. Shortly, to 125 μ l of the GlcNAc containing solution was added 25 μ l of 0.8 M borate (pH=9.1). After incubation at 100 °C for 3 minutes, the samples were put on ice. After cooling down, 750 μ l of a DMAB solution was added (diluted 10 \times from stock with glacial acetic acid just before use). Subsequently, the samples were incubated at 37 °C for 20 minutes. The samples were cooled on ice and absorbance at 585 nm was measured against water (care was taken to avoid erratic absorbance readings due to formation of condense on the cuvettes).

Kean partition assay

A stock solution of methylene blue was prepared by dissolving 0.2 g of methylene blue in 100 ml of a 12.5 mM sulfuric acid solution. The lower phase consisted of 50 μ l methylene blue stock, the proper amount of SDS or Nod factor and water added to a total volume of 500 μ l. Subsequently, 1 ml of organic upper phase was added and the samples were mixed vigorously by vortexing for 10 seconds. After centrifugation, the concentration of methylene blue in the upper phase was quantified by measuring absorbance at 655 nm.

Partitioning of fluorescent Nod factors into upper phase

To 0.25 ml of lower phase (see previous section), 0.5 ml of organic solvent was added, consisting of different percentages of heptane and butanol. Subsequently, 10 μ l of 10 μ M fluorescent LCO was added and mixed thoroughly by vortexing. After phase separation by centrifugation (10 seconds 14,000 g), 100 μ l of upper phase was diluted into 900 μ l of ethanol containing SDS to remove any methylene blue that could possibly quench Nod factor fluorescence. The optical density of the sample was always lower than 0.1. The fluorescence intensity of the solution was measured with a Fluorolog-3 (ISA Inc., Edison, NJ, USA) by excitation at 480 nm (slit width 4 nm) and 516 nm (slit width 4 nm) emission. The 100% value was obtained by adding an equal amount of fluorescent Nod factor directly to the ethanol solution.

Acetylation of LCOs

In case of Nod factors stock solutions in DMSO, DMSO was removed by adding 2 vol H₂O and 2 vol (water saturated) butanol. After separation and isolation of the butanol layer the extraction was repeated three times with the same volume of butanol. Subsequently, the collected butanol layers were evaporated.

For efficient acetylation at least one mole equivalent of catalyst (DMAP) is required relative to the amount of free hydroxyl groups (Gupta et al., 1977), which corresponds to 25 µg DMAP for 20 nmol LCO. To the dried LCO sample 10-20 µl of freshly prepared 5 mg/ml DMAP in acetic anhydride solution was added. The yellowish solution was thoroughly mixed to dissolve the LCOs. The mixture was incubated overnight at room temperature. The reaction mixture can either be used directly (the presence of acetic anhydride and DMAP during the quantification increases the background absorbance slightly, but not the partitioning or the efficiency of ion-pair formation) or can be extracted to remove any DMAP and acetic anhydride. First 50 µl of methanol was added, and incubated for at least 15 minutes, after which 100 µl of CHCl₃ and 50 µl 0.6 M HCl were added. After separation of the layers, the lower layer was washed 2x with 100 µl MeOH/0.6 M HCl (1:1) and evaporated. Alternatively, an acetic anhydride/pyridine mixture can be used for acetylation which can then be easily removed by evaporation as described (Tadano-Aritomi and Ishizuka, 1983). TLC analysis of the reaction mixture was done with silicagel 60 TLC plates using chloroform/methanol 4:1 (v:v) as the mobile phase.

Partitioning of radiolabeled Nod factors into upper phase

First, the radiolabeled Nod factors were acetylated, and the partitioning was done as described above. After phase separation 80% of both phases was transferred to counting vials and the amount of LCO in both layers was determined by liquid scintillation counting.

Acknowledgments

We are grateful to Gideon Oudgenoeg (Lab. for Biochemistry, Wageningen University, The Netherlands) for the LC-MS measurements. We thank Dr. B.M. Gadella (Dept. Veterinary Biochemistry, Utrecht University, The Netherlands) for suggesting the Kean assay he uses for quantification of sulfo-galactoceramides for quantifying sulfated LCOs. This work was supported by the Netherlands Organization for Scientific Research-Council of Earth- and Life Sciences (NWO-ALW) (J.G.), by a NWO-Van Gogh French-Netherlands collaborative research grant (J.J.B. and T.W.J.G.), and by the Royal Netherlands Academy of Arts and Sciences (KNAW) (T.W.J.G.).

**NOD FACTORS INTEGRATE SPONTANEOUSLY IN BIOMEMBRANES,
TRANSFER RAPIDLY BETWEEN MEMBRANES AND TO ROOT HAIRS, BUT
TRANSBILAYER FLIP-FLOP DOES NOT OCCUR****Abstract**

Three novel nodulation (Nod) factors were synthesized from chitotetraose and three structurally different fluorescent BODIPY tagged fatty acids. With fluorescence spectroscopic and microscopic techniques it was studied whether these amphiphilic molecules insert in membranes, whether they transfer between different membranes and whether they are able to transfer from a membrane to a legume root hair. Fluorescence correlation spectroscopy showed that fluorescent Nod factors are present as monomers in PBS buffer at a concentration of 10 nM, but that when either Triton X-100 micelles or dioleoylphosphatidylcholine (DOPC) vesicles are present, the Nod factors are associated with these particles. With time-correlated single photon counting fluorescence spectroscopy it was shown that upon Nod factor-insertion in the membrane, the rotation of the fluorescent acyl chain was markedly reduced. A fluorescence resonance energy transfer assay, was used to study the transfer of Nod factors from one membrane to the other, or from vesicles to root hairs. Nod factors transfer rapidly between membranes or from vesicles to root hair cell walls. However, they do not flip-flop between membrane leaflets. The results provide novel insights for the mode of secretion and transfer of Nod factors during the early steps of the *Rhizobium*-legume interaction.

Joachim Goedhart, Horst Röhrig[§], Mark A. Hink, Arie van Hoek, Antonie J.W.G. Visser, Ton Bisseling and Theodorus W.J. Gadella Jr.

[§]Abteilung Genetische Grundlagen der Pflanzenzüchtung, Max-Planck-Institut für Züchtungsforschung, D-50829, Köln, Federal Republic of Germany.

Introduction

Nodulation (Nod) factors are signal molecules secreted by gram-negative *Rhizobium* bacteria and play a key role in the early steps of nodule formation (Heidstra and Bisseling, 1996; Long, 1996). Root nodules are the result of a *Rhizobium*-legume interaction. In these specialized organs, the rhizobia are present intracellular and convert atmospheric nitrogen into ammonium. In exchange for sugars, the ammonium is fed to the plant. In the initial steps of the interaction, flavonoids secreted by the legume root, induce the expression of the *nod* genes of the bacterium, resulting in the production of Nod factors. The production and secretion of Nod factors is essential for all early steps of nodulation and its chemical structure determines host specificity (Roche et al., 1991). All Nod factors comprise a chitin backbone of 3 to 5 β -1,4-linked N-acetyl glucosamine residues. A fatty acyl chain of 16 to 20 carbon atoms with different degrees of unsaturation is N-linked to the non-reducing terminal sugar. Major determinants of host specificity are the decorations of the chitin backbone which can be acetate, sulfate and fucosyl groups (Lerouge et al., 1990; Price et al., 1992).

Purified Nod factors, either from *Rhizobium* cultures (Lerouge et al., 1990; Spaink et al., 1991) or synthesized (Gadella Jr. et al., 1997b; Nicolaou et al., 1992), are active at picomolar concentrations. They can induce root hair depolarization (Ehrhardt et al., 1992), root hair deformation (Heidstra et al., 1994; Lerouge et al., 1990), cortical cell division (Van Brussel et al., 1992) and primordium formation (Truchet et al., 1991). In order to obtain more insight in the possible mechanisms of secretion and perception of Nod factors, it is necessary to study the molecular behavior of these peculiar amphiphilic molecules. Both in the secretion process by *Rhizobium* bacteria and during perception by root hairs of leguminous plants, membranes play an important role: two bacterial membranes have to be passed to accomplish secretion, and membrane bound receptors have been postulated for Nod factor perception (Niegel et al., 1997). Given the hydrophobic fatty acyl chain of the Nod factors, it is expected that Nod factors will have a high tendency to insert into membranes. Orgambide et al. (1995) show that Nod factors are primarily present in rhizobial membranes. Furthermore, they also speculate that Nod factors diffuse as micelles through the aqueous phase. However, no evidence for this concept is available as no detailed studies on the physicochemical properties of Nod factors have been reported so far.

Recently, the synthesis of fluorescent Nod factor derivatives by attaching a BODIPY fluorophore to the acyl chain has been described (Gadella Jr. et al., 1997b). The labeled molecules enable the characterization of molecular behavior of these amphiphilic molecules by fluorescence spectroscopic and microscopic techniques. A relatively new technique based on the confocal principle, fluorescence correlation spectroscopy (FCS), was used to study the molecular diffusion rates and aggregation state of the fluorescent Nod factors. With FCS fluorescence intensity fluctuations due to movement of fluorescent molecules in and out the confocal volume element are measured. By correlating these fluctuations over time, quantitative

information on mobility and local concentration of fluorescent probes can be obtained (Maiti et al., 1997; Rigler, 1995).

We have synthesized three novel fluorescent Nod factors with different acyl chains, containing red-shifted BODIPY fluorophores. We focus on the molecular behavior of fluorescent Nod factors in the presence and absence of artificial membranes. Both steady state and time-resolved fluorescence spectroscopy were used to report on the molecular environment of the fluorescent tag of the Nod factors. We studied the mode of incorporation of Nod factors in model membranes, their ability to flip-flop between membrane leaflets and their ability to diffuse from one membrane to another or from membranes to root hair cell walls. The implications for both Nod factor secretion and transfer during the early steps of the *Rhizobium*-legume interaction are discussed.

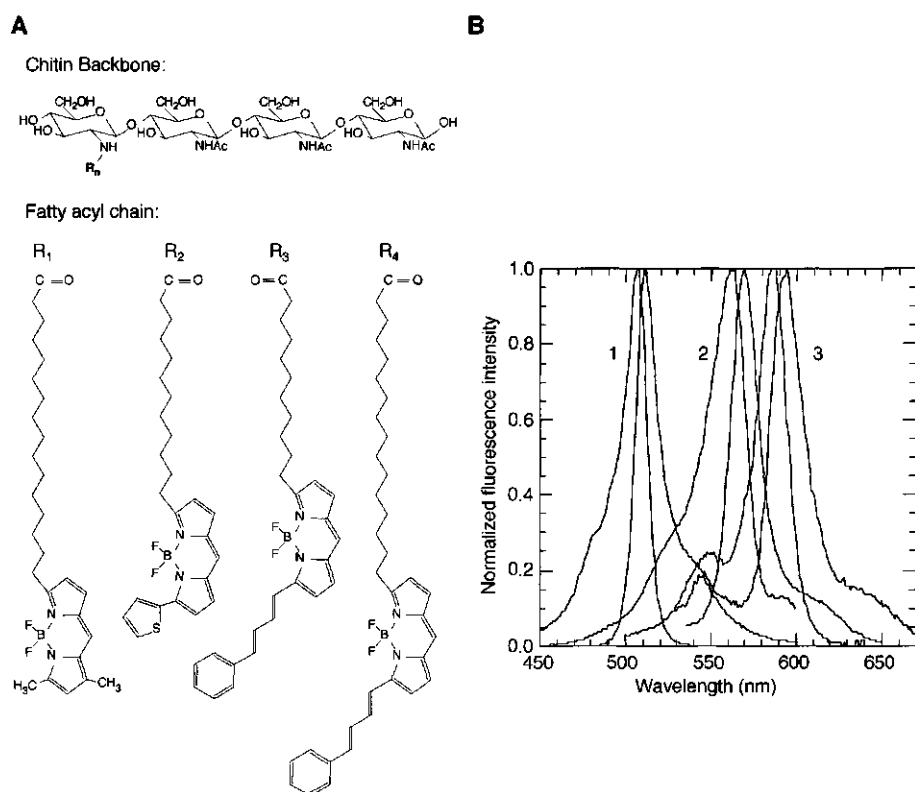


Figure 1: Structure and spectral properties of the four fluorescent Nod factors used in this study.

(A) Chitin backbone and fatty acyl chain structure of the fluorescent Nod factors.

The chitin backbone consists of four β -1,4 linked N-acetylated glucosamine residues, as for Nod factors secreted by *Rhizobium leguminosarum* bv. *viciae*. The four different fatty acyl chains attached to the non-reducing end carrying the fluorophore are BODIPY FL-C₁₆ (R₁), BODIPY 558/568-C₁₂ (R₂), BODIPY 581/591-C₁₁ (R₃) and BODIPY 581/591-C₁₆ (R₄).

(B). Normalized fluorescence excitation and emission spectra of NodRlv-IV (BODIPY FL-C₁₆) (1), NodRlv-IV (BODIPY 558/568-C₁₂) (2), and NodRlv-IV (BODIPY 581/591-C₁₆) (3) recorded in ethanol. The excitation and emission spectra of NodRlv-IV (BODIPY 581/591-C₁₁) were similar to (3).

Results

Synthesis and spectral properties of fluorescent Nod factors

The fluorescent Nod factor derivatives are synthesized by N-acylation of the amino group at the non-reducing end of NodB treated chitotetraose with BODIPY labeled fatty acids and purified on reversed phase HPLC as described (Gadella Jr. et al., 1997b). The structures of the synthesized Nod factors are shown in Figure 1A. Fluorescence emission and excitation spectra of the Nod factors were recorded to evaluate the spectral properties. In Figure 1B, the normalized excitation and emission spectra of NodRlv-IV(BODIPY FL-C₁₆), NodRlv-IV(BODIPY 558/568-C₁₂) and NodRlv-IV(BODIPY 581/591-C₁₆) in ethanol are presented, showing a small difference between excitation and emission maximum (Stokes shift) and narrow spectral bandwidth, typical for BODIPY (Johnson et al., 1991). The excitation and emission spectra of NodRlv-IV(BODIPY 581/591-C₁₆) were identical to the spectra of NodRlv-IV(BODIPY 581/591-C₁₁). The Nod factors labeled with BODIPY 581/591 have superior spectral properties as compared to Nod factors labeled with BODIPY FL (Gadella Jr. et al., 1997b) or NBD (Philip-Hollingsworth et al., 1997), because of i) their very high extinction coefficients (of 150,000 M⁻¹ cm⁻¹), ii) their high fluorescence quantum yields (about 0.9), iii) low sensitivity for environment (Haugland, 1996), and iv) favorable excitation/emission wavelength with respect to root autofluorescence (Gadella Jr. et al., 1997b).

Bioactivity of Nod factors depends on acyl chain structures

The bioactivity of the different fluorescent Nod factors was tested in a root hair deformation assay. As shown in Table 1, NodRlv-IV(BODIPY 581/591-C₁₆), shows root hair deformation at concentrations as low as 10⁻¹⁰ M, approaching the bioactivity of natural Nod factors (Heidstra et al., 1994). This clearly shows that the presence of the relatively bulky BODIPY moiety does not abolish the biological response, as was noted previously also for the second best Nod factor with the BODIPY FL-C₁₆ acyl chain which shows activity down to 10⁻⁹ M. It is very remarkable that a Nod factor also labeled with BODIPY 581/591 but with a 5 carbon atoms shorter acyl chain (NodRlv-IV (BODIPY 581/591-C₁₁)), was found to be completely incapable of inducing root hair deformation even at 10⁻⁷ M. The BODIPY 558/568-C₁₂ labeled Nod factor loses activity at concentrations lower than 10⁻⁸ M in the deformation assay. Our data do not show a clear relationship between bioactivity and Nod factor-acyl chain hydrophobicity since NodRlv-IV (BODIPY FL-C₁₆), NodRlv-IV (BODIPY 558/568-C₁₂), and NodRlv-IV (BODIPY 581/591-C₁₁) having a quite similar hydrophobicity, differ remarkably in bioactivity. Apparently, bulky substitutions at the C₁₁ position of the acyl chain abolish bioactivity. On the other hand, even large hydrophobic modifications at the very end (> C₁₅) of the acyl chain do not seem to interfere with perception. We speculate that this ambiguous structure-response relation could reflect structural features of a fatty-acyl binding pocket of the putative Nod factor receptor.

Table 1: Bioactivity of the fluorescent Nod factors in the root hair deformation assay

Acyl Chain ^a	Concentration [mol l ⁻¹]					
	10 ⁻⁶	10 ⁻⁷	10 ⁻⁸	10 ⁻⁹	10 ⁻¹⁰	10 ⁻¹¹
BODIPY FL-C ₁₆	+	+	+	+/-	-	n.d.
BODIPY 558/568-C ₁₂	n.d.	+	+/-	-	n.d.	n.d.
BODIPY 581/591-C ₁₁	n.d.	-	-	-	n.d.	n.d.
BODIPY 581/591-C ₁₆	n.d.	n.d.	+	+	+	-

^aType of acyl chain attached to the chitin backbone, see Figure 1A.

n.d.: not determined

+: significant deformation in the susceptible zone

+/-: reduced deformation in the susceptible zone

-: no deformation.

FCS on fluorescent Nod factors in presence and absence of artificial membranes

The amphiphilic nature of Nod factors suggests that they will readily incorporate into membranes. To study the association of the Nod factors with membranes, we studied the diffusional behavior of fluorescent Nod factors in the presence and absence of micelles or phospholipid vesicles by FCS. Upon incorporation into micelles or vesicles, the diffusion rate of Nod factors will be markedly reduced and will correspond to the diffusion rate of these membrane-like structures.

In Figure 2A, the autocorrelation functions obtained by FCS with NodRlv-IV(BODIPY FL-C₁₆) in different environments are shown. In PBS, the correlation of signal fluctuations rapidly decreases at time intervals larger than about 100 μ s. From the curve fit of the correlation curves, average diffusion times for the different Nod factors were determined, ranging from 84 μ s to 127 μ s. Using the average diffusion time, and the radius of the laser focus, the diffusion constant can be calculated according to equation 1, giving a value of $2.68 \cdot 10^{-10} \text{ m}^2 \cdot \text{s}^{-1}$ for NodRlv-IV(BODIPY FL-C₁₆). This diffusion constant implies a particle with a hydrodynamic radius of 0.80 nm according to equation 3 and therefore reflects diffusion of Nod factor monomers. When NodRlv-IV(BODIPY FL-C₁₆) is added to a micelle solution, the diffusional mobility decreases considerably, as can be seen in Figure 2A from the shift of the autocorrelation curve to longer diffusion times. Analysis of the curve yields diffusion times around 450 μ s representing the lateral mobility of Triton X-100 micelles (Hink and Visser, 1998). When Nod factors were studied in the presence of small unilamellar vesicles of DOPC the diffusion times were increased further. Curve analysis revealed relatively heterogeneous diffusional behavior, with an average diffusion time of 2.4 ms (Figure 2B). Similar diffusion times were measured for vesicles in which phospholipids with a BODIPY labeled acyl chain were incorporated (Hink and Visser, 1998). This indicates that also in the presence of vesicles, Nod factors incorporate into the vesicles and diffuse with a corresponding slower rate.

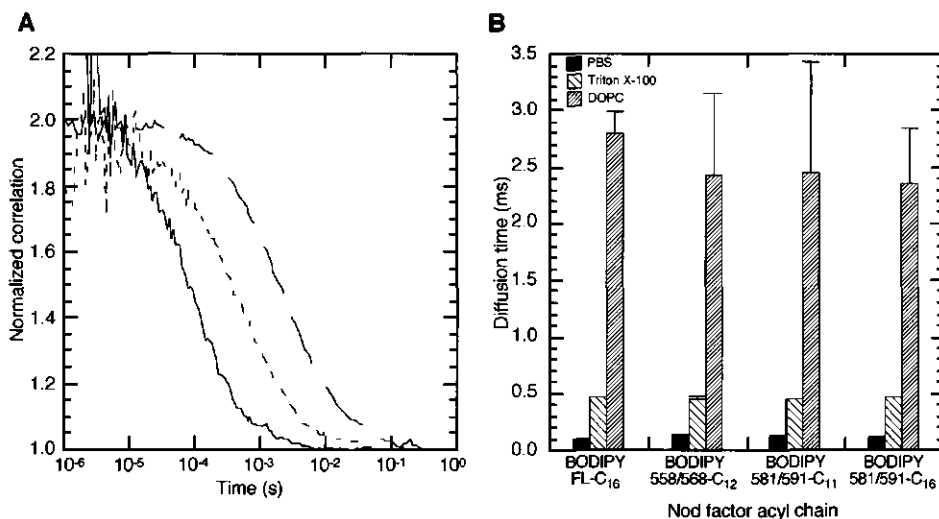


Figure 2: Fluorescence correlation spectroscopy of Nod factors in different environments.

(A). Normalized autocorrelation functions of NodRlv-IV (BODIPY FL-C₁₆). The experiments were all done with 10 nM Nod factor added to a solution of PBS (—), micelles (0.2% (v/v) Triton X-100) (---) or vesicles (50 μM DOPC) (· · ·).

(B). Diffusion times of the four fluorescent Nod factors. Nod factors were added to PBS, 0.2% (v/v) Triton X-100 or 50 μM DOPC. The Nod factor concentration was 10 nM and the diffusion times presented in this figure are the average of five measurements.

In Figure 2B, the average diffusion times determined from the autocorrelation functions of the four fluorescent Nod factors are presented. From this figure it is clear that the diffusion times of the different Nod factors are very similar if they are in the same environment. Regardless of the acyl chain structure all four Nod factors at 10 nM concentration diffuse as monomers in aqueous solution, but in the presence of micelles or phospholipid vesicles, the Nod factors associate completely with these structures and diffuse with corresponding rates, irrespective of the differences of the Nod factor acyl chain.

TCSPC of fluorescent Nod factors in different environments

To study whether upon association with vesicles or micelles the acyl chain of the Nod factor is inserted into the lipid core of these structures, we investigated the rotational mobility of the Nod factor acyl chain in presence and absence of vesicles and micelles. Rotational mobility of fluorophores can be investigated with TCSPC spectroscopy. A short (ps duration) pulse of laser light is used to excite the sample and the intensity and anisotropy of the fluorescence can be monitored as a function of time (ns time scale). In Figure 3A, the experimental anisotropy decay curves for NodRlv-IV (BODIPY FL-C₁₆) in the presence of DOPC vesicles, Triton X-100 micelles or only PBS are shown. From the curvature in the logarithmic plots it can be inferred that the decays are multiexponential. The anisotropy decay in presence of micelles or vesicles

are quite similar. However, the decay of NodRlv-IV(BODIPY FL-C₁₆) in only PBS is much faster, indicating large differences in the rotational freedom of the acyl chain.

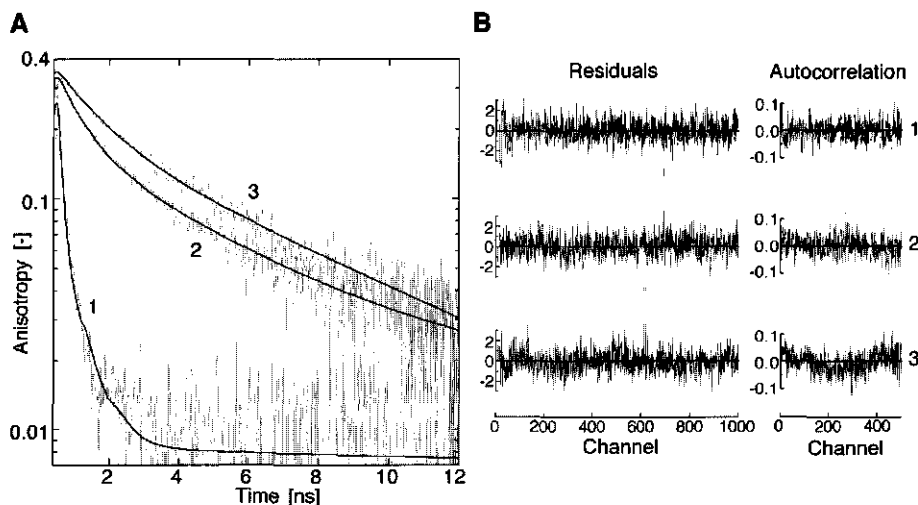


Figure 3: Anisotropy decays of 10 nM NodRlv-IV (BODIPY FL-C₁₆) in different environments. The shown data is a representative result of three experiments.

(A) Experimental anisotropy decays of NodRlv-IV (BODIPY FL-C₁₆) in PBS (1), Triton X-100 micelles (2) or DOPC vesicles (3) and anisotropy decays calculated from the parameters in Table 2.

(B) Residuals and autocorrelation curves depicting the quality of the fits.

The experimental curves were analyzed to obtain the parameters describing the decay, the rotational correlation times ϕ and their contribution β (see Table 2). In some cases, a limiting anisotropy, of which the contribution β_{∞} was analyzed, was included. The theoretical decays of NodRlv-IV(BODIPY FL-C₁₆) constructed from the parameters of the analysis are shown in Figure 3A as smooth lines. The residuals are randomly scattered around zero (Fig. 3B), indicating an accurate fit of the data.

In PBS, NodRlv-IV(BODIPY FL-C₁₆) shows two short rotational correlation times. The longer time ϕ_2 , 0.50 ns, corresponds with motions of the whole molecule, whereas the shorter and predominant time ϕ_1 probably reflects an independent rotational motion of the BODIPY moiety. A limiting anisotropy with a very small contribution β_{∞} is present (3% of r_0), likely reflecting Nod factors adsorbed on the cuvette. According to the Stokes-Einstein relation (equation 3), the rotational correlation time ϕ_2 corresponds to a hydrodynamic radius of 0.78 nm, indicating that the Nod factors are present as monomers. This agrees very well with the hydrodynamic radius that was calculated from FCS measurements of Nod factors in buffer.

When NodRlv-IV(BODIPY FL-C₁₆) is studied in the presence of micelles or DOPC, the very short rotational correlation time disappears, and two longer appear (see Table 2). The absence of the very short correlation times, and the presence of longer correlation times show that the rotational mobility of the Nod factor acyl chain is clearly decreased. The rotational correlation

times observed in presence of micelles represent wobbling (ϕ_1) and translational diffusion (ϕ_2) commonly observed in micellar systems (Hink et al., 1999). The two rotational correlation times of NodRlv-IV (BODIPY FL-C₁₆) in DOPC are comparable to the rotational correlation times of phosphatidylcholine with a BODIPY labeled acyl chain, incorporated in DOPC vesicles (data not shown). Hence, the decreased BODIPY rotational mobility, reflects an insertion of the fluorescent acyl chain of the Nod factor deeply into the hydrophobic core of the micelle or in the lipid bilayer.

Table 2: Anisotropy decay parameters of the four fluorescent Nod factors in different environments.

Acyl chain ^a	solvent	β_1	ϕ_1 (ns)	β_2	ϕ_2 (ns)	β_∞	r_0^b	χ^2
BODIPY FL-C ₁₆	PBS	0.22 (0.10-0.37)	0.07 (0.02-0.16)	0.07 (0.02-0.13)	0.50 (0.31-1.50)	0.008 (0.005-0.010)	0.30	1.48
BODIPY 558/568-C ₁₂	PBS			0.29 (0.18-0.31)	0.24 (0.21-0.56)	0.012 (0.008-0.015)	0.30	1.27
BODIPY 581/591-C ₁₁	PBS			0.29 (0.20-0.31)	0.39 (0.34-0.54)		0.29	1.25
BODIPY 581/591-C ₁₆	PBS			0.25 (0.17-0.33)	0.46 (0.33-0.75)		0.25	1.19
BODIPY FL-C ₁₆	Triton	0.17 (0.13-0.21)	1.19 (0.79-1.66)	0.19 (0.14-0.23)	6.23 (5.23-8.09)		0.35	1.31
BODIPY 558/568-C ₁₂	Triton	0.14 (0.10-0.20)	1.33 (0.80-2.22)	0.20 (0.13-0.25)	6.82 (5.72-9.94)		0.34	1.26
BODIPY 581/591-C ₁₁	Triton	0.20 (0.18-0.23)	4.97 (4.08-5.83)	0.12 (0.09-0.14)	25 ^d		0.32	1.21
BODIPY 581/591-C ₁₆	Triton	0.18 (0.15-0.22)	5.00 (3.91-7.14)	0.14 (0.08-0.16)	25 ^d		0.31	1.24
BODIPY FL-C ₁₆	DOPC	0.17 (0.13-0.20)	0.72 (0.52-1.06)	0.15 (0.11-0.18)	4.32 (3.25-7.06)	0.017 (0.003-0.026)	0.34	1.31
BODIPY 558/568-C ₁₂	DOPC	0.16 (0.13-0.18)	0.85 (0.59-1.19)	0.16 (0.13-0.18)	7.81 (6.63-9.71)		0.32	1.33
BODIPY 581/591-C ₁₁	DOPC	0.08 (0.06-0.11)	0.78 (0.40-1.22)	0.22 (0.20-0.24)	7.04 (5.34-10.7)	0.050 (0.009-0.067)	0.34	1.39
BODIPY 581/591-C ₁₆	DOPC			0.21 (0.20-0.23)	5.83 (4.95-7.04)	0.082 (0.063-0.097)	0.29	1.24

^aType of acyl chain attached to the chitin backbone, see Figure 1A.

^bInitial anisotropy = $\beta_1 + \beta_2 + \beta_\infty$

^cValues between brackets denote 67 % confidence limits.

^dFixed value, corresponding to micellar rotation calculated from FCS measurements (equation 3)

As can be inferred from Table 2, the other fluorescent Nod factors show similar results as obtained with NodRlv-IV(BODIPY FL-C₁₆). When Nod factors carrying an acyl chain with the BODIPY 581/591 fluorophore are inserted into micelles, translational diffusion as well as the rotation of the complete micelle ($\phi \approx 25$ ns) was observed, as has been described for fluorescent phospholipids in presence of Triton X-100 micelles (Hink et al., 1999). Additionally, these Nod factors show a relatively large limiting anisotropy (15-28% of r_0) when inserted in the vesicles, due to the relatively large fluorophore. The limiting anisotropy has also been described for other fluorescent molecules in membrane systems and reflect rotational mobility in a confined geometry or cone (Kawato et al., 1977; Kinoshita Jr. et al., 1977).

Transfer of fluorescent Nod factors between membranes

Given the marked preference of Nod factors to incorporate into membranes, we studied whether Nod factors are able to spontaneously leave one membrane and then insert into another membrane or that they are unable to redistribute between different membranes. Both options would have direct implications for Nod factor-secretion mechanisms occurring in *Rhizobium* bacteria. We developed an assay based on assays for monitoring intermembrane phospholipid exchange (Nichols and Pagano, 1982; Struck et al., 1981; Van Paridon et al., 1988). In short, fluorescent lipids (i.e. Nod factors) are incorporated into so called donor vesicles. By employing fluorescence resonance energy transfer (FRET), the fluorescence of the lipids in the donor vesicles is quenched. Subsequently, an excess of unlabeled acceptor vesicles is added. Upon transfer of the fluorescent lipid from the quenched donor vesicle to an (unquenched) acceptor vesicle, the fluorescence intensity increases, which can be monitored in time.

In addition to NodRlv-IV (BODIPY FL-C₁₆), we incorporated non-exchangeable Texas Red-DHPE as a FRET-acceptor in the donor vesicles to effectively quench the Nod factor fluorescence. Consequently, the NodRlv-IV (BODIPY FL-C₁₆) fluorescence of the donor vesicles was very low, as shown in Figure 4A. Similar results were obtained for donor vesicles prepared with the ethanol injection method or with the sonication method (see methods section). The addition of a ten-fold excess of acceptor vesicles to the sample, resulted in a very rapid increase of the fluorescence intensity quickly reaching a constant level, indicating the rapid transfer of a substantial amount of NodRlv-IV (BODIPY FL-C₁₆) to the acceptor vesicles (Figure 4A). Again no significant differences were observed for the different donor vesicle preparations (i.e. ethanol injection versus sonication). This indicates that the tiny amount of ethanol present after the ethanol injection (0.7% (v/v)) does not affect the transfer rate. After equilibrium was achieved, Triton X-100 was added (arrow C) to disperse and thereby unquench any Nod factors remaining in the donor vesicles. A further fluorescence increase (30-40%) was observed, indicating that in the equilibrium situation, about one third of the NodRlv-IV (BODIPY FL-C₁₆) remained (quenched) in the donor vesicles. As for a control experiment, we incorporated the non-transferable BODIPY 530/550 DHPE instead of fluorescent Nod factor into the donor vesicles. Also for these donor vesicles, the fluorescence intensity in buffer was low. After addition of acceptor vesicles no increase in fluorescence was observed (see Figure 4B). This experiment confirms that BODIPY 530/550 DHPE does not spontaneously transfer between membranes as was also shown for other phosphatidylethanolamines (Nichols and Pagano, 1982). Moreover, it rules out alternative explanations of the fluorescence increase shown in figure 4A at arrow B since i) under the conditions used, Texas Red DHPE (used as a quencher) can not transfer to acceptor vesicles; ii) no fusion of the vesicles is detectable; and iii) the acceptor vesicles have no fluorescence.

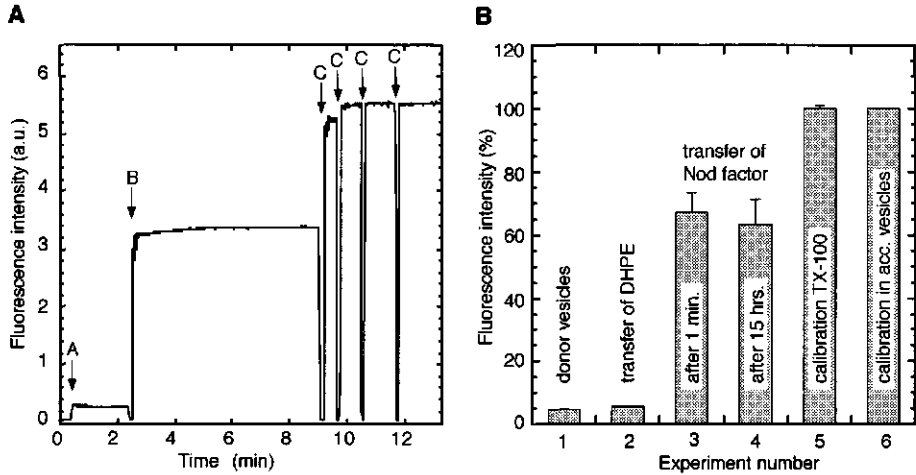


Figure 4: Intermembrane transfer of NodRlv-IV (BODIPY FL-C₁₆) from quenched donor to unquenched acceptor vesicles.

(A) The fluorescence intensity of NodRlv-IV (BODIPY FL-C₁₆) is measured in arbitrary units (a.u.). At the arrow indicated with A, donor vesicles are generated by injection of an ethanolic solution (containing DOPC: DPPA: Texas Red DHPE: NodRlv-IV (BODIPY FL-C₁₆) = 79:10:10:1 mol%, 20 nmol total lipid) into 3 ml Tris buffer under continuous stirring. For initiating spontaneous transfer, a 10-fold excess of acceptor vesicles (containing DOPC: DPPA=90:10 mol%) was added at the arrow indicated with B. After 4 subsequent additions of 25 μ l 10% (v/v) Triton X-100 in PBS (indicated by arrow C) the vesicles are completely solubilized, thereby dispersing and unquenching NodRlv-IV (BODIPY FL-C₁₆).

(B) Normalized fluorescence intensity at various conditions.

(1) Intensity obtained after preparing donor vesicles (DOPC: DPPA: Texas Red DHPE: NodRlv-IV (BODIPY FL-C₁₆) = 79:10:10:1 mol%, 20 nmol total lipid in 3 ml Tris) (n=4).

(2) Intensity obtained after adding acceptor vesicles to donor vesicles containing, instead of NodRlv-IV (BODIPY FL-C₁₆), the phospholipid BODIPY 530/550 DHPE (n=2).

(3) Fluorescence intensity observed after the addition of a 10-fold excess of acceptor vesicles to the donor vesicles prepared according to (1) (n=4).

(4) Fluorescence intensity observed if the mixture (3) is incubated for 15 more hours (n=2).

(5) The emission after unquenching donor vesicles by solubilizing with 100 μ l of 10% (v/v) Triton X-100 (n=4).

(6) The fluorescence intensity of 200 nmol unquenched acceptor vesicles consisting of DOPC: DPPA:NodRlv-IV (BODIPY FL-C₁₆) =89.5:9.5:1 mol% in 3 ml Tris. This signal represents a 100% transfer situation and is equal to (5) and validates the calibration by solubilization with 100 μ l 10% (v/v) Triton X-100 (n=3).

The experiment shown in figure 4A indicates that despite their distinct preference for membranes, Nod factors rapidly equilibrate between different membranes. Similar observations have been made for lipids with a bulky polar head group and relatively low total hydrophobicity (i.e. phospholipids with short fatty acyl chains) (Homan and Pownall, 1988). The critical transition for intermembrane transfer is the energy required for desorption of a lipid monomer from the membrane surface (Bai and Pagano, 1997; Nichols and Pagano, 1981). Obviously, the chitin moiety of the Nod factor provides ample opportunities for hydrogen bonding in the aqueous phase, thereby lowering the activation energy for Nod factor desorption and subsequent spontaneous monomeric transfer.

The average percentage of transferred NodRlv-IV(BODIPY FL-C₁₆) varied between 60-70% in several experiments, which corresponds well with the relative surface of the outer leaflet of small

unilamellar vesicles (Gadella Jr. and Wirtz, 1994; Johnson et al., 1971; Van Paridon et al., 1988). Hence, the immobile fraction reflects the Nod factor population trapped in the inner leaflet of the donor vesicles. Even at 15 hours after mixing the donor and acceptor vesicles, no further increase in fluorescence intensity was observed and subsequent calibration again indicated transfer of 60-70% (Figure 4B). This demonstrates that spontaneous flip-flop of Nod factors between inner and outer leaflets of membranes is prohibited. For transbilayer exchange (flip-flop), the bulky hydrophilic chitin moiety has to pass the hydrophobic lipid interior of the membrane. Apparently, this transition is highly unfavored and requires a high activation energy similarly as observed for lipids with a bulky polar head group (Bai and Pagano, 1997; Homan and Pownall, 1988).

Transfer of fluorescent Nod factors from vesicles to root hairs

To examine whether the Nod factors can transfer spontaneously from membranes (e.g. bacterial outer membranes) to the cell wall of root hairs, vesicles containing both NodRlv-IV(BODIPY FL-C₁₆) and the non-exchangeable quencher Texas Red-DHPE, were added to vetch roots in Fåhrens slides. To allow detection of NodRlv-IV(BODIPY FL-C₁₆) above the autofluorescence of the root hairs, a concentration of 0.6 μ M was used, and a bandpass emission filter was employed excluding Texas Red fluorescence.

After application of the vesicles, this resulted in an increase of green fluorescence of the cell wall of the root hairs, as shown in Figure 5A. The labeling pattern is identical to the one observed when the Nod factors were added without vesicles (data not shown). Also a clear Texas Red fluorescence could be observed at the root hair cell wall, indicating that at least part of the vesicles applied adhere at the root hair surface. Three hours after addition of the vesicles, root hairs were deformed normally, indicating that Nod factor perception is not different when Nod factors are administered as monomers or as vesicle-bound structures. In a control experiment the BODIPY FL labeled Nod factor was replaced by BODIPY FL-DHPE (a non-exchangeable phospholipid). After addition of these vesicles (figure 5B), the green fluorescence intensity of the root hairs was similar to the root hair autofluorescence intensity detected on untreated plants (compare with Figure 5C), but also a distinct Texas Red fluorescence signal could be observed at the root hair surface (data not shown). This indicates that the increase in NodRlv-IV(BODIPY FL-C₁₆) fluorescence as shown in Figure 5A truly reflects desorption of Nod factor monomers from (adhered) vesicles and transfer to the root hairs, and not association or disintegration of vesicles at the cell wall. Given the comparable physicochemical properties of all four fluorescent Nod factors in relation to membranes, the results of the transfer experiments performed with NodRlv-IV(BODIPY FL-C₁₆) are most likely representative for the other fluorescent Nod factors and moreover, natural occurring Nod factors.

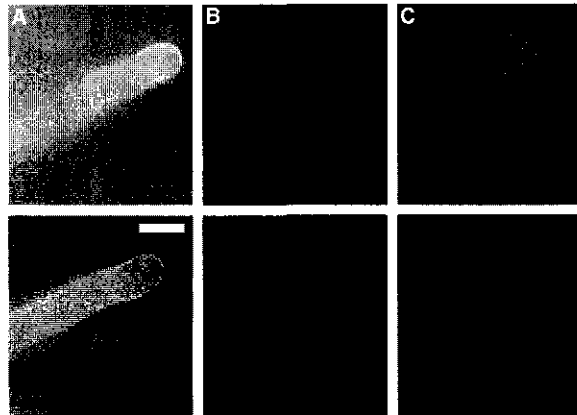


Figure 5: Images of *Vicia sativa* (vetch) root hairs, showing the fluorescence after incubation with quenched vesicles containing BODIPY labeled Nod factors or phospholipids. All images shown are representative data of multiple (at least triplicate) experiments. Image exposure times, microscopy settings, and image processing (contrast stretching) was identical for all 6 subimages. Bar represents 15 μm .

(A) Fluorescence of root hairs 10 minutes after incubation with quenched donor vesicles (DOPC: DPPA: Texas Red DHPE: NodRlv-IV (BODIPY FL- C_{16})= 79.4:10:10:0.6 mol%, 100 nmol total lipid in 1 ml PGM without CaCl_2) containing Nod factor.

(B) Fluorescence of root hairs 10 minutes after incubation with quenched donor vesicles (DOPC: DPPA: Texas Red DHPE: BODIPY FL DHPE= 79.4:10:10:0.6 mol%, 100 nmol total lipid in 1 ml PGM without CaCl_2) containing a non-transferable lipid.

(C) Autofluorescence of non-treated roots.

Discussion

In this study the behavior of fluorescently labeled Nod factors was investigated. The capability to deform root hairs of *Vicia sativa* seedlings was used to evaluate their bioactivity. It appears that the introduction of the hydrophobic BODIPY moieties at carbon atom C_{16} of the fatty acyl chain does not seriously interfere with perception efficiency. This makes us feel confident that these fluorescent Nod factors can be used as truthful representatives of their natural counterparts, also in other systems.

Since Nod factors are amphiphilic molecules, with an acyl chain of 16 carbon atoms or more, special attention was given to their properties in the presence of membranes. No transbilayer movement of the Nod factors is observed within 15 hours. In view of the cytoplasmic localization of the enzymes involved in the Nod factor biosynthesis in rhizobia (Barny and Downie, 1993; Bloemberg et al., 1994; Schlaman et al., 1990), the inability of Nod factors to flip-flop spontaneously has direct implications for the bacterial Nod factor-secretion mechanism. Our observations imply that after biosynthesis in the cytoplasm, the Nod factors are trapped in the inner leaflet of the inner membrane of the bacterium. As a consequence, for enabling bacterial Nod factor secretion, there is an absolute requirement for a transfer mechanism in both bacterial membranes to effectively move Nod factors from the inner leaflet

of the inner membrane to the outer leaflet of the outer membrane, e.g. an ATP dependent flippase-like transport system (reviewed for aminophospholipids by (Devaux, 1992)). Indeed three rhizobial proteins have been identified (NodI, NodJ and NodT) which enhance secretion of Nod factors, but are not involved in the Nod factor biosynthesis (Rivilla et al., 1995; Spaink et al., 1995). For flippase activity, NodI is the most probable candidate, given its membrane association and ATP binding motif (Downie, 1998; Spaink et al., 1995). Further studies using model membranes containing NodI and fluorescent Nod factor as described here can elucidate whether these enzymes act as flippases.

FCS and time-correlated fluorescence spectroscopy revealed that, at 10^{-8} M, the fluorescent Nod factors are present as monomers in buffer and do not have the tendency to aggregate in micelles. We did not investigate whether Nod factors do form micelles at higher concentrations, but given the fact that Nod factors can elicit responses in legume root hairs at concentrations down to 10^{-12} M (Heidstra et al., 1994; Roche et al., 1991) we can exclude that formation of micellar structures by Nod factors is part of a biological activation mechanism at physiological concentrations. All four Nod factors have a high tendency to insert in exogenously applied micelles or vesicles. From this it is concluded that the physicochemical properties of the fluorescent Nod factors are quite similar, irrespective of the distinct differences in bioactivity (Gadella et al. (1997) and Table 1).

The transfer experiments show that NodR1v-IV(BODIPY FL-C₁₆) is able to redistribute between outer leaflets of different vesicles very rapidly. Although we did not perform detailed kinetic studies, we hypothesize that like for the well studied spontaneous transfer of short acyl chain phospholipids between membranes, the transfer mechanism involves desorption of monomers from the outer membrane leaflet (Bai and Pagano, 1997; Homan and Pownall, 1988; Nichols and Pagano, 1981; Roseman and Thompson, 1980). This view is supported by the *in vivo* transfer experiments which showed that the Nod factors are able to desorb from vesicles to diffuse to the cell wall of root hairs, without significant fusion or disintegration of the vesicles. Given the observations we postulate that Nod factors also will be able to spontaneously diffuse from the outer membrane of *Rhizobium* bacteria to the root hair cell wall and cell membrane, without the need for the bacterium to provide a specific mechanism for enhancing desorption of Nod factor monomers from the bacterial outer membrane. This again supports our notion that the *nod* gene products indicated to be involved in rhizobial Nod factor secretion (Rivilla et al., 1995; Spaink et al., 1995) are involved in intrabacterial transbilayer transport of Nod factors.

In conclusion we have shown that Nod factors are water soluble at physiological concentration, insert in membranes but are not able to flip-flop between membrane leaflets and that they spontaneously transfer from membranes to legume root hairs. These observations provide novel and direct insight on how Nod factors behave in the presence of biomembranes and root hairs which increased our understanding of the mode of secretion and transfer of Nod factors during the early steps of the *Rhizobium*-legume interaction.

Materials and Methods

Materials

All fluorescent probes, except for erythrosine B (Eastman Kodak, Rochester, NY), were purchased from Molecular Probes Europe (Leiden, The Netherlands), BODIPY 581/591-C₁₆ was a Molecular Probes custom synthesis product. Triton X-100 (for gas chromatography), ethanol, and DMSO (spectroscopic grade) were from Merck (Darmstadt, Germany). DOPC, the sodium salt of DPPA and mannitol (plant cell culture tested) were from Sigma (Zwijndrecht, The Netherlands). In order to make DPPA soluble in ethanol, DPPA was converted to the acid form by acidic extraction by dissolving in CHCl₃:CH₃OH:0.6 M HCl (1:2:0.8 v/v), phase separation by addition of 1/4 volume of H₂O and CHCl₃, and subsequent evaporation of the isolated lower phase (Folch et al., 1957).

Fluorescent Nod factors

The synthesis of NodR1v-IV(BODIPY FL-C₁₆) is described in (Gadella Jr. et al., 1997b). Correspondingly, three novel Nod factors differing both in acyl chain length and fluorophore structure are synthesized and purified. According to the nomenclature proposed by Roche et al. (1991) the Nod factors are indicated as NodR1v-IV(BODIPY 558/568-C₁₂) NodR1v-IV(BODIPY 581/591-C₁₁) and NodR1v-IV(BODIPY 581/591-C₁₆).

Plant material

Seeds of *Vicia sativa*, subspecies *nigra*, were germinated and grown in modified Fåhrens slides (Bhuvaneswari and Solheim, 1985) as described earlier (Heidstra et al., 1994; Van Brussel et al., 1982). The plant growth medium (PGM) was composed of 2.72 mM CaCl₂, 1.95 mM MgSO₄, 2.20 mM KH₂PO₄, 1.26 mM Na₂HPO₄ and 0.08 mM Fe(III) citrate. Root hair deformation assays were done as described before (Heidstra et al., 1994). DMSO and ethanol concentrations were never higher than 0.1% (v/v).

Fluorescence spectroscopy

Nod factors were dissolved in ethanol and pipetted in 1 ml quartz cuvettes. All excitation and emission spectra were recorded on a SPF-500C spectrofluorimeter (SLM instruments, Urbana, IL, USA). Excitation spectra were recorded by monitoring emission (slit 5 nm) at 560 nm, 610 nm and 650 nm and scanning excitation (slit 2 nm) from 400 to 550 nm, 450 to 600 nm and 500 to 630 nm for BODIPY FL, BODIPY 558/568 and BODIPY 581/591 respectively. Emission spectra were recorded by excitation (slit 5 nm) at 450 nm, 500 nm and 520 nm and scanning emission (slit 2 nm) from 460 to 600 nm, 510 to 650 nm and 530 to 570 nm for BODIPY FL, BODIPY 558/568 and BODIPY 581/591 respectively.

Preparation of micelles and vesicles

Phosphate buffered saline (PBS) consisted of 10 mM phosphate (pH=7.4) and 154 mM NaCl. Triton X-100 was added to a final concentration of 0.2% in PBS (v/v) to obtain micelles. Small unilamellar vesicles were made as described (Batzri and Korn, 1973) by injecting 10 μ l of a solution of DOPC in ethanol into 1 ml of PBS, to yield a final concentration of 50 μ M DOPC. The fluorescent Nod factors were added from DMSO stock solutions to PBS, Triton X-100 micelles or DOPC vesicles to a final Nod factor concentration of 10 nM.

For transfer experiments, donor vesicles were made as described above, by injecting 20 μ l of an ethanolic solution of 790 μ M DOPC, 100 μ M DPPA, 10 μ M NodRlv-IV(BODIPY FL-C₁₆) or 10 μ M BODIPY 530/550 DHPE and 100 μ M Texas Red DHPE into 3 ml Tris buffer (20 mM Tris (pH=7.4), 100 mM NaCl, 1 mM EDTA, 1 mM EGTA), under continuous stirring. Alternatively, the ethanolic solution was evaporated, 3 ml of Tris buffer was added followed by sonication using a Branson tip sonifier (Danbury, CT, USA) for three minutes with an output power of 15 W (30% duty cycle). Acceptor vesicles were prepared by mixing 3600 nmol DOPC and 400 nmol DPPA in chloroform. After evaporation of the chloroform, the lipids were dissolved in 2 ml of Tris buffer by vortexing, followed by sonication for 3 min. To monitor transfer from vesicles to roots, donor vesicles prepared by sonication consisted of 80 μ M DOPC, 10 μ M DPPA, 10 μ M Texas Red DHPE and 0.6 μ M NodRlv-IV(BODIPY FL-C₁₆) or 0.6 μ M BODIPY FL DHPE (final concentration in PGM without calcium).

Nod factor transfer assay

The emission of NodRlv-IV(BODIPY FL-C₁₆) was monitored continuously on an Aminco SLM-8000 (SLM instruments, Urbana, IL) by excitation at 490 nm (slit 4 nm) and emission at 513 or 550 nm (slit 4 nm). To start the assay, 100 μ l of acceptor vesicles were added to 3 ml of donor vesicles, and the fluorescence intensity was monitored as a function of time. For calibration, aliquots of 25 μ l 10% (v/v) Triton X-100 in PBS were added, until the fluorescence intensity did not increase.

Fluorescence microscopy

Fluorescence microscopy was performed with the FRIM system described by Gadella et al. (Gadella Jr. et al., 1997b) based on a Leica DMR microscope (Leitz, Wetzlar, Germany) with Leitz fluotar 10 \times NA 0.3 air or fluotar 40 \times NA 0.5-1.0 oil immersion objectives. In addition to the CH250 CCD-camera, images were captured by a Quantix CCD-camera (Photometrics, Tucson, AZ, USA) interfaced through a PCI-card to an Apple Macintosh PowerPC 8500/180 computer (Apple computer, Cupertino, CA, USA) and controlled by IPLab 3.1 software (Signal Analytics, Vienna, VA, USA). Fluorescence of BODIPY FL was acquired by excitation with a 100 W USH-102D mercury lamp (Fairlight, Rotterdam, The Netherlands) and an Omega (Omega Optical, Brattleboro, VT, USA) 490DF20 nm bandpass filter. The emission was

separated by an Omega 505 DRLP dichroic mirror and passed through a 525DF30 bandpass filter.

Fluorescence Correlation Spectroscopy

FCS measurements were performed with a Zeiss-EVOTEC ConfoCor (Carl-Zeiss, Jena, Germany and Evotec Biosystems, Hamburg, Germany). Briefly, the system consists of an Zeiss inverted confocal microscope, and uses either an air-cooled argon ion laser (488 nm) or a helium-neon laser (543 nm) for excitation. Standard confocal epi-fluorescence microscope optics are used, including dichroic mirrors (510 nm or 560 nm for the respective laser lines), a Zeiss water immersion objective (C-Apochromat 40 \times , 1.2 NA, 440052), and bandpass filters for selecting the fluorescence emission (515-565 nm or 565-610 nm for the respective laser lines). The emission was spatially filtered through a pinhole (diameter 40 μ m) and detected by an avalanche photodiode coupled to a fast digital correlator. Data acquisition and analysis were performed using the FCS ACCESS software package (EVOTEC/Zeiss, Inc., version 1.0.12) running under Windows95 (Microsoft, Inc.). The system is described in detail elsewhere (Hink et al., 1999; Hink and Visser, 1998). Samples were measured and calibration (see below) was performed in 8-chamber coverglasses (Nalge Nunc Int., Naperville, IL, USA) having a borosilicate bottom with a thickness of 0.135 mm. The laser beam was focused 150 μ m above the bottom of the chamber. Acquisition times for calibration and samples were 30-60 s. All experiments were done at room temperature.

Calibration was done by rhodamine green in H₂O for 488 nm excitation and by tetramethylrhodamine or tetramethylrhodamine-dextran (MW 10,000) in H₂O for 543 nm excitation, which have known diffusion constants of $2.8 \cdot 10^{-10} \text{ m}^2 \cdot \text{s}^{-1}$, $2.8 \cdot 10^{-10} \text{ m}^2 \cdot \text{s}^{-1}$ and $1.36 \cdot 10^{-10} \text{ m}^2 \cdot \text{s}^{-1}$, respectively (Rigler et al., 1992). The triplet time constant was fixed to 5 μ s during evaluation of the calibration results because of the use of air-saturated solutions. From these results, the axial radius of the laser beam at the focal plane, ω_1 , at 488 nm and 543 nm excitation was calculated, which were 0.30 μ m and 0.36 μ m respectively. The diffusion constants are related to diffusion times according to equation 1 (Hink and Visser, 1998):

$$\tau = \frac{\omega_1^2}{4D} \quad (1)$$

in which τ is the diffusion time in seconds and D is the diffusion constant in $\text{m}^2 \cdot \text{s}^{-1}$. The volume, V , of the confocal element (m^3) can be calculated from the axial laser radius ω_1 and structural parameter (SP) obtained from the calibration (Hink and Visser, 1998):

$$V = 2\pi\omega_1^3 SP \quad (2).$$

The radius, r , of spherical particles is related to the diffusion constant via the Stokes-Einstein equation (Edward, 1970):

$$r = \frac{kT}{6\pi\eta D} = \sqrt[3]{\frac{3kT\phi}{4\pi\eta}} \quad (3).$$

For the viscosity, η , the value of water is taken ($10^{-3} \text{ kg}\cdot\text{m}^{-1}\cdot\text{s}^{-1}$), T is the absolute temperature, ϕ is the rotational correlation time obtained by anisotropy decay analysis, and k the Boltzmann constant.

Time-correlated single photon counting

Time-resolved experiments were done on the TCSPC set-up as described in detail elsewhere (Van den Berg et al., 1998; Van Hoek and Visser, 1992). The excitation wavelength was 510 nm (coumarine 460 dye as laser medium, pumped by a mode-locked Nd-YLF laser), emission was detected using a Schott (Mainz, Germany) OG 530 nm cut-off and Balzers Filtraflex K55 bandpass filter (Balzers, Liechtenstein) for BODIPY FL emission, a Schott 570.3 nm bandpass filter for BODIPY 558/568 emission or a Schott KV 550 nm cut-off and an Omega 580DF30 nm bandpass filter for BODIPY 581/591 emission. For each decay 1024 channels were collected with a time spacing of 25 ps. Ten to twenty cycles were acquired for the sample, three cycles for the reference and two to eight for the blank, depending on the signal intensity. Erythrosine B in H_2O ($\text{OD}_{\text{max}} < 0.1$), with a known single lifetime of 80 ps was used as a reference for deconvoluting the instrumental response function. Total fluorescence decay- and fluorescence anisotropy decay experiments were analyzed according to a multiexponential decay law using a global analysis program, which principle has been described previously (Beechem et al., 1992) and which is based on a Marquardt nonlinear least squares procedure (Marquardt, 1963). The complete anisotropy decays were analyzed and χ^2 values were calculated starting from channel 25, at which the fluorescence reached the maximal intensity. The 67% confidence limits of the rotational correlation times were determined by a rigorous error analysis (Beechem et al., 1992).

Acknowledgments

We are grateful to Jürgen Schmidt and Michael John (Abteilung Genetische Grundlagen der Pflanzenzüchtung, Max-Planck-Institut für Züchtungsforschung, Köln, Germany) for their continuous interest and help in the synthesis of the fluorescent Nod factors.

IN VIVO* FLUORESCENCE CORRELATION MICROSCOPY (FCM) REVEALS ACCUMULATION AND IMMOBILIZATION OF NOD FACTORS IN ROOT HAIR CELL WALLS*Abstract**

Fluorescence correlation microscopy (FCM), is a new single molecule detection technique based on the confocal principle to quantify molecular diffusion and concentration of fluorescent molecules (particles) with submicron resolution. FCM is applied to study the diffusional behavior of fluorescent Nod factor-analogs on living *Vicia sativa* root hairs. Three recently described Nod factors with a fluorescent acyl chain (Goedhart et al., 1999, *Biochemistry* 38, 10898-10907) are used. Plasmolysis of fluorescently labeled root hairs shows that the Nod factors are predominantly located in the cell wall, as hardly any fluorescence can be detected in the plasma membrane. After Nod factor-induced root hair deformation, the new outgrowth is not labeled, indicating a lack of migration of Nod factors to the newly synthesized cell wall. In agreement, FCM shows a >1000-fold reduction of molecular mobility of the fluorescence Nod factors upon binding to the cell wall. In addition, FCM demonstrates that Nod factors, when exogenously applied in aqueous solution at 10 nM, markedly concentrate in the cell wall of root hairs (up to 50-fold). The feasibility of applying FCM for the study of living plant cells as well as the implications of our results for the perception of Nod factors are discussed.

Joachim Goedhart, Mark A. Hink, Antonie J.W.G. Visser, Ton Bisseling and Theodorus W.J. Gadella Jr.

Introduction

Fluorescence correlation spectroscopy (FCS) is a fluorescence microscopic technique that gives information on diffusion rate and absolute numbers of fluorescently tagged molecules. FCS measures fluorescence intensity fluctuations due to movement of single fluorescent molecules into and out of an open confocal volume element. The fluctuations are correlated over time, yielding quantitative information on molecular mobility and local concentration (Maiti et al., 1997; Rigler, 1995). The theoretical concept was developed in the early 1970s (Ehrenberg and Rigler, 1974; Elson and Magde, 1974; Magde et al., 1972). Nowadays, as a result of new technological advances, FCS instruments routinely allow detection of single molecules in a confocal volume of less than a femtoliter (Maiti et al., 1997). Typical fluorophore concentrations which are measured are in the nanomolar range, making it an attractive new technique for monitoring sparse molecules.

Applications of FCS include measuring diffusion constants (Magde et al., 1974), aggregation states (Berland et al., 1996), hybridization of oligonucleotides (Kinjo and Rigler, 1995; Oehlenschläger et al., 1996) and receptor-ligand interactions (Rauer et al., 1996). The use of FCS in combination with microscopy (FCM) (Brock and Jovin, 1998) to study molecular diffusion and concentration in living cells has been limited. To date, only few papers have been published describing the use of FCS for *in vivo* studies (Berland et al., 1995; Brock et al., 1998; Brock and Jovin, 1998; Brock et al., 1999; Politz et al., 1998; Schwille et al., 1999; Visser, 1998). In this study we describe the application of FCM to reveal the behavior of fluorescent derivatives of Nod factors in relation to their perception by legume root hairs.

Nod factors are signaling molecules that are secreted by Gram-negative *Rhizobium* bacteria and are essential in the early steps of the *Rhizobium*-legume interaction (Heidstra and Bisseling, 1996; Long, 1996). The precise structure of the Nod factors differs for each *Rhizobium* species, but they all consist of a chitin backbone of 3 to 5 N-acetylglucosamine residues to which a fatty acyl chain is attached at the non-reducing end. Therefore, Nod factors are often referred to as lipo-chitooligosaccharides (LCOs). Purified Nod factors at picomolar concentrations can elicit specific responses in roots of leguminous plants in the absence of *Rhizobium* bacteria, encompassing root hair depolarization (Ehrhardt et al., 1992), root hair deformation ((Heidstra et al., 1994; Lerouge et al., 1990), cell division (Van Brussel et al., 1992) and primordium formation (Truchet et al., 1991). Some of these responses are very fast: 15 seconds after Nod factor application to alfalfa a depolarization across the plasma membrane of root hairs and an intracellular pH increase are observed (Ehrhardt et al., 1992; Felle et al., 1995; Felle et al., 1996). So far, four efforts have been made to localize Nod factors in plants using either epipolarization microscopy of radioactively tagged Nod factors (Heidstra et al., 1994), immunolocalization on fixed nodules (Timmers et al., 1998) or fluorescence microscopy of fluorescent Nod factor derivatives (Gadella Jr. et al., 1997b; Philip-Hollingsworth et al., 1997). We have shown that a Nod factor labeled with a BODIPY FL-C₁₆ acyl chain (NodRIv-IV(BODIPY FL-C₁₆))

predominantly binds to the cell surface of the root hairs and atrichoblasts, and that there is an increased labeling at the tips of root hairs (Gadella Jr. et al., 1997b). Furthermore, this Nod factor analog can induce root hair deformation at concentrations down to 10^{-9} M (Gadella Jr. et al., 1997b). The autofluorescence of *Vicia sativa* root hairs is significantly lower if the excitation is shifted from blue (480 nm, necessary for excitation of BODIPY FL) to green or yellow (510-580 nm). For this reason 3 novel red-shifted NodRlv-IV Nod factor analogs were synthesized containing a BODIPY 558/568-C₁₂, BODIPY 581/591-C₁₁ or a BODIPY 581/591-C₁₆ acyl chain (Goedhart et al., 1999). In the root hair deformation assay (Heidstra et al., 1994), two of these new Nod factor analogs were found to be bioactive. Root hair deformation could be observed at concentrations down to 10^{-10} M and 10^{-8} M for the NodRlv-IV analogs containing a BODIPY 581/591-C₁₆ and BODIPY 558/568-C₁₂ acyl chain, respectively, whereas the NodRlv-IV(BODIPY 581/591-C₁₁) was found to be inactive (Goedhart et al., 1999). Due to the higher bioactivity and the greatly improved spectral properties of the NodRlv-IV(BODIPY 581/591-C₁₆) Nod factor, its *in situ* localization and binding to root hairs can be studied at much lower and more physiological concentrations. Moreover, the lower autofluorescence background permits the application of FCM, which can add important information on mobility as well as concentration of the fluorescent Nod factors. For example, upon binding of Nod factors to a receptor or other binding protein, as has been described for *Medicago truncatula* (Bono et al., 1995) and *Dolichos biflorus* (Etzler et al., 1999), the diffusion of Nod factors will be reduced markedly. Additionally, the number of Nod factors bound to the complex and the concentration of the complex itself can be quantified.

In this study, the detailed localization of the fluorescent Nod factors at nanomolar concentration is described. FCM is used to relate these results to quantitative information on molecular mobility in living plant root hairs. Furthermore, FCM is used to obtain absolute Nod factor concentrations in both the cell wall and cytoplasm of the root hairs. In addition to the novel insights on the *in situ* behavior of Nod factors on legume root hairs, the new perspectives of the application of the FCM technique to *in vivo* plant studies are discussed.

Principle of FCS

A strongly focused laser beam continuously illuminates a spot in the sample. The out-of-focus emission is rejected by a pinhole, thereby creating a confocal volume (fig. 1a). Unlike confocal laser scanning microscopy (CLSM), the position of the excited volume is fixed throughout the measurement. Fluorescent molecules diffusing in and out of the continuously excited volume will give rise to fluctuations in emission intensity. As small particles will diffuse more rapidly through the confocal volume than large molecules, (compare curve 1 and 2 in figure 1b) the intensity fluctuations will contain information on the diffusion speed of the molecules.

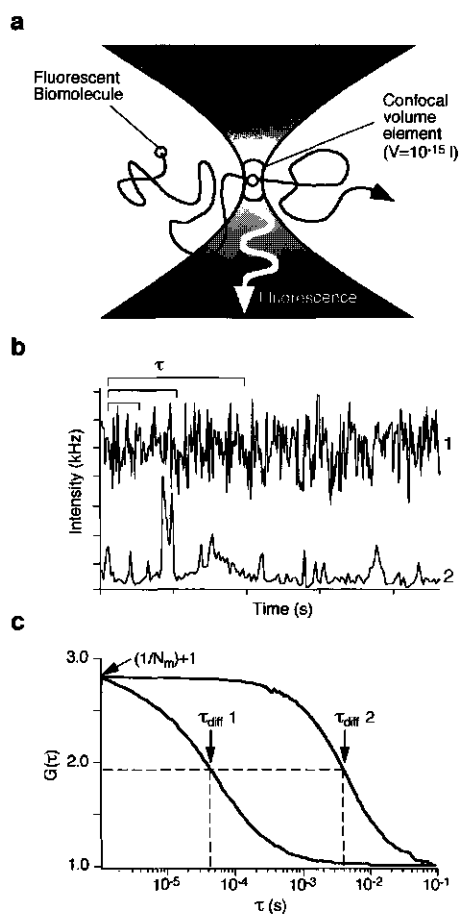


Figure 1: Principle of FCS. A fixed confocal volume is continuously illuminated by a strongly focused laser beam (a). Fluorescent molecules entering the confocal volume will give rise to bursts of photons (given in thousands of counts per second (kHz)), of which the duration is dependent on the time they spend in the confocal volume. This is illustrated in panel b by curve 1 and 2, showing intensity fluctuations caused by diffusion of small organic fluorophores (rhodamine green in H_2O) and large vesicles labeled with fluorescent lipids respectively. Autocorrelation of the intensity fluctuations gives the respective autocorrelation curves $G(\tau)$ shown in panel c. The amplitude of the autocorrelation curve at a time value τ indicates whether intensities measured at a time interval τ in panel b are correlated (yielding $G(\tau)$ values >1). The time τ at which the amplitude has dropped to 50% of its maximum corresponds roughly to the diffusion time τ_{diff} . The $G(\tau)$ curves can be analyzed to yield the average number of particles N_m in the confocal volume, and the diffusion time τ_{diff} (see equations 1-3).

The diffusion constant for translational movement can be determined from the normalized autocorrelation function $G(\tau)$, which relates the fluorescence intensity, I , at a time t to that at an incremental time τ seconds later:

$$G(\tau) = \frac{\langle I(t) \cdot I(t+\tau) \rangle}{\langle I \rangle^2} = \frac{\langle I \rangle^2 + \langle \delta I(t) \cdot \delta I(t+\tau) \rangle}{\langle I \rangle^2} \quad (1)$$

Here δI denotes the fluctuation of the fluorescence intensity around the mean value $\langle I \rangle$. It should be noted, that fluctuations in fluorescence intensity are only monitored when the number of molecules in the volume element is *low* enough, thus determining the *upper* concentration limit at which FCS can be used (around 10^{-7} M). The lower concentration limit is defined by background and can be as low as 10^{-12} M (Rigler, 1995). Assuming a Gaussian shaped laser focus in three dimensions, the autocorrelation function can be written as:

$$G(\tau) = 1 + \frac{(1 - F + F \cdot e^{-\lambda\tau})}{N_m (1 + \tau / \tau_{diff}) (1 + (\omega_{xy} / \omega_z)^2 \cdot \tau / \tau_{diff})^{3/2}} \quad (2)$$

where τ_{diff} denotes the diffusion time in seconds and N_m indicates the number of fluorescent particles in the detection volume (figure 1c). The equation also contains a term F , describing the fraction of molecules in the triplet state and the characteristic triplet decay rate λ . The constants ω_{xy} and ω_z describe the dimensions of the volume element. These are defined as the distance from the center of the laser focus in the radial, ω_{xy} , and axial direction, ω_z , where the fluorescence intensity has dropped to e^{-2} ($\approx 13.5\%$) of its peak value. Typical values of ω_{xy} and ω_z are $0.3 \mu\text{m}$ and $2.1 \mu\text{m}$ respectively, creating a confocal volume that can be approximated by a cylinder with a diameter of $0.6 \mu\text{m}$ and height of $4.1 \mu\text{m}$. The laser radii can be resolved by calibration using reference compounds with known diffusion constants. The autocorrelation can easily be extended for multiple contributions (Brock et al., 1998). However, quantum yields of different species contributing to the autocorrelation should be taken into account (Meseth et al., 1999). The diffusion constant D_{tran} is related to the diffusion time τ_{diff} according to equation 3:

$$\tau_{diff} = \frac{\omega_{xy}^2}{4 \cdot D_{tran}} \quad (3)$$

The volume, V , of the cylindrically shaped confocal element (m^3) can be calculated from the laser radii.

$$V = 2\pi \omega_{xy}^2 \cdot \omega_z \quad (4)$$

The hydrodynamic radius r of the fluorescent particles, assuming a spherical shape, is related to the diffusion constant via the Stokes-Einstein equation (Edward, 1970):

$$r = \frac{kT}{6\pi\eta D_{tran}} \quad (5)$$

in which η is the viscosity, T is the absolute temperature and k the Boltzmann constant.

Results

Nod factors label root hair tips

To localize Nod factors on *Vicia sativa* root hairs, 10 nM NodRlv-IV(BODIPY 581/591-C₁₆) in PGM was added to the roots. Immediately after addition, the root hairs were fluorescent on the outside (see Figure 2a). After three hours, deformation of the root hairs occurred, clearly demonstrating the bioactivity of this Nod factor derivative (fig. 2b1). In figure 2c1-2c4 the location of NodRlv-IV(BODIPY 581/591-C₁₆) during swelling and deformation of root hairs is shown. As is clear from figure 2d, the new outgrowth was far less fluorescent than the cell wall or membrane of the swelling from which the outgrowth originated. The fluorescence inside the root hairs (fig. 2c and 2d) mainly originated from out of focus fluorescence which is nicely shown by the low 'cytoplasmic' fluorescence intensity in the outgrowth of a deformed root hair (fig. 2d2). When fluorescent Nod factors were reapplied, the outgrowths did become labeled (data not shown). This indicates that the initial negative stain of outgrowths was caused by exhaustion of the supply of extracellular Nod factors and low lateral mobility at the root hair surface, rather than by the lack of Nod factor binding sites at these root hair areas.

Nod factors are associated with the cell wall

To investigate whether the fluorescent Nod factors associate with the cell wall or the plasma membrane, plasmolysis was induced after labeling *Vicia sativa* roots with 10 nM NodRlv-IV(BODIPY 581/591-C₁₆). As can be inferred from figure 2e, the cell wall remained labeled. The cell wall labeling pattern was very similar to that observed before the induction of plasmolysis, indicating that plasmolysis does not induce a significant change in localization. Occasionally (< 5% of the hairs examined), only a very low level of fluorescence was observed at the plasma membrane. This indicates that the affinity of Nod factors for the cell wall is much higher than for the plasma membrane, which is remarkable given the distinct preference of Nod factors for membranes (Goedhart et al., 1999). When higher (non-physiological) concentrations of Nod factor were applied (1 μ M) and subsequently plasmolysis was induced, besides cell wall labeling also (uniform) plasma membrane (but no cytosolic or endomembrane) labeling was visible in all plasmolyzed root hairs (data not shown). Hence, at much higher Nod factor concentrations the binding sites in the cell wall become saturated and non-specific membrane labeling appears. This shows that the cell wall is permeable for the Nod factors and confirms that the primary Nod factor-binding sites are in the cell wall.

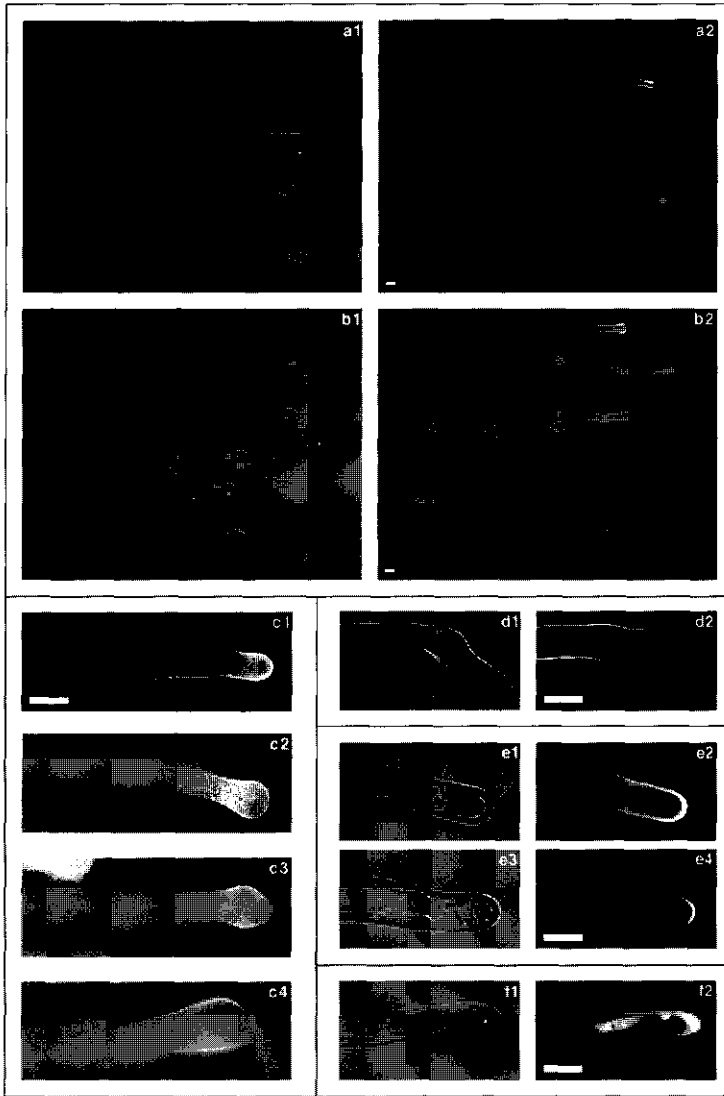


Figure 2: Phase contrast and fluorescence images of *Vicia sativa* root hairs after incubation with BODIPY labeled Nod factors or fatty acid. All images shown are representative data of multiple (at least triplicate) experiments. Bars represent 15 μ m.

Phase contrast (a1, b1) and fluorescence images (a2, b2) of root hairs of *Vicia sativa* 10 minutes (a) and 3 hours (b) after incubation with 10 nM NodRlv-IV (BODIPY 581/591-C₁₆).

Images at higher magnification showing the location of NodRlv-IV (BODIPY 581/591-C₁₆) after 10 minutes (c1) and after 1.5-2 hours (c2-c4) of addition.

Differential interference contrast (d1) and fluorescence (d2) images of a deformed root hair 3 hours after addition of 10 nM NodRlv-IV (BODIPY 581/591-C₁₆).

Phase contrast (e1, e3) and fluorescence (e2, e4) images of root hairs labeled with NodRlv-IV (BODIPY 581/591-C₁₆) and plasmolyzed with 0.45 M mannitol 10 minutes after addition of Nod factor. The arrow head shows the extent to which the plasma membrane is withdrawn from the cell wall.

Differential interference contrast (f1) and fluorescence (f2) images of a root hair showing the location of 10 nM BODIPY 558/568-C₁₂ acyl chain after 10 minutes of addition.

A BODIPY-fatty acid is rapidly taken up and is located in the cytosol

To investigate whether the cell wall labeling of the fluorescent Nod factors is related to the presence of the BODIPY fluorophore, *Vicia sativa* roots were labeled with a BODIPY-labeled fatty acid. Unlike the corresponding Nod factor, the fatty acyl chain was internalized within minutes. By comparing the fluorescence image of the fatty acid (fig. 2f2) to the phase contrast image (fig 2f1), it is clear that the fatty acyl chain localized in the cytoplasm and the nucleus. Hardly any labeling of the vacuole and cell wall was observed. From this experiment it can be ruled out that the BODIPY-label itself causes the cell wall association observed for the fluorescent Nod factors.

Nod factors are immobilized in the cell wall

The remarkable observation that the new outgrowth was not labeled by fluorescent Nod factor (fig. 2b and 2d) indicates that the diffusion of Nod factors through the cell wall is slow and that the concentration of Nod factors in the medium is low. To examine Nod factor mobility after binding, the diffusion times of the fluorescent Nod factors on root hairs were studied by FCM. Only at 543 nm excitation (i.e. not at 488 or 514 nm) was the autofluorescence intensity low enough to perform FCM experiments, therefore it was not possible to study NodRlv-IV(BODIPY FL-C₁₆). So we used BODIPY 558/568 and BODIPY 581/591 labeled Nod factors, which can be effectively excited at 543 nm. A scan of the Nod factor diffusional behavior across the root hair tip was made by employing root hair growth, shown in figure 3. The first (extracellular) curve revealed fast diffusion of Nod factor, typical for Nod factor monomers in solution (Goedhart et al., 1999). As soon as the root hair tip grew inside the confocal volume element the fluorescence intensity increased many-fold (figure 3a), reflecting a significant increase in local Nod factor concentration, and the autocorrelation curve shifted to diffusion times around 100 ms indicating very slow diffusion (figure 3b). This clearly shows that Nod factors concentrate in the cell wall and concurrently become immobilized. A few minutes later, the confocal volume element was positioned in the cytosol of the growing root hair. The count rate (fluorescence intensity) in the cytosol was much less as compared to the cell wall but still was two to three times higher than in hairs of plants incubated with unlabeled Nod factors or untreated plants. In addition, the autocorrelation curve shifted to faster values, indicating approximately a sevenfold increase of diffusional mobility in the cytosol as compared to the cell wall.

To investigate the diffusional behavior quantitatively, several individual measurements were performed on cell walls (close to the tip) and cytoplasm of root hairs labeled with the different Nod factors. Analysis with a single diffusion time did not accurately describe the experimental curves, whereas a two-component model was satisfactory. At present we do not have a physical explanation for the apparent complex diffusional behavior (being a mix of slower and faster diffusing molecules), but we note that in other FCM studies also complex intracellular diffusional behavior was observed (Brock et al., 1998; Brock et al., 1999; Schwille et al., 1999).

Schwille et al. introduced an anomalous diffusion constant, after which the use of only two fit parameters (instead of the three used here) could describe the data (Schwille et al., 1999).

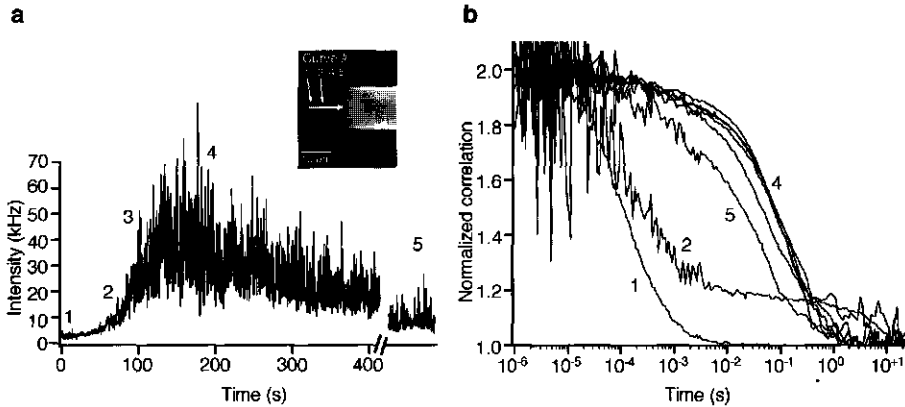


Figure 3: FCM experiments on a living *Vicia sativa* root hair incubated with 10 nM NodRlv IV(BODIPY 581/591-C₁₆) for ten minutes.

The confocal volume element was positioned outside the root hair, but close to the root hair tip. Subsequently, the fluctuations in intensity were monitored (a), giving the autocorrelation curves shown in panel b. The root hair tip grew into the confocal volume element, which resulted in a scan of Nod factor diffusional behavior across the root hair axis at the root hair tip. The different positions of the root hair with respect to the confocal volume are indicated: the root hair just outside the confocal volume (1), the tip of the root hair touching the confocal volume (2+3), the volume element across the cell wall (4), and the confocal volume completely in the cytosol (5). The steep increase of fluorescence (3) gives rise to an aberrant correlation curve that can not be analyzed and therefore this curve was omitted in the figure. The experiment was repeated at least 3 times for both the NodRlv IV(BODIPY 581/591-C₁₆) and NodRlv IV(BODIPY 558/568-C₁₂) Nod factors and essentially similar curves were acquired.

To come to a better comparison between the different experiments we calculated an average diffusion time, $\langle\tau_{diff}\rangle$ from both diffusion times and their relative contribution (see table 1). In the cell wall, the analysis showed a shorter diffusion time of 2.5 to 7.0 ms and a longer diffusion time ranging from 112 to 335 ms for all three Nod factors. The average diffusion time of the different Nod factors in the cell wall (90 to 218 ms) was considerably slower than for free Nod factor in medium (0.1 ms), showing that Nod factor diffusion was approximately $10^3 - 2 \times 10^3$ -fold reduced in the cell wall. In the cytosol, the average diffusion times of Nod factors were faster as compared to the cell wall, and were similar to diffusion times observed in the cytosol of unlabeled plants. This implies that autofluorescent and Nod factor labeled cytosolic particles diffuse with comparable rates. It is striking that the diffusion characteristics of the most active and inactive Nod factor (for bioactivity see materials and methods), NodRlv-IV(BODIPY 581/591-C₁₆) and NodRlv-IV(BODIPY 581/591-C₁₁), respectively, were nearly identical.

Apart from diffusional behavior, also the average number of fluorescent particles (N_m) and fluorescence intensity inside the confocal volume element can be estimated with FCM. In the cytosol on average 9 particles containing NodRlv-IV(BODIPY 558/568-C₁₂) were localized within the confocal volume element, whereas for both NodRlv-IV(BODIPY 581/591-C₁₁) and

NodRlv-IV(BODIPY 581/591-C₁₆) about 20 particles were detected. The latter value was obtained after correcting for autofluorescence which gave 10 particles with nearly identical intensity (counts) per particle and diffusion time. Given the calibrated size of the confocal volume element of approximately $1.15 \cdot 10^{-15}$ L, this would imply a concentration of particles containing fluorescent Nod factor of about 14 nM, assuming one Nod factor per particle. Because the counts per particle in the cytosol was similar to that observed extracellularly in PGM, in which we know that Nod factors diffuse as monomers (Goedhart et al., 1999), this is a reasonable assumption. Moreover, the quantum yield of BODIPY fluorescence is similar in water, lipid bilayers and different organic solvents (Johnson et al., 1991).

Table 1: Parameters^a describing the analysis of FCM experiments performed with fluorescent Nod factors on *Vicia sativa* root hairs

Nod factor ^b (10 nM)	location	number of experiments	percentage of τ_{diff1}	τ_{diff1} (ms)	τ_{diff2} (ms)	$\langle \tau_{diff} \rangle$ (ms)	Count rate (kHz)	N_m^c
none	cytosol	11	39 ± 21	1.8 ± 1.5	95 ± 65	52 ± 30	6 ± 2	10 ± 6
none	cell wall	27	25 ± 15	1.7 ± 2.2	54 ± 29	39 ± 16	14 ± 4	5 ± 2
BODIPY 558/568-C ₁₂	cytosol	15	41 ± 15	1.9 ± 1.3	77 ± 48	44 ± 23	13 ± 6	9 ± 4
BODIPY 558/568-C ₁₂	cell wall	9	31 ± 13	7.0 ± 4.6	335 ± 197	218 ± 111	55 ± 21	34 ± 19
BODIPY 581/591-C ₁₁	cytosol	7	37 ± 14	3.2 ± 1.6	123 ± 49	63 ± 33	16 ± 5	31 ± 10
BODIPY 581/591-C ₁₁	cell wall	4	16 ± 7	2.5 ± 1.3	170 ± 64	145 ± 58	52 ± 18	47 ± 7
BODIPY 581/591-C ₁₆	cytosol	6	39 ± 15	3.6 ± 1.2	122 ± 25	75 ± 20	17 ± 5	30 ± 8
BODIPY 581/591-C ₁₆	cell wall	8	19 ± 6	3.9 ± 4.3	112 ± 36	90 ± 27	46 ± 16	49 ± 22

^aStandard deviations shown in the table are calculated from experiments on different root hairs and hence reflect true variations in Nod factor-mobility in different root hairs rather than reflecting the standard error of the fitted parameters in one single experiment (which are much smaller).

^bAcyl chain of the added Nod factor, chitin backbone was NodRlv-IV for all Nod factors

^cAverage number of particles in the confocal volume element

At the cell wall, the number of particles containing fluorescent Nod factors inside the confocal volume element was estimated to be 35-50, representing a particle concentration of 50-72 nM. Considering the dimensions of the xy-plane of the volume element (diameter of 0.6 μ m), the cell wall thickness of approximately 0.15 μ m (Sherrier and VandenBosch (1994) and A.M.C. Emons, personal communication), and the orientation of the cell wall of the root hair tip, being parallel to the z axis of the confocal volume, only a quarter of the confocal volume element could be occupied by the cell wall at any time. Consequently, the concentration of fluorescent particles at the cell wall calculated above should be four times higher. As the number of counts per particle was twofold higher in the cell wall as compared to the cytosol (see Table 1), this implies that each detected particle in the cell wall contained on average 2 times more Nod factors than in the cytosol. Taken together, this would yield an approximate Nod factor concentration of 500 nM in the cell wall, i.e. 50-fold higher than initially added. If we assume a uniform labeling of the entire root hair surface, and calculate the total number of Nod factors associated to the cell

wall of one root hair (with average dimensions length 300 μm , diameter 13 μm , cell wall thickness 0.15 μm), the 500 nM local Nod factor concentration implies that under the employed conditions roughly about 550,000 Nod factor molecules (10^{-18} mol) were bound at a cell wall of a single root hair. Because Nod factors seem more concentrated at the tip of the root hair (where the FCM measurements have been performed, e.g. see fig. 2), this number would be an overestimation, setting a clear upper limit to the total number of Nod factor-binding sites per root hair required for inducing root hair deformation. In this respect it is of interest to note that even at a 100-fold lower concentration of this Nod factor, deformation can still be induced (Goedhart et al., 1999).

The fluorescence arising from the cytoplasm after application of fluorescent Nod factor was significantly higher than autofluorescence, but could be detected only with the very sensitive FCM technique and not by confocal laser scanning microscopy (CLSM) or fluorescence digital imaging microscopy (FDIM) (due to low signal to noise and to high out-of-focus cell wall fluorescence levels, respectively). It should be noted that the diameter of the Gaussian confocal volume element in the axial direction (two times ω_z) was about 4.1 μm with the employed objective. As root hairs have a diameter of 10-15 μm , it cannot be ruled out completely that some fluorescence of the cell wall was picked up, especially at positions close to the root hair tip. However, the difference in diffusional behavior shows that most of the signal picked up in the cytosol cannot be attributed to out-of-focus fluorescence of the cell wall.

The minor intracellular portion implies that some Nod factors or degradation products thereof entered the cytosol. In a recent systematic *in vivo* FCS study by Schwille et al. it was described that cytoplasmic diffusion is 4-10 times slower than diffusion in aqueous buffers (Schwille et al., 1999). However, in our experiments the Nod factor-diffusion speed in the cytosol was approximately 100 times slower than in aqueous solution (see fig. 3). Equation 3 (under certain assumptions) predicts that we observed particles with diameters of roughly 700 nm. Therefore, we think that the fluorescence in the cytosol reflects endomembrane-association (possibly cytosolic vesicles) rather than single diffusing molecules. It is of note that very similar particle numbers and diffusion times were found in the cytosol after incubation with a 100-fold lower concentration (i.e. 0.1 nM) of BODIPY- C_{12} fatty acid which was readily taken up in the cytoplasm (see Figure 2f). Thus, cleavage of only 1% of the applied Nod factors releasing the acyl chain could explain the observed intracellular diffusion times. In addition, if intact Nod factors were indeed present in the cytosol, an active uptake mechanism is required (i.e. endocytosis) since Nod factors by themselves are unable to cross a membrane (Goedhart et al., 1999). Hence, we favor the idea that the cytosolic fluorescence after Nod factor application reflects the accumulation of a fluorescent degradation product or possibly a small fraction of internalized (membrane linked) down-regulated Nod-factor receptors, rather than a primary Nod factor-signaling event.

Discussion

FCM is especially powerful for obtaining detailed information on molecular interactions (protein-protein, ligand-receptor etc.) at low concentration (Berland et al., 1996; Brown and Royer, 1997; Rauer et al., 1996; Rigler, 1995). It is of great importance to utilize this potential for plant cell studies, thereby fully exploiting the submicron spatial resolution of the technique. By successfully applying FCM for monitoring *in vivo* molecular behavior of fluorescent Nod factors in living plant root hairs, our study represents a first step towards achieving this goal.

We obtained well defined *in vivo* correlation curves (e.g. see Figure 3b), demonstrating that in plant root hairs autofluorescence levels at the employed excitation wavelength (543 nm) are low enough for enabling the application of the very sensitive (single molecule detection) FCM technique. Of course FCM is not restricted to studies of Nod factor behavior. FCM is generally suitable for monitoring fluorescent molecules active at (sub)nanomolar concentrations, which just happens to coincide with the physiologically relevant Nod factor concentrations.

Two important parameters can be quantified with FCS with high spatial resolution: the local diffusion speed and the average number of fluorescent particles in the submicron FCM-confocal excited volume. As discussed below, quantifying these parameters for fluorescently tagged Nod factors in living root hairs provides new insights in Nod factor-perception mechanisms.

Firstly, Nod factors concentrate 50-fold in the cell wall (to 500 nM) and the extracellular supply of Nod factors (10 nM initially) is nearly exhausted 3 hours after application. This, demonstrates, quantitatively and for the first time, the extensive Nod factor-binding capacity of the cell wall.

Secondly, the very slow lateral diffusion of Nod factors in the cell wall and the inability of Nod factors to diffuse from the cell wall to the plasma membrane, are indicative of tight (i.e. high affinity) binding to the cell wall. Bono et al. (1995) characterized a Nod factor binding site in root extracts of *Medicago truncatula*. Interestingly, this binding site (with a K_d of 86 nM) was most abundant in a high density fraction containing cell wall material, which does support our observations. Using the dissociation constant of 86 nM, we calculated the extent of equilibrium binding of Nod factors at binding site concentrations of 500 nM (this is the occupied binding site concentration in cell walls as estimated by FCM) or 100-fold higher binding site concentration (see methods section). The 100-fold higher site concentration was taken into account because the Nod factor binding was not saturated at 10 nM exogenously applied Nod factor, and consequently the actual binding site concentration must be > 500 nM. At a binding site concentration of 500 nM, the 86 nM dissociation constant predicts that about 85% of the added Nod factors are bound to the sites. At a 100-fold higher site concentration this value is 99.8%, which fits well with the observed concentration of Nod factors in the cell wall and the concomitant near exhaustion of extracellular applied Nod factors, as judged from the unlabeled outgrowth. The more recently described high-affinity binding sites from *Medicago varia*

(Gressent et al., 1999) would even predict higher binding efficiencies. The accumulative properties of the cell wall imply that if one aims at assessing binding constants under *in vivo* conditions, not only the concentration of externally added Nod factors, but also the time of exposure and the total incubation volume should be considered. For the root hair deformation assay we use, it is known that in order to get a full response to Nod factors at 10^{-11} M, the roots should be exposed to Nod factor solution for at least 10 minutes (Heidstra et al., 1994). This might reflect a minimum accumulation threshold that is required for deformation.

Thirdly, irrespective of the difference in biological activity of the fluorescent Nod factors, their location on *Vicia sativa* roots is very similar (data not shown) and FCM experiments show no apparent differences in accumulation and degree of immobilization of the Nod factors at the cell wall. Furthermore, addition of NodRlv-IV (BODIPY 558/568-C₁₂) to roots of the non-legume *Arabidopsis thaliana*, also showed cell wall labeling of root hairs albeit at reduced levels (approximately 5-fold lower, data not shown). Thus, binding to the cell wall is not strictly correlated with the capability of a factor to induce root hair deformation. Interestingly, the Nod factor binding site studies by Bono et al. show similar results: Nod factors incapable of inducing root hair deformation in *Medicago* can bind effectively to the binding site, and also in tomato root subcellular fractions, a Nod factor binding activity was found with the same K_d as observed for the *Medicago* root extract, but with a 4-fold reduced amount of binding sites (Bono et al., 1995). These findings suggest that the cell wall associated binding sites are not the putative signaling receptors. Nonetheless, we think that the binding sites in the cell wall can play an important role in concentrating and immobilizing Nod factors prior to exposing them to the putative signaling receptor for which the plasma membrane is the most probable location. This may serve two goals: i) a more efficient detection mechanism than direct binding to a (possibly much lower abundant) receptor molecule; or ii) a localization mechanism pinpointing the site of Nod factor secretion (i.e. the *Rhizobium* bacteria). Besides the Nod factor binding sites characterized (Bono et al., 1995; Gressent et al., 1999; Niebel et al., 1997), chitinases and chitinase-like receptors (Kawamura et al., 1999; Kim et al., 1998; Staehelin et al., 1994b) or the recently discovered apyrases (with lectin binding sites) (Etzler et al., 1999) are likely candidates for accomplishing these two goals. In this respect it is of interest to note that binding of a single Nod factor molecule secreted by one *Rhizobium* bacterium ($1 \times 2 \mu\text{m}$) to the adjacent root hair cell wall, already represents a local concentration of 6 nM (assuming a cell wall thickness of $0.15 \mu\text{m}$). Our results indicate that if many more Nod factor molecules are secreted, a steep lateral Nod factor gradient can appear in the cell wall due to the extensive binding capacity and slow lateral diffusion at the cell wall. We speculate that such local Nod factor concentration gradients can be instrumental for directing root hair curling and for localizing infection thread initiation. Future experiments should indicate whether local Nod factor application (e.g. Nod factor decorated beads) can cause root hair curling in the absence of rhizobia.

In conclusion, the new FCM technique provided detailed insight in the behavior of Nod factor molecules on living root hairs. Particularly, the observation that Nod factors are immobilized

and concentrated many-fold in cell walls (possibly preceding the interaction with a signaling receptor) urges for a re-definition of Nod factor receptor affinity in terms of equilibrium dissociation constants. Our findings demonstrate the usefulness and exciting future potential of FCM for measuring molecular behavior of molecules at low concentrations with minimal perturbation in living plant cells. Especially the study of the fate and interactions between signaling (ligand) molecules and the study of oriented diffusion (due to cytoplasmic streaming or other means of active transport) are promising research areas for future *in situ* plant studies with the FCM technique.

Materials and Methods

Materials

BODIPY 558/568-C₁₂ was purchased from Molecular Probes Europe (Leiden, The Netherlands). DMSO (spectroscopic grade) was from Merck (Darmstadt, Germany). Mannitol (plant cell culture tested) was from Sigma (Zwijndrecht, The Netherlands).

Fluorescent Nod factors

The synthesis and bioactivity of NodRlv-IV(BODIPY FL-C₁₆) [10⁻⁹ M], NodRlv-IV(BODIPY 558/568-C₁₂) [10⁻⁸ M] NodRlv-IV(BODIPY 581/591-C₁₁) [Not active ≤ 10⁻⁷ M] and NodRlv-IV(BODIPY 581/591-C₁₆) [10⁻¹⁰ M] is described by (Gadella Jr. et al., 1997b) and (Goedhart et al., 1999). The numbers between brackets denote the lowest concentration at which the Nod factor derivatives are bioactive in the root hair deformation assay (Heidstra et al., 1994).

Plant material and root hair deformation assay

Seeds of *Vicia sativa*, subspecies *nigra*, were germinated and grown in modified Fåhrens slides (Bhuvaneswari and Solheim, 1985) as described earlier (Heidstra et al., 1994; Van Brussel et al., 1982). The plant growth medium (PGM) was composed of 2.72 mM CaCl₂, 1.95 mM MgSO₄, 2.20 mM KH₂PO₄, 1.26 mM Na₂HPO₄ and 0.08 mM Fe(III) citrate. Root hair deformation assays were done as described by (Heidstra et al., 1994). DMSO concentrations were never higher than 0.1% (v/v). Plasmolysis of the root hairs was done by replacing the PGM by 0.45 M mannitol in water.

Arabidopsis thaliana seeds were surface-sterilized in 70% ethanol for 5 minutes, followed by 20% bleach and 0.05% (v/v) Triton X-100 for 5 minutes. After sterilization, they were washed 3 times in sterile water and stored in water at 4 °C. After germination, plantlets were transferred to Fåhrens slides (spacing between object and coverglass of 0.3 mm), and grown in half strength (2.2 g/l) Murashige and Skoog medium (Murashige and Skoog, 1962) including vitamins (Duchefa Biochemie B.V., Haarlem, The Netherlands) at 20 °C with a 16 hr light period. Four to five days after germination they were used for microscopy.

Fluorescence correlation microscopy

FCS measurements were performed with a Zeiss-EVOTEC ConfoCor (Carl-Zeiss, Jena, Germany and Evotec Biosystems, Hamburg, Germany). The system is described in detail elsewhere (Hink et al., 1999; Hink and Visser, 1998). Briefly, the system consists of an Zeiss inverted confocal microscope, and uses either an air-cooled argon ion laser (488 and 514 nm) or a helium-neon laser (543 nm) for excitation. Standard confocal epi-fluorescence microscope optics are used, including dichroic mirrors (510 nm or 560 nm for the respective laser lines), a Zeiss water immersion objective (C-Apochromat 40×, 1.2 NA, 440052), and bandpass filters for selecting the fluorescence emission (515-565 nm or 565-610 nm for the respective laser lines). The emission was spatially filtered through a pinhole (diameter 40 μm) and detected by an avalanche photodiode coupled to a fast digital correlator. Data acquisition and analysis were performed using the FCS ACCESS software package (EVOTEC/Zeiss, Inc., version 1.0.12). For all FCM experiments, Fåhrus slides (Bhuvaneswari and Solheim, 1985) were used (also for calibration). Fåhrus slides were inverted in such way that the cover glass was facing the objective. The laser beam was focused approximately 150 μm above the bottom of the cover glass. The calibration is performed using tetramethylrhodamine in H₂O as described before (Goedhart et al., 1999) and yielded values of ω_{xy} (see equation 2-3) around 0.3 μm. Acquisition times for calibration and samples were 30-60 s. All experiments were done at room temperature.

Fluorescence microscopy

The root system of *Vicia sativa* was incubated with 1 ml 10 nM Nod factor in Fåhrus slides for 10 minutes to 3 hours. Fluorescence microscopy was performed with the FRIM system described by (Gadella Jr. et al., 1997b) based on a Leica DMR microscope (Leitz, Wetzlar, Germany) with Leitz fluotar 10× NA 0.3 air or fluotar 40× NA 0.5-1.0 oil immersion objectives. In addition to the CH250 CCD-camera, images were captured by a Quantix CCD-camera (Photometrics, Tucson, AZ) interfaced through a PCI-card to an Apple Macintosh PowerPC 8500/180 computer (Apple computer, Cupertino, CA) and controlled by IPLab 3.1 software (Signal Analytics, Vienna, VA).

Fluorescence of BODIPY 558/568 or BODIPY 581/591 was observed by excitation at 568 nm with an Innova 70 Ar/Kr mixed-gas laser or by passing the excitation light of a 100 W USH-102D mercury lamp (Fairlight, Rotterdam, The Netherlands) through a Omega 546DF10 nm or 577DF10 nm bandpass filter, emission was separated by a dichroic mirror (555 nm or 595 nm) and passed through an Omega 580DF40, 605DF50 or 625DF50 bandpass or a Schott (Mainz, Germany) OG575 nm longpass filter.

Calculation of equilibrium binding of Nod factors to a Nod factor binding site

The calculations were made on basis of the equilibrium dissociation constant definition: $K_d = [N]_{\text{free}} \times [S]_{\text{free}} / [S]_{\text{bound}} = \{(N_0 - X) \times (S_0 - X)\} / X$. Here N stands for Nod factor, S for binding

sites, N_0 is the total Nod factor concentration (bound+free), S_0 is the total binding site concentration, and X is the bound Nod factor concentration. After rearranging this expression $X=(N_0+S_0+K_d-\text{SQRT}\{(N_0+S_0+K_d)^2-4\times N_0\times S_0\})/2$ is obtained. The percentage of bound Nod factors (Y) is then given by $Y=(X / N_0)\times 100\%$

Acknowledgments

We are grateful to Horst Röhrig, Jürgen Schmidt and Michael John (Abteilung Genetischen Grundlagen der Pflanzenzüchtung, Max-Planck-Institut für Züchtungsforschung, Köln, Germany) for their continuous interest and help in the synthesis of the fluorescent Nod factors. We thank Tijs Ketelaar (Laboratory for Plant Cytology and Morphology, Wageningen Agricultural University, The Netherlands) for providing us with Arabidopsis seedlings in Fährus slides. The fluorescence correlation spectroscopy setup was made available by an investment grant awarded by the Netherlands Organization for Scientific Research (NWO). J.G. and M.A.H. are supported by the Netherlands Council of Earth- and Life Sciences (ALW), T.W.J.G. by the Royal Netherlands Academy of Arts and Sciences (KNAW).

LOCALIZATION, IMMOBILIZATION AND CELL WALL ACCUMULATION OF SULFATED AND NON-SULFATED NOD FACTORS IS IDENTICAL IN ROOT HAIRS OF HOST AND NON-HOST LEGUMES**Abstract**

Nod factors are signaling molecules secreted by *Rhizobium* bacteria. These lipochitooligosaccharides (LCOs) are required for the early steps of symbiosis with legumes and are capable of eliciting specific responses at subnanomolar concentrations on a compatible host legume. The bioactivity of three fluorescent sulfated LCOs was tested in a root hair deformation assay on the model plant *Medicago truncatula*, showing a relatively high bioactivity (>1 nM) for the different derivatives. A green fluorescent derivative was used for a transfer assay, showing fast transfer between phospholipid vesicles, but no transbilayer flip-flop. A novel orange fluorescent derivative carrying a BODIPY 558/568-C₁₂ acyl chain could induce root hair deformation at concentrations down to 0.1 nM and is used to study the location and diffusional mobility on root hairs. Fluorescence microscopy of plasmolyzed root hairs shows that fluorescent Nod factors accumulate in the cell wall of root hairs, whereas they are absent from the plasma membrane when applied at 10 nM. Fluorescence correlation microscopy was used to study in detail the mobilities of fluorescent Nod factors on a host and a non-host legume. The results show that Nod factors hardly diffuse and strongly accumulate in root hair cell walls of *Medicago truncatula* and *Vicia sativa*, independent of the sulfate group. Experiments on root hairs of the *hcl* mutant, which is disturbed in root hair curling, show a similar distribution of fluorescent Nod factors compared to wild-type plants. These results indicate that the mutant is not disturbed in Nod factor immobilization. The implications for the perception of Nod factors are discussed.

Joachim Goedhart, Jean-Jacques Bono[§], Ton Bisseling and Theodorus W.J. Gadella Jr.

[§]Laboratoire de Biologie Moléculaire des Relations Plantes-Microorganismes, UMR 215 INRA-CNRS, BP 27 31326 Castanet-Tolosan, France.

Introduction

Nod factors are signaling molecules produced by rhizobia and are required to accomplish symbiosis with a compatible legume (Heidstra and Bisseling, 1996; Long, 1996). Nod factors are lipo-chitooligosaccharides (LCOs) comprising a chitin backbone of three to five β -1,4-linked N-acetylglucosamine (GlcNAc) residues and an acyl chain which is N-linked to the non-reducing terminal sugar. Nod factors, either purified from rhizobial cultures or chemically synthesized, elicit a wide variety of specific responses at picomolar concentrations on their compatible host plant (Downie and Walker, 1999). These responses include ion-fluxes (Felle et al., 1998), calcium spiking (Ehrhardt et al., 1996; Wais et al., 2000; Walker et al., 2000), activation of phospholipases (Den Hartog et al., 2001; Pingret et al., 1998) all within ten minutes, followed by root hair deformation (Heidstra et al., 1994; Lerouge et al., 1990) and gene expression (Pingret et al., 1998) after a few hours. The substitutions on the chitin backbone are the main determinants of host-specificity. Also the structure of the acyl chain can modulate activity (Demont-Caulet et al., 1999; Goedhart et al., 1999; Spaink et al., 1991). Nod factors produced by *Rhizobium leguminosarum* bv. *viciae* have an acetate on the non-reducing GlcNAc as the only substitution on the chitin backbone (Spaink et al., 1991). *Sinorhizobium meliloti* secretes a similar Nod factor with the main exception being a sulfate group on O-6 of the reducing GlcNAc (Lerouge et al., 1990). The sulfate group is essential for accomplishing symbiosis with host plants like *Medicago truncatula* and *Medicago sativa* (Roche et al., 1991). As a consequence, mutation of the rhizobial *nodH* gene (a sulfotransferase), responsible for the 6-O-sulfation of Nod factors, renders the bacteria completely inactive on their host plant *Medicago sativa*. However, the same mutation confers compatibility with the non-host *Vicia sativa*, which is not observed with the wild-type *Sinorhizobium meliloti* bacteria (Roche et al., 1991). Hence, when these two legumes are considered, the presence or absence of the sulfate group is the primary determinant of host specificity.

The high specificity and the low concentration at which Nod factors are active strongly suggest the involvement of a Nod factor receptor. Although several Nod factor binding proteins have been characterized biochemically (Bono et al., 1995; Etzler et al., 1999; Gressent et al., 1999; Niebel et al., 1997), so far no Nod factor receptor has been identified. Bono and coworkers have characterized two different binding activities in an extract from *Medicago truncatula* roots and from extracts of a *Medicago varia* cell culture (Bono et al., 1995; Gressent et al., 1999; Niebel et al., 1997). A low affinity binding site (termed NFBS1, $K_d=86$ nM) found in the root extract from *Medicago truncatula* was also present in the non-legume tomato (Bono et al., 1995). Besides a low affinity site, a high affinity site was found in a *Medicago varia* cell culture extract (NFBS2, $K_d=4$ nM), which was enriched in the microsomal fraction (Gressent et al., 1999). Interestingly, both binding activities do not discriminate between sulfated and non-sulfated Nod factors. Recently, a lectin with Nod factor binding capability has been isolated from the legume *Dolichos biflorus*. Biochemical studies have revealed that the lectin has phosphohydrolase

activity which can be induced by Nod factors and that it is present on the surface of root hairs (Etzler et al., 1999).

Using genetic approaches, several mutants that are disturbed in Nod factor signaling have been isolated (Cullimore et al., 2001). Mutants disturbed in Nod factor perception should not display any early Nod factor responses such as calcium spiking, which was used to characterize several mutants (Wais et al., 2000; Walker et al., 2000). However, to date it is not clear whether any of the mutants that are disturbed in calcium spiking are blocked in signaling at the level of the Nod factor receptor.

Another strategy in obtaining insight in the mechanism of Nod factor perception is to study the location and molecular behavior of Nod factors when added to roots. A prerequisite is the presence of a sensitive and specific label on the Nod factor, which is satisfied by using a fluorescent reporter group. The use of ligands tagged with a fluorescent group has been successfully applied for several decades for the study of ligand-binding to receptors in mammalian cell cultures (Shechter et al., 1978). A variety of dedicated fluorescence techniques can be employed for studying ligand-receptor interactions (for a review see (Hovius et al., 2000)). So far, only a limited number of fluorescently labeled ligands have been used for plant studies. Previously, we described the use of non-sulfated fluorescent Nod factor derivatives in the study of Nod factor perception by the compatible legume host *Vicia sativa* (Gadella Jr. et al., 1997b; Goedhart et al., 2000). We could show that Nod factors, when applied at low concentration, are located within the cell wall, and are absent from the plasma membrane (Goedhart et al., 2000). In the same study, fluorescence correlation microscopy (FCM) was used to monitor the diffusional characteristics of the fluorescent Nod factors on the root hairs of *Vicia sativa*. FCM measures intensity fluctuations originating from single fluorescent molecules moving across a continuously excited laser spot, which can be related to diffusion constants and particle numbers (Maiti et al., 1997). The FCM experiments revealed that the fluorescent Nod factors accumulate and immobilize within root hair cell walls of *Vicia sativa* (Goedhart et al., 2000). Together these results were surprising, since it has been shown that in the presence of membrane-like structures, Nod factors insert their lipid tail into the hydrophobic core of the membrane, suggesting association with the root hair plasma membrane (Goedhart et al., 1999). Moreover, in order to transduce the Nod factor signal across the plasma membrane, it is likely that putative Nod factor receptors are located within the plasma membrane. In this study we compare the perception of non-sulfated and sulfated Nod factors on the legume species *Vicia sativa* and *Medicago truncatula*. Novel fluorescent sulfated Nod factors are described and like the non-sulfated Nod factor analogs used for studying root hair deformation, location and diffusional behavior *in situ* on both host and non-host legume root hairs. These studies enable us to directly assess the influence of the sulfate group on the Nod factor binding and perception *in vivo*.

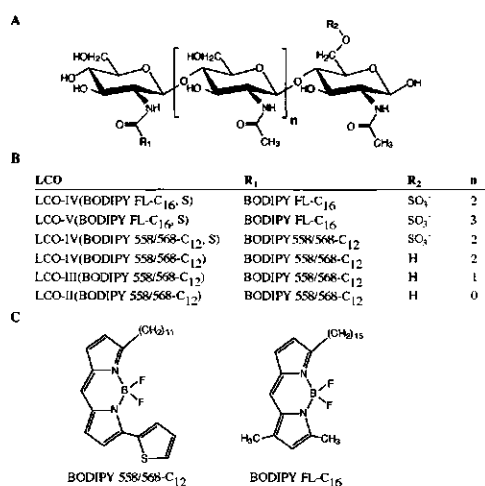


Figure 1: Structures of the fluorescent LCOs described in this study. The chitin-like headgroup (A) with different acyl chains (R₁), sulfated or non-sulfated (R₂) and different degrees of GlcNAc polymerization referred to as pentamers (n=3), tetramers (n=2), trimers (n=1) and dimers (n=0). (B) The novel fluorescent sulfated Nod factors have two different fluorescent acyl chains, either the green fluorescent BODIPY FL-C₁₆ or the orange fluorescent BODIPY 558/568-C₁₂ (C). Note that LCO-IV(BODIPY 558/568-C₁₂) is identical to the previously described NodRiv-IV (BODIPY 558/568-C₁₂) (Goedhart et al., 1999).

Results

Fåhrens slide system for the study of Medicago truncatula root hairs

Root hair deformation on *Vicia sativa* grown in Fåhrens slides has been used as an assay for bioactivity of Nod factors (Heidstra et al., 1994). This assay is relatively fast, semi-quantitative and allows to study the root hairs in real-time by (fluorescence) microscopy. In previous studies this system was used by us to evaluate the bioactivity of fluorescent LCO-IV, its location on the root hairs and diffusional behavior (Gadella Jr. et al., 1997b; Goedhart et al., 2000; Goedhart et al., 1999).

In order to study fluorescent sulfated LCOs and to compare the results with the unsulfated derivatives it was necessary to evaluate whether the Fåhrens slide system, used for *Vicia sativa*, was also suitable for *Medicago sativa* and *Medicago truncatula*. It appeared that upon addition of plant growth medium, lacking Nod factors, morphogenic responses such as swelling were induced in the root hairs of *M. sativa*, rendering these plants useless for deformation studies in our Fåhrens slide system (data not shown). The root hairs of *Medicago truncatula* retained their normal morphology after transferring them to the Fåhrens slide, and application of 10⁻⁹ M NodRm-IV (Ac,S) (a natural Nod factor) induced clear root hair deformations within three hours, whereas replacing the medium, without Nod factor, did not show any effect. Hence, we decided to focus on *M. truncatula* as the host plant for studying sulfated LCOs in the deformation assay. An advantage of the *M. truncatula* root hairs is that the air-grown root hairs

maintain their cytoarchitecture after transfer from the agarose plates to PGM containing Fåhrens slides, which is in contrast with root hairs of *Vicia sativa*.

Table 1: Three fluorescent sulfated Nod factors were tested for their root hair deforming activities on *Medicago truncatula*.

Nod factor	10 ⁻⁸ M	10 ⁻⁹ M	10 ⁻¹⁰ M	10 ⁻¹¹ M
LCO-IV(BODIPY FL-C ₁₆ , S)	+	+/-	-	nt
LCO-V(BODIPY FL-C ₁₆ , S)	+	+	-	nt
LCO-IV(BODIPY 558/568-C ₁₂ , S)	+	+	+	-

+ : significant deformation
 +/-: reduced level of deformation
 - : no deformation
 nt : not tested

Bioactivity of Sulfated Nod factors

Since the Fåhrens system can be used for root hair deformation tests on *Medicago truncatula*, we used this assay to examine the bioactivity of the fluorescent sulfated Nod factor analogs. Three fluorescent sulfated Nod factors were used: LCO-IV(BODIPY FL-C₁₆, S), LCO-V(BODIPY FL-C₁₆, S) and LCO-IV(BODIPY 558/568-C₁₂, S), see figure 1. The bioactivity of these Nod factors in the root hair deformation assay on *Medicago truncatula* is listed in table 1. All three Nod factors are bioactive at concentrations down to 1 nM, although the activity of LCO-IV(BODIPY FL-C₁₆, S) is reduced at this concentration.

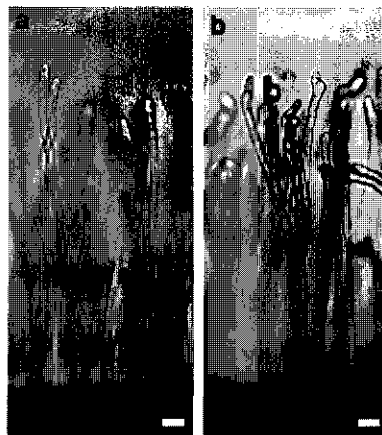


Figure 2: Root hair deformation on *Medicago truncatula* using a fluorescent Nod factor derivative. Three hours after addition of PGM containing (b) 0.1 nM LCO-IV(BODIPY 558/568-C₁₂, S) and 0.1% DMSO or (a) only 0.1% DMSO a clear deformation of the root hairs has taken place only when fluorescent Nod factors are present. Bars represent 30 μ m.

The orange fluorescing Nod factor derivative, LCO-IV(BODIPY 558/568-C₁₂, S), induces root hair deformation even at 10⁻¹⁰ M (figure 2), which is an order of magnitude higher than the green fluorescing sulfated Nod factors. In contrast, none of the three sulfated fluorescent LCOs was capable of inducing root hair deformation on the non-host legume *Vicia sativa* at the highest concentration tested of 10⁻⁷ M (data not shown).

Intermembrane transfer but no flip-flop of sulfated LCOs

To examine the dynamics of membrane association and intramembrane flip-flop of sulfated LCOs, we designed a similar transfer assay as was described previously for non-sulfated Nod factors (Goedhart et al., 1999). Phospholipid vesicles containing sulfated LCOs and a non-transferable fluorescence quencher were prepared by injection of an ethanolic solution of phospholipids, Texas Red DHPE and LCO-IV(BODIPY FL-C₁₆, S) in aqueous buffer solution. As can be inferred from figure 3, the fluorescence of LCO-IV(BODIPY FL-C₁₆, S) is very low directly after the ethanol injection (see arrow A). The very low fluorescence is caused by quenching by the fluorescence resonance energy transfer (FRET) acceptor Texas Red DHPE which was present in the vesicles. Because the FRET occurs only at distances <10 nm, this result demonstrates quantitative association of the Nod factor with the vesicles. Subsequently, a 10-fold excess of unlabeled acceptor vesicles is added, after which a fast increase in fluorescence is observed.

The rapid dequenching indicates that the Nod factors are rapidly transferred from the quenched donor vesicles to the unquenched acceptor vesicles. The increased level of fluorescence intensity remained stable over at least 25 minutes. Only after the addition of Triton X-100, which disrupts all vesicles thereby releasing the remaining quenched Nod factors, the fluorescence intensity increased. These results show that approximately 40% of the fluorescent Nod factors are not available for transfer to the acceptor vesicles and therefore remain within the quenched vesicles. These observations can be explained by the fact that Nod factors located in the inner leaflet of the original donor vesicles will have to flip-flop to the outer leaflet of the vesicle before transfer can occur. Hence, within the 25 minutes observation time no transmembrane flip-flop of Nod factors takes place. These results are very similar to the results obtained for non-sulfated Nod factor (Goedhart et al., 1999).

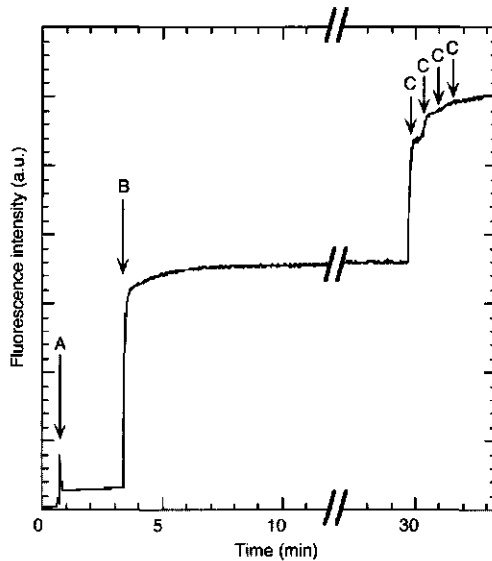


Figure 3: Intermembrane transfer of LCO-IV(BODIPY FL-C₁₆, S) from quenched donor to unquenched acceptor vesicles. The fluorescence intensity of LCO-IV(BODIPY FL-C₁₆, S) is measured in arbitrary units (a.u.). At the arrow indicated with A, donor vesicles are generated by injection of an ethanolic solution (containing DOPC: DPPA: Texas Red DHPE: LCO-IV(BODIPY FL-C₁₆, S) = 79:10:10:1 mol%, 20 nmol total lipid) into 3 ml Tris buffer under continuous stirring. For initiating spontaneous transfer, a 10-fold excess of acceptor vesicles (containing DOPC: DPPA=90:10 mol%) was added at the arrow indicated with B. After 4 subsequent additions of 25 μ l 10% (v/v) Triton X-100 in PBS (indicated by arrow C) the vesicles are completely solubilized, thereby dispersing and dequenching LCO-IV(BODIPY FL-C₁₆, S).

Location of fluorescent LCOs on Vicia sativa and Medicago truncatula roots

Although the bioactivity of the green fluorescent Nod factor derivatives is relatively high, they are less well suited for *in vivo* localization studies by fluorescence microscopy at physiological relevant concentrations due to a relative high contribution of root autofluorescence at these excitation/emission wavelengths (Gadella Jr. et al., 1997b). Red-shifted fluorescent Nod factor derivatives however, have excellent spectral properties for localization and diffusional studies at a relative low concentration as shown before (Goedhart et al., 2000; Goedhart et al., 1999). The spectroscopic properties of the novel LCO-IV(BODIPY 558/568-C₁₂, S) are identical as described for the non-sulfated Nod factor (Goedhart et al., 1999), and ideally suited for *in vivo* labeling studies.

In spite of the advantageous spectral properties it is not possible to image the orange fluorescent LCO at the threshold concentration of biological activity of 0.1 nM (data not shown). To obtain images with a reasonable signal-to-background level, the LCOs need to be applied at a concentration of 10 nM or higher. Upon application of 10 nM LCO-IV(BODIPY 558/568-C₁₂, S) to the roots of *M. truncatula*, an increase in fluorescence on the root hairs was detected, with a concomitant decrease of fluorescence in the medium near the root hair tips. Fluorescence imaging revealed surface labeling of the root hairs. To verify whether the fluorescence

represented cell wall or plasma membrane labeling, plasmolysis was induced by replacing the medium with a 0.45 M mannitol solution. After the plasma membrane was withdrawn from the cell wall, all the fluorescence was still associated with the cell wall and no fluorescence was observed in the plasma membrane (figure 4). It is of note that the acyl chain (BODIPY 558/568-C₁₂) alone accumulates immediately into the cytoplasm of *M. truncatula* root hairs (data not shown), as was also observed for *V. sativa* (Goedhart et al., 2000).

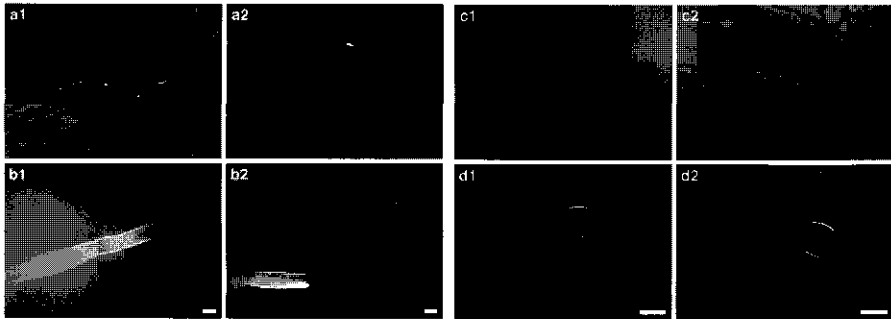


Figure 4: Digital images of *Medicago truncatula* incubated with 10 nM LCO-IV(BODIPY 558/568-C₁₂, S). After ten minutes the PGM is replaced with 0.45 M mannitol to induce plasmolysis which can be seen in the phase contrast images (a1, a2) as a retraction of the plasma membrane from the cell wall. The plasma membrane is indicated with an arrow head. The fluorescence images (b1, b2) show predominant location of the fluorescent Nod factor in the cell wall. After three hours the root hairs are deformed due to the presence of the Nod factor. The new outgrowth is clearly visible in the phase contrast images (c1, c2). Fluorescence images representing the location of LCO-IV(BODIPY 558/568-C₁₂, S) show a lack of fluorescence in the new outgrowth. Bars represent 15 μ m.

When the seedlings were incubated for three hours with 10 nM LCO-IV(BODIPY 558/568-C₁₂, S), the root hairs were clearly deformed. As can be inferred from figure 4, the newly formed outgrowths were hardly labeled, whereas the older part of the root hair was still clearly fluorescent, indicating a lack of diffusion of the LCO through the cell wall. These results are similar to the results obtained with non-sulfated fluorescent Nod factor derivatives on *V. sativa* (Goedhart et al., 2000).

FCM of fluorescent LCOs

The plasmolysis and deformation experiments point to affinity of Nod factors for the cell wall and a reduced mobility of the sulfated Nod factors in the root hair cell wall as observed for *V. sativa* labeled with non-sulfated Nod factors. In order to obtain more detailed information on the behavior of the fluorescent LCO on root hairs, fluorescence correlation microscopy (FCM) experiments were performed. A focused laser beam is positioned at the preferred location in the specimen and the fluorescence intensity fluctuations originating from the confocal volume element are measured. These fluctuations are autocorrelated, yielding information on the diffusion time that is necessary for the fluorescent molecules to cross the volume element.

Additionally, the amplitude of the autocorrelation is inversely related to the average number of fluorescent molecules inside the volume element. By fitting the autocorrelation curve, both the diffusion time and the particle number can be determined. When the dimensions of the confocal volume element are determined by calibration, the diffusion constant (see equation 1) and the concentration of the fluorescent molecules can be calculated (Goedhart et al., 2000).

Autocorrelation curves obtained from 10 nM LCO-IV(BODIPY 558/568-C₁₂, S) in PGM represented diffusion of monomers (curve 2 in figure 5) as observed before, for non-sulfated fluorescent LCOs in aqueous media (Goedhart et al., 2000; Goedhart et al., 1999). Autocorrelation curves obtained from intensity fluctuations measured in root hair tips after addition of 10 nM LCO-IV(BODIPY 558/568-C₁₂, S) to the roots of *M. truncatula* are also shown in figure 5. Qualitatively, these curves represent very long diffusion times, typical for molecular interactions on immobilized structures (Brock et al., 1999; Schwille et al., 1999). The greatly reduced mobility of sulfated Nod factor on *M. truncatula* (3 orders of magnitude) compares favorably with the immobility of their non-sulfated counterparts on *V. sativa* (Goedhart et al., 2000).

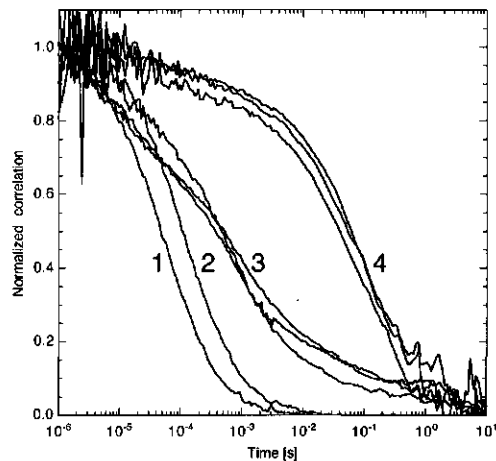


Figure 5: Normalized autocorrelation curves of TMR and LCO-IV(BODIPY 558/568-C₁₂, S) measured by FCM. The confocal volume element was positioned in the medium (1,2) to measure the diffusion of TMR (1) or LCO-IV(BODIPY 558/568-C₁₂, S) (2) or at the tip of *Medicago truncatula* root hairs to measure the mobility of TMR (3) or LCO-IV(BODIPY 558/568-C₁₂, S) (4). For the measurement in root hairs (3,4) representative curves from three individual root hairs are shown.

To further examine this reduced mobility, i.e. whether this is a result of aspecific interactions, we measured the mobility of carboxy-tetramethylrhodamine (TMR) in the presence of root hairs as well. TMR is a standard fluorescent compound often used to calibrate FCM measurements since it has a known diffusion constant and optimal spectroscopic properties for 543 nm excitation, yet it has no known biological function. Interestingly, upon application of TMR to

Medicago roots, a moderate accumulation in the root hair cell wall, but no internalization into the root hair cytosol was observed, qualitatively mimicking Nod factors. The diffusional behavior of TMR in plant growth medium was identical to the reference situation in pure H₂O (figure 5, curve 1). When the confocal volume element was positioned in the cell wall at the tip of a growing root hair and TMR-fluorescence intensity fluctuations were monitored, autocorrelation curves were shifted to longer times (see figure 5). This indicates that the mobility of TMR is reduced in root hair cell walls relative to diffusion in aqueous solution. However, TMR is still two orders of magnitude more mobile than Nod factors in root hair cell walls. Furthermore, for TMR it was possible to acquire proper autocorrelation curves in the older root hair cell wall further from the tip, whereas this was not possible for fluorescent LCOs due to very strong immobilization and consequently severe bleaching (data not shown). These data demonstrate that Nod factor binding to cell walls is strong, and clearly surpasses levels that can be explained by aspecific interactions such as observed with TMR.

Table 2: Results of the analysis of the autocorrelation curves obtained by FCM of root hair cell walls

Plant	Probe ^a	n ^b	D1 ^c ($\times 10^{11}$) m ² /s	% D1	D2 ^d ($\times 10^{13}$) m ² /s	N ^e	c ^f (nM)
<i>M. truncatula</i>	TMR	8	2.3 \pm 0.5	82 \pm 6	2.3 \pm 1.3	25 \pm 6	53 \pm 13
<i>M. truncatula</i>	LCO-IV(S)	7	3.2 \pm 2.3	20 \pm 5	2.1 \pm 0.7	52 \pm 24	113 \pm 52
<i>M. truncatula</i>	LCO-IV	8	4.8 \pm 3.7	22 \pm 5	2.3 \pm 1.4	44 \pm 16	90 \pm 33
<i>V. sativa</i>	LCO-IV(S)	8	4.7 \pm 2.3	16 \pm 9	3.2 \pm 0.9	72 \pm 36	147 \pm 74
<i>V. sativa</i>	LCO-IV	7	8.2 \pm 7.3	13 \pm 2	3.3 \pm 1.0	57 \pm 9	112 \pm 18

^aThe fluorescent Nod factor derivatives carry the BODIPY 558/568-C₁₂ acyl chain.

^bNumber of experiments

^cAverage fast diffusion constant (\pm SD)

^dAverage slow diffusion constant (\pm SD)

^eAverage number of molecules in the confocal volume (\pm SD)

^fAverage concentration in the confocal volume (\pm SD) calculated from N and the volume determined by calibration. Considering that the cell wall occupies approximately 25% of the volume element (Goedhart et al., 2000), the Nod factor concentration in the cell wall is approximately 4-fold higher than the tabulated values.

Using FCM we analyzed the mobility of the sulfated and non-sulfated Nod factors on the surface of root hairs of either *M. truncatula* or *V. sativa*. To enable a quantitative comparison, all measurements were performed by positioning the confocal volume in the cell wall at the tip of nearly full-grown root hairs. When the autocorrelation curves of TMR and fluorescent LCOs in root hair cell walls were analyzed, two diffusion constants were necessary for a proper fit as described before (Goedhart et al., 2000). The obtained parameters are listed in table 2. Interestingly, the diffusion constants for TMR and LCOs were quite similar. However, the fast diffusion constant was most significant for TMR (contributing at least 75% to the curve), whereas the contribution of the fast diffusion constant was small for fluorescent Nod factors. For all Nod factors, the slower diffusion constant contributed 80-90% and had an average value

of 2.1×10^{-13} - 3.3×10^{-13} m²/s. This is 1000-fold reduced as compared to the value of 2.68×10^{-10} m²/s for free Nod factor (Goedhart et al., 1999). Interestingly, no difference was observed when the sulfated and non-sulfated LCO were compared and also the diffusional mobility on the two different plant species was similar. These results indicate that the accumulation and mobility of Nod factors does not depend on the presence of the sulfate group, and is comparable in *V. sativa* and *M. truncatula*.

Depletion of LCOs from the medium

The observation that the new outgrowth after deformation is unstained with fluorescent LCO, implies that the root hair cell walls very efficiently absorb Nod factors from the medium. Depletion of Nod factors from the medium was confirmed with FCM by positioning the confocal volume element in the growth medium at different distances from the root hairs. It was observed that the Nod factor concentration in the medium near the root hairs was lower than the Nod factor concentration further away from the root (data not shown).

To visualize the depletion of fluorescent Nod factors from the medium, we incubated the root system of *Medicago truncatula* with 10 nM LCO-IV(BODIPY 558/568-C₁₂, S) and captured digital images of the fluorescence in the medium surrounding the root using a stereoscope equipped with a highly sensitive liquid-cooled CCD-camera. Because of the low numerical aperture of the stereoscope lens and the very low amount of label used, long exposure and camera integration times were needed. A series of fluorescence images of the root and the surrounding medium is shown in figure 6. The first image already shows that the medium close to the root hairs is less fluorescent than the medium further away from the root. During time, the fluorescence intensity of the medium decreases, with the most dramatic decrease near the root hairs. In this way the root creates a concentration gradient of fluorescent LCOs in the growth medium. These results demonstrate the remarkable capability of root hairs to absorb and concentrate Nod factors and for the first time directly and quantitatively visualize the depletion of Nod factors from the medium. It is remarkable that the steepest Nod factor gradient is observed near the region of the root containing young root hairs. Exactly these hairs are predominantly susceptible to infection by rhizobia.

Nod factor binding by the hcl mutant

It has been proposed (Goedhart et al., 2000) that the observed immobilization of Nod factors in the cell wall implies that they can provide positional information on the site where the Nod factors are secreted (i.e. the position of the *Rhizobium* bacteria). This information seems essential in order to accomplish the formation of a root hair curl around these bacteria. A recently characterized *hcl* mutant is disturbed in curling, and shows only root hair deformation in the presence of rhizobia (Catoira et al., 2001). A possible mechanism could be that this mutant is unable to immobilize Nod factors in the cell wall of root hairs and thereby is unable to perceive a localized signal in the presence of bacteria.

To study whether this was indeed the case we applied fluorescent sulfated Nod factors to the roots of mutant B56, and studied the binding characteristics. Initial binding was as for wild-type *Medicago truncatula*. Plasmolysis experiments showed that the Nod factor was located in the cell wall of root hairs of the *hcl* mutant. After three hours root hair deformation was observed, of which the reinitiated outgrowth was essentially non-fluorescent. These results are identical as compared to wild-type root hairs and show that Nod factors are also immobilized by the *hcl* mutant. Hence, also in the *hcl* mutant, Nod factors still can carry positional information, pinpointing the location of the rhizobia on the root hair.

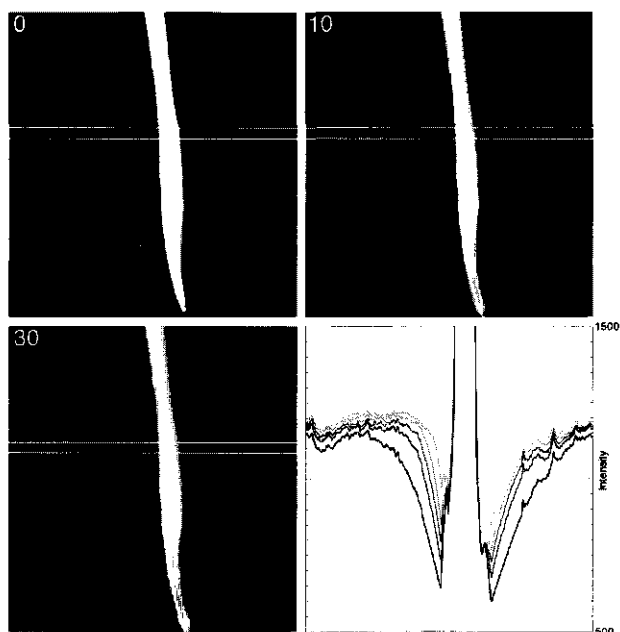


Figure 6: Fluorescent Nod factors are depleted from the growth medium by the *Medicago truncatula* root. 10 nM fluorescent LCO-IV(BODIPY 558/568-C₁₂, S) was added to the medium of a *Medicago truncatula* root, after which the fluorescence was imaged. The time series (time in minutes) show the decrease of fluorescence intensity in the medium, especially in areas close to the root. The figure in the lower right corner shows profile plots corresponding to the regions of interest shown in the digital images. The average value of each column of pixels was plotted versus the pixel number for 0, 2, 5, 10 and 30 minutes after addition of Nod factor.

Chitinase activity on roots

Plant roots exhibit Nod factor hydrolyzing activity (Heidstra et al., 1994; Staehelin et al., 1994b). To examine whether breakdown products contributed significantly to mobility measurements by FCM, we extracted and analyzed the fluorescent components from the roots after different incubation times. *Vicia sativa* root systems were incubated with 500 nM LCO-IV(BODIPY 558/568-C₁₂) for 10, 30, 60 and 750 minutes, after which both the medium was isolated and the roots were ground. Nod factors were isolated from both fractions by n-butanol extraction. When the extracts from roots were analyzed by TLC it was observed that some

fluorescent compounds from the root were present in the butanol layer, as can be seen in the first lane of the TLC in figure 7. Still, the Nod factor fluorescence can be clearly detected above the background fluorescence. From the TLC analysis of the root extracts shown in figure 7, it can be inferred that no breakdown of Nod factors is detected within the first 10 minutes. After 30 minutes less than 5% of the Nod factors was degraded. After prolonged incubation, the majority of the Nod factors is degraded to LCO-III(BODIPY 558/568-C₁₂) and LCO-II(BODIPY 558/568-C₁₂). Extracts of the medium after 10-60 minutes only showed LCO-IV(BODIPY 558/568-C₁₂), whereas LCO-II(BODIPY 558/568-C₁₂) was the major compound (>50%) present after 750 minutes (data not shown). The kinetics of Nod factor hydrolysis by roots corresponds with previous studies using radiolabeled compounds (Heidstra et al., 1994). Essentially similar results were obtained for either LCO-IV(BODIPY 558/568-C₁₂, S) or the non-sulfated derivative upon application to *Medicago truncatula* roots (data not shown). From these results we conclude that Nod factor breakdown products are a minor fraction and thereby do not interfere with the FCM measurements which are performed within 30 minutes after application of Nod factors.

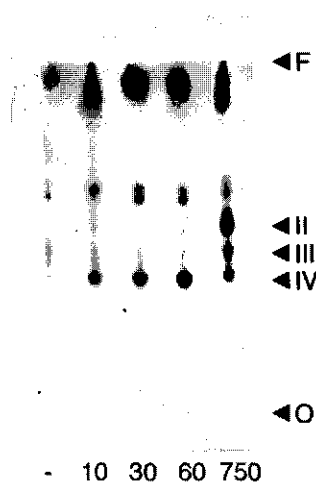


Figure 7: TLC analysis of Nod factor hydrolyzing activity of *Vicia sativa* roots. Root extracts, before and 10, 30, 60 or 750 minutes after addition of 500 nM LCO-IV(BODIPY 558/568-C₁₂), showing the degradation to LCO-III(BODIPY 558/568-C₁₂) and LCO-II(BODIPY 558/568-C₁₂).

Discussion

In this study we examined the characteristics of novel sulfated fluorescent LCOs and compared the binding by both *Vicia sativa* and *Medicago truncatula* root hairs with non-sulfated LCOs. Nod factor induced root hair deformation can be studied on the model legume *M. truncatula* in Fåhrens slides similar to *V. sativa*. This agrees with the study of Catoira et al., reporting successful root hair deformation tests on *M. truncatula* transferred to Fåhrens slides (Catoira et al., 2000). The three fluorescent LCOs have a relative high bioactivity in the root hair deformation assay. The novel sulfated BODIPY 558/568-C₁₂ labeled LCO is remarkably active (down to 10⁻¹⁰ M) which is comparable to the threshold concentration of the most active non-sulfated fluorescent Nod factor for *V. sativa* (Goedhart et al., 1999). Interestingly, *V. sativa* preferred (non-sulfated) LCOs with a BODIPY FL-C₁₆ acyl chain over those labeled with BODIPY 558/568-C₁₂ (chapter 3), whereas *M. truncatula* preferred (sulfated) LCOs carrying BODIPY 558/568-C₁₂ over those with a BODIPY FL-C₁₆ acyl chain. This difference in acyl chain preference of both species might reflect that the putative Nod factor signaling receptors in both species have a structurally different lipid-binding pocket. For further discussion see chapter 7.

LCO-IV(BODIPY FL-C₁₆, S) was used to study the properties of sulfated LCOs in the presence of membranes. The Nod factor associated with vesicles, transferred rapidly between vesicles and no transmembrane flip-flop occurred, as was observed previously for non-sulfated Nod factors (Goedhart et al., 1999). Hence, like postulated for the non-sulfated Nod factors, an active flip-flop mechanism is required for secretion of sulfated Nod factors by rhizobia. Otherwise, Nod factors which are synthesized in the cytosol and inner leaflet of the inner rhizobial membrane would be trapped inside the bacteria and would never cross both bacterial membranes. For LCO-IV(BODIPY 558/568-C₁₂, S) it is clear from FCM experiments that it diffuses as monomers in plant growth medium when applied at a concentration of 10 nM. Hence, the physicochemical properties of LCOs and their affinity for membranes is hardly or not dependent on the presence of the sulfate group.

In addition to the bioactivity in the root hair deformation assay, the fact that fluorescent Nod factors can be hydrolyzed by root chitinases provides additional support that the derivatives are truthful representatives of their natural counterparts. Nod factor breakdown products represent only a minor fraction on the legume root system relative to intact Nod factor within the first 30 minutes. Therefore, the fluorescence which is observed within the first 30 minutes, e.g. to study initial binding and to study the diffusional behavior of the Nod factors on root hair tips, represents the intact fluorescent LCO.

LCO-IV(BODIPY 558/568-C₁₂, S) accumulated in the cell walls of *M. truncatula* root hairs. The plasmolysis experiments show the absence of fluorescence associated in plasma membrane, when these LCOs are applied at 10 nM. The strong binding to the cell wall was also evident from the lack of diffusion of Nod factor to the newly formed outgrowth induced by the Nod

factors. It is of interest that the initial binding of Nod factors to root hair cell walls of a compatible and non-compatible host (sulfated LCOs on *V. sativa* and non-sulfated LCOs on *M. truncatula*) is similar.

To study the binding characteristics in detail, the diffusional behavior and accumulation of Nod factors was measured by FCM. Quantitative analysis of the FCM autocorrelation curves showed marked immobilization, but no difference in diffusional characteristics and accumulation of sulfated and non-sulfated LCOs on root hair cell walls of host and non-host legumes. This implies that (i) the molecular structure of the root hairs of the two plants are very similar, (ii) the binding of Nod factors to the cell wall is independent of the sulfate group and (iii) the extent of binding to the root hair cell wall is not related to the bioactivity. Although binding of the Nod factor to the cell wall needs the chitin backbone, since the free acyl chain is directly taken up into the root hair cytosol, the presence of a sulfate group is not sufficient to change the binding or targeting. For a detailed discussion on the mode of Nod factor perception, the reader is referred to the summarizing discussion.

For comparison, a biologically non-relevant fluorophore, TMR, was included in the FCM analysis. TMR showed moderate accumulation in root hair cell walls and a slower diffusion as compared to diffusion in aqueous medium. However, the average diffusion of TMR in root hair cell walls is still 100-fold faster than the diffusion of fluorescent LCOs. This clearly shows that Nod factors are much tighter bound to the cell wall than aspecific lipophilic molecules such as TMR. The FCM data analysis was performed using a two-component diffusion model requiring a fit of two diffusion constants and a fractional contribution.

Interestingly, the diffusion constants determined for TMR are similar to those determined for the LCOs, although the contributions differ markedly (table 2). Although the model with two diffusion times can accurately describe the data, allowing a quantitative comparison between the LCOs, it is not possible to judge whether this model is physically correct: i.e. that it actually describes that Nod factors move as two, rather independent, populations of faster and slower diffusing molecules in a root hair cell wall. In this respect, it is of note that the mathematically derived two-component model assumes a homogeneous solution of fluorescent particles continuously occupying the confocal volume element (Maiti et al., 1997). We know that the cell wall is too thin to occupy the volume element completely. Also, we do not know whether the diffusion in all parts of the cell wall is similar. In addition, it is difficult to model the effect of the orientation of the cell wall with respect to the volume element in a physical theory (Gennerich and Schild, 2000). Hence, two diffusion times (i) could reflect Nod factors diffusing relatively fast in the outer part of the cell wall (but still significantly slower than in solution) and the majority being more immobilized in the inner part of the cell wall, (ii) it could reflect Nod factors freely diffusing in aqueous microdomains of the cell wall being hindered (slowed down) due to volume exclusion by cell wall polymers and another (larger) fraction being bound to the cell wall, or (iii) it could reflect an asymmetry of Nod factor diffusion in the root hair cell wall perpendicular to the optical axis of the microscope versus parallel to the optical axis of the

microscope inside. Because an accurate physical meaning of the two-component model is lacking, we rather would refer to the data as reflecting "complex diffusion" also observed by others in different cellular systems (Brock et al., 1998; Brock et al., 1999; Schwille et al., 1999). Still, qualitatively, the curves observed for LCOs and TMR on root hairs differ markedly from each other and when compared to curves obtained in solution (note the logarithmic scale of the horizontal axis in figure 5), clearly indicating the usefulness of the FCM technique.

Another way to show accumulation of Nod factors by legume roots is to visualize the decrease of fluorescent LCOs in the medium surrounding the roots. Directly after application of fluorescent Nod factors, a decrease of fluorescence in the medium is apparent near the root hairs (figure 6). The fluorescence near the root hairs decreases, until almost all Nod factors near the root hairs are absorbed. However, at locations further from the root the Nod factor concentration hardly drops. The concentration gradient in the medium was visualized for the first time, and can only exist if there is a continuous uptake of Nod factors by the root surface that acts like a sink. This experiment also demonstrates that in assessing Nod factor bioactivity, not only the applied concentration is important, but also the applied volume and time of incubation needs to be taken into account.

In a first effort to obtain information on the importance of Nod factor immobilization for root hair curling by the use of mutants, the Nod factor binding on the *hcl* mutant that is disturbed in root hair curling (Catoira et al., 2001) was characterized. Binding of LCO-IV(BODIPY 558/568-C₁₂, S) was similar as observed on wild-type *M. truncatula* plants, indicating that the mutant is not disturbed in immobilization of the Nod factor. Apparently, a downstream process, probably unrelated to Nod factor binding but necessary to relay the positional information to the morphogenesis machinery during the curling process, is disturbed in the *hcl* mutant. Bibikova et al. (1997) described that in *A. thaliana* root hairs a localized influx of calcium, generated by UV-uncaging of a caged calcium ionophore, was sufficient to induce transient reorientation of tip-growth to the site where the calcium concentration was increased. This clearly shows that intracellular processes unrelated to Nod factor perception can spatially restrict signaling leading to morphogenesis. Whether the *hcl* mutant is affected in calcium signaling remains to be established.

In summary, we have described three fluorescent sulfated Nod factor analogs and studied their bioactivity on *M. truncatula* and *V. sativa*. It turned out that, like the natural non-fluorescent counterpart, the sulfate group on the reducing sugar of the LCO mediates host-specificity of the biological response. Surprisingly, by detailed analysis of the *in situ* binding characteristics of both sulfated and non-sulfated fluorescent LCOs on the two legumes, we could not see any difference: both LCOs concentrated in cell walls to a similar extent, both LCOs were markedly immobilized in cell walls and both LCOs did not label the plasma membrane. From these results we conclude that it is likely that two different molecules are involved in the initial Nod factor perception process: i) a Nod factor binding molecule with high abundance in the cell wall, low Nod factor specificity and a high affinity for Nod factors and ii) a Nod factor signaling receptor

of low abundance and recognition sites for presence or absence of a sulfate group and a lipid binding pocket. Because the localization studies only yield information on the abundant Nod factor binding sites, the localization and binding affinity of the signaling receptor can not be studied by our approach. A more detailed discussion on the mode of perception of Nod factors by legume root hairs will be given in chapter 7.

Materials and Methods

Materials

Synthesis of the fluorescent sulfated Nod factors will be described elsewhere (De Medina et al., manuscript in preparation). The fluorescent Nod factor derivatives are named LCO-IV(BODIPY FL-C₁₆, S), LCO-V(BODIPY FL-C₁₆, S) and LCO-IV(BODIPY 558/568-C₁₂, S). The non-sulfated Nod factor has been described previously (Goedhart et al., 1999) as NodR1v-IV (BODIPY 558/568-C₁₂) and is denoted here as LCO-IV(BODIPY 558/568-C₁₂). For the structures of fluorescent Nod factors used in this study see figure 1.

Transfer assay

For transfer experiments, quenched donor vesicles were prepared by injecting 20 μ l of an ethanolic solution of 790 μ M DOPC, 100 μ M DPPA, 10 μ M LCO-IV(BODIPY FL-C₁₆, S) and 100 μ M Texas Red DHPE into 3 ml Tris buffer (20 mM Tris (pH=7.4), 100 mM NaCl, 1 mM EDTA, 1 mM EGTA), under continuous stirring (Batzri and Korn, 1973). Acceptor vesicles were prepared by mixing 3600 nmol DOPC and 400 nmol DPPA in chloroform. After evaporation of the chloroform, the lipids were dissolved in 2 ml of Tris buffer by vortexing, followed by sonication for 3 min. The emission of NodR1v-IV(BODIPY FL-C₁₆) was monitored continuously on an Aminco SLM-8000 (SLM instruments, Urbana, IL) by excitation at 490 nm (slit 4 nm) and emission at 513 or 550 nm (slit 4 nm). To start the transfer, 100 μ l of acceptor vesicles was added to 3 ml of donor vesicles, and the fluorescence intensity was monitored as a function of time. For calibration, aliquots of 25 μ l 10% (v/v) Triton X-100 in PBS were added, until the fluorescence intensity did not increase.

Plant Material

Experiments on *Vicia sativa* were performed as described (Heidstra et al., 1994). *Medicago truncatula* ecotype A17 or alfalfa seeds were treated for 5-10 minutes with concentrated H₂SO₄, washed with H₂O, treated with concentrated bleach for 5-10 minutes and washed extensively with H₂O. Subsequently, seeds were transferred to 1% agarose plates and incubated at 4 °C for 2-3 days. After two days at 20 °C seedlings were transferred to Fåhreus slides containing PGM (2.72 mM CaCl₂, 1.95 mM MgSO₄, 2.20 mM KH₂PO₄, 1.26 mM Na₂HPO₄ and 0.08 mM Fe(III) citrate).

Root hair deformation on *Medicago truncatula* is done similar to *Vicia sativa*, except that two plants are grown per Fåhrens slide parallel to the long side because the roots grow faster compared to *Vicia sativa*. Root hair deformation experiments were performed one day after transfer of seedlings to the slides containing PGM. For each Nod factor concentration three slides containing two seedlings each were scored blindly (i.e. without prior knowledge of the treatment) three hours after addition of the Nod factor.

Fluorescence microscopy

Digital imaging of root hairs was performed as described (Goedhart et al., 2000), except that in some cases the fluorescent LCO solution was removed after 15 minutes of incubation by washing two times with PGM. For imaging whole roots, a Leica MZFLIII stereomicroscope (Leitz, Wetzlar, Germany) with 545DF10 excitation and 605DF50 emission filters was equipped with a slow scan series 200 (CH250) liquid cooled CCD camera (Photometrics, Tucson, AZ), interfaced onto the Nubus slot of a Macintosh PowerPC 8100 computer and controlled using the IPlab Spectrum image processing software (Signal Analytics, Vienna, VA). To fully replace the medium surrounding the root hairs with PGM containing 10 nM LCO-IV(BODIPY 558/568-C₁₂, S), the root was thoroughly washed with PGM containing the fluorescent LCO, after which imaging was started immediately. All images were background and flat-field corrected.

Chitinase activity

To a Fåhrens slide containing five seedlings of *V. sativa* or two seedlings of *M. truncatula*, 0.5 µM fluorescent Nod factor in PGM was added. After the appropriate time, the medium was removed and extracted with 300 and 200 µl water saturated n-butanol. The roots were washed with water twice, after which they were cut from the seedling and ground after freezing in liquid nitrogen. To the ground roots, 1 ml of water saturated butanol was added and mixed. After addition of 4 ml H₂O, the mixture was transferred to a tube, and phase separation was induced by centrifugation. After removal of the upper phase (approx. 200 µl) the lower phase was re-extracted with 200 µl water saturated butanol. The collected butanol phases were evaporated in a speedvac and redissolved in 20 µl n-butanol. The fluorescent products were separated by TLC according to Heidstra et al. (1994) and visualized by recording the blue-excited fluorescence on a STORM 840 (Molecular Dynamics Inc., Sunnyvale, CA).

FCM

The calibration procedure and FCM measurements were performed as described before (Goedhart et al., 2000). The laser radius in the xy plane (ω_{xy}) was calculated from the measured diffusion time τ_{diff} of TMR and the known diffusion constant D of 2.8×10^{-10} m²/s according to:

$$\tau_{diff} = \frac{\omega_{xy}^2}{4 \cdot D} \quad (1).$$

The value of ω_{xy} differed from day to day and ranged from 240 nm to 290 nm. The structural parameter was also obtained from the measured autocorrelation curves of TMR and was between 6.4 and 9.1. For the *in vivo* measurements a two component fit procedure was used to obtain two diffusional times and their relative contribution (Goedhart et al., 2000). The diffusion time τ_{diff} was converted to the diffusion constant D according to equation 1, using the laser radius ω_{xy} obtained from the calibration.

Acknowledgments

We are grateful to M.A. Hink (Laboratory for Biochemistry, Wageningen University, The Netherlands) for helpful suggestions and comments on the FCM analysis. This work was supported by the Netherlands Organization for Scientific Research-Council of Earth- and Life Sciences (NWO-ALW) (J.G), by a NWO-Van Gogh French-Netherlands collaborative research grant (J.J.B. and T.W.J.G.), and by the Royal Netherlands Academy of Arts and Sciences (KNAW) (T.W.J.G.). Seeds of the *hcl* mutant were a kind gift of Jean Dénarié.

SYNTHESIS AND USE OF PHOTORELEASEABLE PHOSPHATIDIC ACID TO STUDY LIPID SIGNALING**Abstract**

Caged compounds that release a biologically active molecule upon exposure to UV light can be used to initiate signaling pathways with high spatial and temporal resolution. In order to study lipid signaling, the caging strategy was applied to the phospholipid phosphatidic acid (PtdOH). To simplify the analysis of caging and uncaging, a fluorescent PtdOH derivative was synthesized. First, phosphatidylcholine labeled with a BODIPY 558/568-C₁₂ acyl chain at the sn-2 position was prepared. After purification, the product was converted to fluorescent PtdOH by phospholipase D. The product was caged by addition of a 1-(2-nitrophenyl)ethyl moiety and subsequently purified. TLC analysis showed that the purified caged compound releases PtdOH *in vitro* after exposure to UV (365 nm).

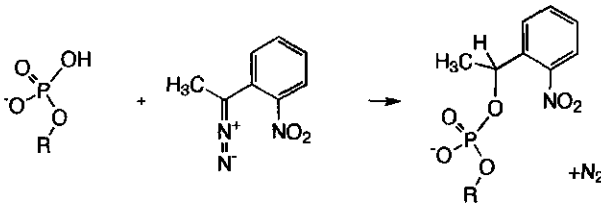
Caged PtdOH was applied to the swimming green alga *Chlamydomonas moewusii*. The cells arrested swimming only after exposure to UV, due to (PtdOH induced) excision of flagella. This well-characterized response to PtdOH was not observed in absence of the caged compound or when control caged compounds (caged acetic acid) were added. When the caged compound is applied to legume roots, it readily passes through cell wall and plasma membrane and accumulates in intracellular membranes. These results indicate that caged PtdOH can be used to specifically manipulate PtdOH levels in living cells, and show that it is a promising phospholipid precursor for studying phospholipid signaling in plants.

Introduction

Nod factor perception by legumes elicits a number of responses in root hairs (Downie and Walker, 1999). An influx of calcium is the earliest response, which is followed by an efflux of chloride and potassium (Felle et al., 1998). After approximately ten minutes perinuclear calcium spiking is observed (Ehrhardt et al., 1996). A pharmacological study suggests that G-proteins and phospholipases are involved in the Nod factor signaling cascade (Pingret et al., 1998). Mastoparan was used as a G-protein agonist, inducing the expression of an early noduline similarly to the induction by Nod factors. The response to both mastoparan and Nod factor could be blocked by neomycin and the phospholipase C inhibitor U73122. In a more detailed study of the role of phospholipases in Nod factor signaling, den Hartog et al. (2001) monitored changes in phospholipid levels by labeling roots with ^{32}P and subsequent lipid analysis by TLC. It was shown that both mastoparan and Nod factors increased the levels of phosphatidic acid (PtdOH) and diacylglycerolpyrophosphate due to the activation of both phospholipase C and phospholipase D (Den Hartog et al., 2001). They also showed that both root hair deformation and elevation of PtdOH levels could be blocked by neomycin, corroborating the results of Pingret et al. These results indicate that phospholipids in general and PtdOH in particular are important players in Nod factor signaling.

To study phospholipid signaling *in vivo* several approaches can be taken. Monitoring phospholipid turn-over in single living cells has been shown using specific lipid binding domains tagged with a fluorescent protein (Stauffer et al., 1998; Venkateswarlu et al., 1998). Another way to study the role of phospholipids is administering them to cells. In some cell systems it has been shown that external application of the lipid of interest is sufficient to have an effect (Derman et al., 1997; Moolenaar et al., 1986; Munnik et al., 1995). However, for charged phospholipids which have to pass the membrane passive loading is highly inefficient. In addition, the experimenter has poor temporal and spatial control over the phospholipid concentration *in vivo*. To achieve both spatial and temporal control over the increase of a second messenger in a single cell photosensitive precursors are ideal (Adams and Tsien, 1993). The molecule of interest, i.e. a second messenger, is derivatized with a photosensitive protecting group rendering the compound inactive (figure 1). By exposure to UV light this so-called "cage" is removed, releasing the original (bioactive) second messenger (McCray and Trentham, 1989). Well known examples of photoreleasable second messengers are caged $\text{Ins}(1,4,5)\text{P}_3$ (Walker et al., 1987), caged Ca^{2+} (Kaplan, 1990) and caged cGMP/cAMP (Nerbonne et al., 1984).

Caging:



Uncaging:

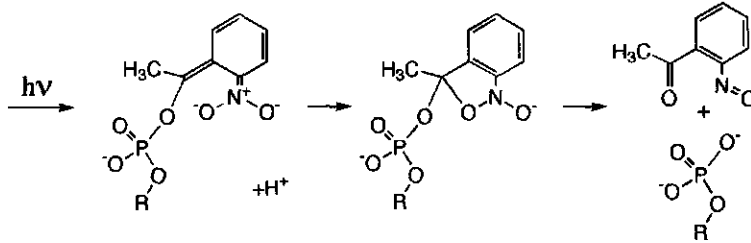


Figure 1: Caging; the phosphate group is derivatized by a reaction with 1-(2-nitrophenyl)ethyldiazoethane in CHCl_3 which yields the photosensitive NPE moiety. Uncaging; upon exposure to UV (365 nm), an aci-nitro intermediate is formed after which intramolecular transfer of the oxygen from the nitro-group takes place which yields the original compound and the by-product 2-nitrosoacetophenone. R=diacyl-glycerol for PtdOH.

PtdOH levels are markedly increased in *Vicia sativa* roots upon Nod factor induced signaling (Den Hartog et al., 2001). Also in many other plant signaling events this lipid is implicated as a second messenger (Munnik, 2001). In this chapter we describe the synthesis of photoreleasable PtdOH. By following the caging strategy, we hope to be able to manipulate PtdOH levels in plants by using UV light. For monitoring loading efficiencies *in vivo* and localization purposes also a fluorescent caged analog was synthesized.

Results

Synthesis of BODIPY labeled PtdOH

Fluorescent PtdOH can be synthesized from fluorescent acyl chain labeled phosphatidylcholine after PLD treatment (Somharju et al., 1985). We preferred to equip PtdOH with a red fluorescent dye as this is more compatible with plant studies. Plant autofluorescence generally decreases upon increasing the excitation wavelength and is minimal when exciting with 543 nm or 568 nm laser lines or with 546 nm or 577 nm mercury lines. Since the commercially available most red-shifted fluorescent phosphatidylcholine (PtdCho) is prone to oxidation (Pap et al., 1999) we decided to synthesize an orange fluorescent PtdCho with a BODIPY 558/568- C_{12} acyl chain. From earlier studies it appeared that this probe has excellent spectroscopic and biological properties to study location of signaling molecules at low concentration (Goedhart et

al., 2000). The fluorescent PtdCho is prepared by reacting lyso-PtdCho with the anhydride of BODIPY 558/568-C₁₂, which is purified on CM-cellulose and then treated with PLD to prepare fluorescent PtdOH. The preparation of BODIPY 558/568-C₁₂ labeled PtdOH by the action of PLD on fluorescent PtdCho typically yields >90% PtdOH (see lane A, figure 2). For further experimental details see materials and methods.

Caging of phosphatidic acid

We have caged PtdOH by the addition of a 1-(2-nitrophenyl)ethyl (NPE) moiety onto the free phosphate as reported by Williger et al. (1995). Fluorescent NPE-PtdOH was prepared by using fluorescent PtdOH extracted from the PLD incubation. The crude preparation was directly incubated with 1-(2-nitrophenyl)diazoethane. The subsequent application of the caged compound to a silica gel column serves two purposes. First, the remaining 1-(2-nitrophenyl)diazoethane is inactivated by a reaction with the silica gel. Second, both the contaminants PtdCho and unreacted PtdOH bind to the column, whereas the caged PtdOH is eluted with chloroform. The purity of NPE-PtdOH is excellent as can be inferred from TLC (figure 2, lane B). Similarly, natural PtdOH was caged and purified.

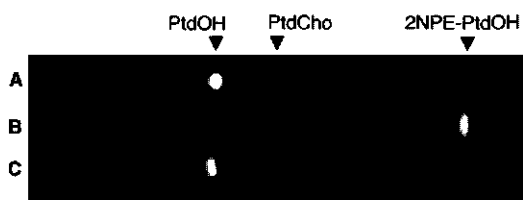


Figure 2: TLC analysis of the synthesis and photolysis of fluorescent NPE-PtdOH. (A) Fluorescent PtdOH produced by the action of PLD on BODIPY 558/568-C₁₂ labeled PtdCho. (B) Fluorescent NPE-PtdOH obtained after reaction of PtdOH with 1-(2-nitrophenyl)diazoethane and subsequent purification. (C) Release of PtdOH from NPE-PtdOH after illumination with UV (365 nm).

Uncaging of NPE-phosphatidic acid

Using fluorescent NPE-PtdOH, the photorelease of PtdOH *in vitro* can be easily evaluated by TLC analysis. When a sample of NPE-PtdOH is exposed to UV and subsequently run on a TLC, it is directly apparent that PtdOH is released from the caged compound (lane C, figure 2). Another compound is also present on the TLC after irradiation. As checked with a standard, this product was not diacylglycerol, but probably an uncaging intermediate since it was not present after prolonged exposure of caged PtdOH to UV, yielding only PtdOH (data not shown).

PtdOH is implicated as a second messenger in several plant responses (Munnik, 2001). A relative well-characterized signaling process takes place when the green alga *Chlamydomonas moewusii* is exposed to mastoparan. The G-protein agonist elevates the level of PtdOH, thereby inducing the excision of its flagella. It has been shown that addition of PtdOH vesicles is sufficient to induce excision of the flagella (Munnik et al., 1995). This response can be easily

observed since after deflagellation the cells are unable to swim. Hence, by monitoring the mobility of the alga in the absence and presence of UV light and NPE-PtdOH we have a convenient assay to study the photorelease of PtdOH *in vivo*.

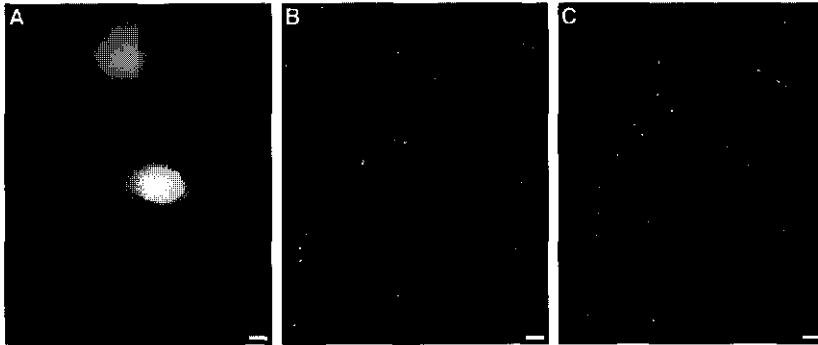


Figure 3: *In vivo* uncaging by spatially restricted UV exposure and subsequent fluorescence imaging. (A) The fluorescence that is induced due to uncaging of caged fluorescein-dextran in glycerol was used to quantify the UV intensity in the illuminated spots. (B) After incubation of *Chlamydomonas moewusii* with $0.7 \mu\text{M}$ NPE-PtdOH, the sample was illuminated for 5 minutes with UV at the spots corresponding to panel A. In the regions that are exposed to UV, cells are accumulated as visualized by monitoring their chlorophyll autofluorescence. The fluorescence image is acquired with a long integration time, which effectively shows only non-swimming cells, since swimming cells are blurred due to movement. (C) As a control, cells were incubated with $25 \mu\text{M}$ NPE-Ac and exposed to UV, showing that the UV exposure or the released cage alone are not sufficient to stop the cell motility. Bars represent $50 \mu\text{m}$.

The location of UV exposure in the sample was calibrated by illuminating a solution of caged (non-fluorescent) fluorescein, and subsequently taking an image of the uncaged and fluorescent fluorescein (fig. 3A). Swimming *Chlamydomonas moewusii* cells were observed under a microscope. Continuous illumination of the spots shown in figure 3A with UV light did not impair the motility of untreated cells that crossed these spots. When the same experiment was done after application of $0.7 \mu\text{M}$ NPE-PtdOH to the *Chlamydomonas moewusii* cells, swimming arrested specifically at the illuminated spots, indicating that the combination of NPE-PtdOH and UV light was required and sufficient to stop the cells (fig. 3B). The photolysis of NPE-PtdOH yields a side-product which is 2-nitrosoacetophenone. To investigate whether this compound might be harmful for the cells, a control experiment was performed in which either caged fatty acid or caged acetic acid (NPE-Ac) was used. As shown in figure 3C, even when a 35-fold excess of NPE-Ac was used, no change in swimming speed of the cells was observed upon illumination with UV, indicating that the side-product is not responsible for the arrest in motility. These experiments show that the release of PtdOH from its caged precursor leads to motility arrest of the cells, thereby providing direct *in vivo* evidence for the second messenger function of this phospholipid.

The image shown in figure 3B shows that the spot at which cells that are unable to swim accumulate correlates with the intensity of UV light shown in figure 3A. To quantitatively relate

deflagellation with the light intensity we developed an image correlation method. First of all, the images of cells (3B and 3C) are thresholded and converted to binary images, in which pixels corresponding with cells are given the value of 1 and background pixels a value of 0. The binary image is multiplied with the UV intensity image. This yields an image in which the background has a value of 0, and cells have a pixel value corresponding to the UV intensity. A histogram of the intensities in this image represents the probability of finding a non-swimming cell as a function of the local UV intensity. This histogram however, has to be divided by the probability of finding a certain intensity of UV light intensity, i.e. the histogram of the UV intensity distribution in figure 3A. The normalized histogram shows the probability of finding a cell at a certain UV intensity. In case of a random distribution of cells, there should be no correlation of the location of the cells with respect to the UV intensity. On the other hand, when cells accumulate in the UV exposed areas, a positive correlation between the UV intensity and the number of cells is expected. The data of two experiments with NPE-PtdOH present and one control experiment are analyzed using this procedure. The results are shown in figure 4. Clearly a positive and surprisingly linear correlation between UV intensity and the number of accumulated cells is seen for cells incubated with NPE-PtdOH, whereas no such trend is seen in cells incubated with NPE-Ac. Hence, the analysis routine is capable of extracting the PtdOH specific response and allows a quantitative comparison with control situations.

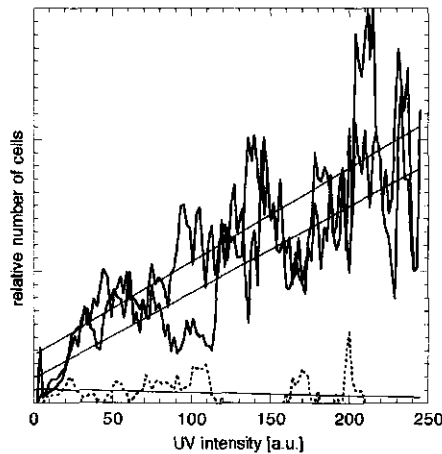


Figure 4: Histograms showing the accumulation of cells at a location with a certain UV intensity. Also the linear fit through the data points is shown. In case of NPE-PtdOH loaded cells (straight lines), there is a positive correlation with the UV intensity, whereas no positive correlation (dashed line) is observed when cells are incubated with NPE-Ac.

NPE-PtdOH accumulates in root hairs

In order to evaluate whether the caged lipid could be useful for studying lipid signaling in root hairs, the purified caged product (lane B figure 3) was administered to *Vicia sativa* roots. As can

be inferred from figure 5, intracellular membranes, as well as the plasma membrane, are labeled. Apparently, the reduced negative charge on the phosphate group in combination with the hydrophobic nature of the cage enables the molecule to cross cellular membranes by passive diffusion. Cytoarchitecture, polar cell growth and cytoplasmic streaming remained unchanged during loading, indicating that NPE-PtdOH is biochemically inactive and does not disturb cell physiology at this concentration.

To investigate whether UV irradiation of NPE-PtdOH loaded root hairs could produce a morphogenic response (i.e. root hair deformation), NPE-PtdOH treated and control root hairs were irradiated with UV-light of variable duration. Interestingly, UV irradiation of NPE-PtdOH labeled root hairs resulted in a few root hair deformation events. However, this was also the case when the root hairs were not incubated with the caged compound, indicating that prolonged exposure to UV is potentially harmful. Because no focused spot of UV could be generated with the current microscopy system, we were unable to study the effect of local (e.g. tip-located) production of PtdOH on the root hair morphology.

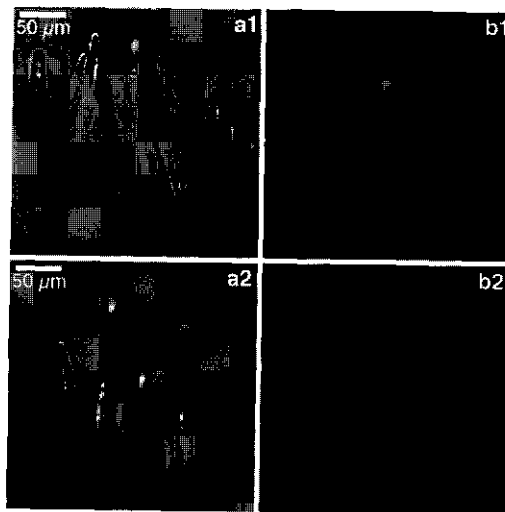


Figure 5: *Vicia sativa* root hairs accumulate fluorescent NPE-PtdOH. Phase contrast (a1, a2) and fluorescence (b1, b2) images of *Vicia sativa* root hairs after application of fluorescent NPE-PtdOH to the growth medium. Subcellular structures of root hairs corresponding to the cytosol (c) and nucleus (n) show increased fluorescence, whereas the vacuole (v) remains unlabeled. This indicates that the caged compound can readily pass the plasma membrane and within the cell transfers to endomembranes and the nucleus.

Discussion

Photolysis of caged second messengers is an elegant method to achieve spatiotemporal control over the increase of a second messenger. The structurally simple lipid phosphatidic acid is important in a great number of signaling cascades both in plant (Munnik, 2001) and animal cells (English et al., 1996). Therefore caged PtdOH derivatives are of great interest. In this report the

synthesis and purification of a fluorescent and caged phosphatidic acid starting from a fluorescent PtdCho is described. The fluorescent reporter allows sensitive and convenient analysis of the uncaging process by TLC.

It has been shown that adding phosphatidic acid at millimolar concentration also induces deflagellation of the swimming green alga *Chlamydomonas moewusii* (Munnik et al., 1995). The deflagellation response to PtdOH was used to test the ability of NPE-PtdOH to release PtdOH *in vivo* upon exposure to UV. The loss of flagella is easily observed under a microscope because the alga stop swimming. By spatially restricting the UV exposure it was possible to show that the arrest of swimming was related to the spots that are exposed to UV. These experiments show that photolysis of NPE-PtdOH can efficiently release biologically active PtdOH. In the experiments described in this chapter, NPE-PtdOH was added at a concentration which is at least three orders of magnitude lower than the added concentration of PtdOH in a previously described study (Munnik et al., 1995). The fact that a 1000-fold lower concentration of uncaged NPE-PtdOH can be as effective as PtdOH can be explained by the highly efficient loading of NPE-PtdOH in cells. PtdOH which is much more polar than NPE-PtdOH will not be able to accumulate as efficiently in intracellular membranes and flip-flop between membrane leaflets. The low concentration of NPE-PtdOH that is able to elicit the deflagellation response provides direct evidence that PtdOH acts as a second messenger in flagellar excision. In addition, the linear correlation of UV intensity with the chance of deflagellation also demonstrates a clear dose-response relation between levels of (photoreleased) PtdOH and deflagellation.

When the fluorescent NPE-PtdOH is applied to legume roots it readily crosses both the cell wall and the plasma membrane of root hairs and accumulates in intracellular membranes. The accumulation within cells is also observed for mammalian cell cultures (K. Jalink, personal communication). This property greatly facilitates the use of NPE-PtdOH in cell biological studies. Unfortunately, it turned out that root hairs were sensitive to UV exposure under the conditions used. Probably, UV irradiation of root hairs is less disturbing when only a limited area of the cell instead of a whole microscopy field is exposed. Therefore, it is important for future studies to use lasers rather than a mercury lamp as an UV source, yielding a more focused excitation spot. In this respect, a publication reporting the effects of the photolysis of a caged calcium ionophore by laser scanning on *A.thaliana* root hairs without any damaging effect of the UV, is encouraging (Bibikova et al., 1997). Moreover, laser scanning enables exact control over the uncaging position. It will be of interest to expose cells to UV at various locations within the cell, to examine the importance of PtdOH at a subcellular level. For example, it could be of importance to spatially restrict the second messenger release when studying Nod factor signaling, since it is evident that local signaling is required for the induction of root hair curling.

Materials and Methods

Materials

BODIPY 558/568-C₁₂ was from Molecular Probes (Leiden, The Netherlands), CM52 cellulose (pre-swollen) was from Whatmann (Maidstone, England). Lyso-PtdCho, phosphatidic acid (from egg yolk lecithin), PLD, activated Mn(IV)O₂, hydrazine hydrate and 2-nitroacetophenone were from Sigma-Aldrich (Zwijndrecht, The Netherlands).

Biological material

Seedlings of *Vicia sativa* were germinated and grown as described (Goedhart et al., 2000). *Chlamydomonas moewusii* cells were cultured and prepared for experiments as described (Munnik et al., 1995).

Synthesis of PtdCho with a BODIPY 558/568-C₁₂ acyl chain

Acylation of 5 µmol lyso-PtdCho was done according to (Gupta et al., 1977) after preparing the anhydride of 10 µmol BODIPY 558/568-C₁₂ in dry CHCl₃ as reported (Selinger and Lapidot, 1966). Purification of the fluorescent PtdCho was done on CM-cellulose (Comfurius and Zwaal, 1977), from which the product eluted at 4 % methanol as verified by TLC.

Synthesis of PtdOH from PtdCho by PLD

When PLD from cabbage was used, PtdCho was dissolved in 200 µl ether which was added to 200 µl 100 mM acetate buffer (pH=5.6) containing 100 mM CaCl₂ and 5 units of PLD. After incubation at 30 °C for 90 min. the ether was evaporated and the lipids extracted with CHCl₃/MeOH. When PLD from *S. chromofuscus* was used, the PtdCho was suspended in 50 mM Tris (pH=8.0) and 10 mM CaCl₂ and incubated for 60 min. at 37 °C in absence of ether.

Caged compounds

The precursor 2-nitroacetophenone hydrazone was prepared as described (Walker et al., 1988; Walker et al., 1989). For a caging reaction, a ten-fold excess of 2-nitroacetophenone hydrazone was dissolved in chloroform, after which 8 mole equivalent of MnO₂ was added. After stirring vigorously for 5 minutes the red solution was filtered through silanized glass wool. This solution was added to a chloroform solution of phosphatidic acid and incubated for at least 30 minutes. Subsequently, the solution was applied to a silica column from which the caged PtdOH was eluted with chloroform. Similarly, caged fatty acid was prepared. To prepare caged acetic acid (NPE-Ac), a 40-fold excess of glacial acetic acid was added to 1-(2-nitrophenyl)diazoethane which immediately turned yellow. Unreacted acetic acid could easily be removed by extracting the chloroform solution with water.

Photorelease with a microscope

Generally, exposure to UV with an excitation bandpass 365HT25 (Omega, Brattleboro, VT) and a 430DCLP dichroic mirror was at 20× magnification. Subsequently an image was acquired at 10× magnification with a Quantix CCD camera (Photometrics, Tucson, AZ) controlled by IPLab spectrum software (Signal Analytics, Vienna, VA). To calibrate the position of UV exposure within the microscope field, 50 µg/ml DMNB-fluorescein dextran in 80% glycerol in a microcuvette with an internal diameter of 0.1 mm (VibroCom, Mountain Lakes, NJ) was exposed for 1 s after which an image with fluorescein filter settings was taken immediately. Chlorophyll fluorescence of *Chlamydomonas moewusii* was acquired with 10 times reduced excitation power and a LP610 emission filter. An integration time for image acquisition of 10 seconds was used to selectively image non-swimming cells, since the signal of swimming cells is spatially averaged.

Image processing

Image processing was done with NIH image v1.62 (<http://rsb.info.nih.gov/nih-image>). Digital images were imported using the IPLab import macro. A threshold was applied to separate cells from the background, and the image was converted to a binary image in which cells were given a value of 1, and background a value of 0. This image was multiplied by the UV intensity distribution image (fig. 3A). The histogram of the multiplied image was divided by the histogram of the UV intensity image, yielding a histogram that correlates the probability of finding a cell with the intensity of UV light. Further details are discussed in the results section.

Acknowledgments

We thank Martine den Hartog (Plant physiology, University of Amsterdam) for the continuous supply of fresh and happily swimming *Chlamydomonas moewusii* cells.

SUMMARIZING DISCUSSION*Fluorescent Nod factors*

The main part of this thesis describes the use of fluorescent Nod factor derivatives aiming to increase the knowledge of Nod factor perception in the *Rhizobium*-legume interaction. The first report of a fluorescent Nod factor derivative was published in 1997 by Gadella et al., describing a Nod factor in which the natural acyl chain at the non-reducing terminal sugar was replaced by a green fluorescent acyl chain. A month later a paper was published by Philip-Hollingsworth et al. (1997), who have prepared fluorescent LCOs by derivatizing the reducing sugar via a dicarbon spacer to a NBD fluorophore. From these two studies it was immediately clear that the autofluorescence of root hairs was seriously limiting the use of green fluorescent Nod factors at low concentrations. In order to detect fluorescence of Nod factors *in vivo* they had to be applied at 1 μM , which is relatively high since the threshold concentration at which natural Nod factors are active is several orders of magnitude lower.

This thesis describes the synthesis of novel red-shifted Nod factors by using acyl chains with orange and red-fluorescent probes to increase sensitivity. When using fluorescent or otherwise tagged biomolecules it is of major importance to verify that the label does not seriously interfere with the bioactivity. Therefore, the first experiment was to test novel fluorescent Nod factors for root hair deforming activity on their host plant. As described in chapter 3 the most active fluorescent Nod factor NodRlv-IV (BODIPY 581/591- C_{16}) can still elicit root hair deformation on *Vicia sativa* when administered at 10^{-10} M. This is excellent when compared to NodRlv-V with a fully saturated C18 acyl chain (stearic acid) which loses root hair deforming activity at 10^{-11} M (Heidstra et al., 1994). The second class of fluorescent Nod factors containing similar acyl chains carry a sulfate group at their reducing terminal sugar. The most active novel sulfated Nod factor induces root hair deformation at a concentration down to 10^{-10} M on *Medicago truncatula* (chapter 5). These results clearly indicate that it is possible to prepare labeled Nod factors while retaining bioactivity suggesting that these fluorescent derivatives reliably represent the natural Nod factor.

Characterization of Nod factors in vitro by spectroscopic techniques

The general structure of Nod factors is amphiphilic, suggesting that Nod factors are present as micelles in solution (Hirsch, 1992; Orgambide et al., 1995). However, no studies on the physicochemical properties of Nod factors were reported to corroborate this idea. Therefore the behavior of Nod factors in aqueous solution and in the presence of model membranes was studied using different fluorescence spectroscopic techniques (chapter 3). Time-resolved fluorescence spectroscopy experiments complemented with FCS measurements at physiological relevant concentrations (10 nM) show that Nod factors despite their amphiphilic nature do not

form micelles but instead are present as monomers in aqueous solution at 10 nM. When membrane-like systems are present, such as Triton X-100 micelles or phospholipid vesicles, the Nod factor acyl chain inserts into the hydrophobic core of these structures. Interestingly, experiments with vesicles show that transfer of Nod factors between the vesicles is very rapid, and also that Nod factors can transfer from vesicles to root hairs. Presumably, in a natural environment in which the aqueous solution is absent, physical contact between the bacterium and the root hair is required for efficient transfer of Nod factors.

Interestingly, it was observed that Nod factors are not able to pass the membrane by passive flip-flop. Both the absence of micelle formation and the absence of flip-flop can be attributed to the extensive hydrophilic oligosaccharidic moiety of the Nod factors. The properties described in chapter 3 are not limited to Nod factors from *Rhizobium leguminosarum* since lipochitooligosaccharides secreted by other *Rhizobium* species usually contain a more extensive and sometimes charged chitin backbone. For example, in chapter 5 it is shown that the sulfated fluorescent Nod factor LCO-IV(BODIPY FL-C₁₆, S) also transfers rapidly between vesicles, whereas intramembrane flip-flop does not occur. Also the preference for membrane-like structures can most likely be extrapolated to all Nod factors described so far.

Role of acyl chain in perception of Nod factors - targeting or recognition?

Not all of the new fluorescent Nod factor were highly active in the deformation assay. NodRlv-IV(BODIPY 581/591-C₁₁) is inactive, whereas compounds with a similar hydrophobicity, NodRlv-IV(BODIPY FL-C₁₆) and NodRlv-IV(BODIPY 558/568-C₁₂), are active at 10⁻⁹ M and 10⁻⁸ M respectively, indicating that the hydrophobicity of the compound is not correlated with activity. Furthermore, the FCM experiments (chapter 4) show that the derivatives accumulate to a similar extent on *Vicia sativa* root hairs and have a similar molecular mobility. Since the physicochemical properties and the *in vivo* binding behavior of the fluorescent Nod factor derivatives are not depending on the acyl chain, their bioactivity provides information on the role of the acyl chain in Nod factor recognition.

It was already shown that the *cis* double bond present in natural LCOs secreted by *Rhizobium leguminosarum* (at position C11) and *Rhizobium meliloti* (at position C9) is not required for bioactivity (Demont-Caulet et al., 1999; Heidstra et al., 1994). However, it seems to be important for root hair deformation that the Nod factor acyl chain can adopt the conformation of a *cis*-bond at the position at which these unsaturations are naturally found. Obviously, this requirement is met by a fully saturated acyl chain. The proposed requirement of the acyl chain to be able to adopt a *cis*-bond is concluded from the root hair deformation experiments with the fluorescent Nod factors, as will be discussed below.

In case of Nod factors from *Rhizobium leguminosarum*, the *cis*-bond is located at position C11. The fluorescent Nod factor with a BODIPY 581/581-C₁₁ acyl chain did not show root hair deforming activity. As can be inferred from figure 1, this acyl chain is completely lacking the

ability to adopt the *cis* configuration, since carbon atom number 12 is part of the extensive fluorophore. The acyl chain that is one carbon atom longer is BODIPY 558/568-C₁₂. The Nod factors carrying this acyl chain have reduced activity, suggesting that not only the configuration is important but also the presence of an acyl chain beyond the *cis* double bond rather than an extensive fluorophore. This is supported by the fact that the fluorescent Nod factors with an acyl chain of 16 carbon atoms between the backbone and fluorophore are the most bioactive. NodRlv-IV (BODIPY 581/591-C₁₆) closely approaches the bioactivity of a natural fully saturated Nod factor. These bioactivity data nicely fit with the proposed importance of the *cis* configuration at position C11, although they do not explain why the bioactivity of NodRlv-IV (BODIPY FL-C₁₆) is at least 10-fold lower as compared to NodRlv-IV (BODIPY 581/591-C₁₆).

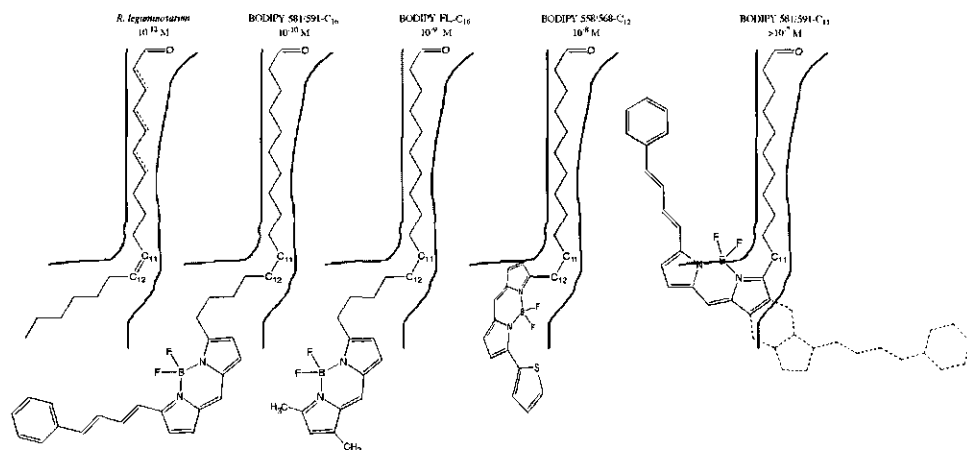


Figure 1: Natural and fluorescent synthetic acyl chains of NodRlv factors used in this study and their minimal concentration to induce root hair deformation on a compatible host legume (A putative consensus lipid-binding pocket of the Nod factor receptor, in which only acyl chains with a *cis*-configuration around C11 fit, is indicated by the bold lines enclosing the acyl chain). The dashed bonds indicate *trans* double bonds found in acyl chains of natural Nod factors. All natural Nod factors produced by *Rhizobium leguminosarum* *bv. viciae* contain a *cis* double bond at position C11. The fluorescent acyl chains are shown in a configuration that mimics the *cis* configuration of the natural acyl chain. The BODIPY 558/568-C₁₂ does not completely fit within the putative binding pocket, but can adopt a comparable conformation by rotating the BODIPY moiety out of the plane of the figure as illustrated. The consequently induced strain, could explain the reduced activity. For BODIPY 581/591-C₁₁, two configurations are given of which both will not fit within the proposed binding pocket, causing it to be inactive.

Since the *cis* double bond in the natural Nod factor from *Rhizobium meliloti* is located at position C9, being two atoms closer to the chitin backbone relative to NodRlv, it can be anticipated that the fluorophore can also be closer to the chitin backbone without losing bioactivity. This is nicely demonstrated by LCO-IV (BODIPY 558/568-C₁₂, S) which is still fully active in the root hair deformation assay on *Medicago truncatula* at a concentration down

to 10^{-10} M. The acyl chain can easily adopt the cis-bond configuration at C9. Of course, this is also true for sulfated Nod factors carrying BODIPY FL-C₁₆, which is bioactive at concentrations down to 10^{-9} M. Because only two different acyl chains were tested for sulfated LCOs, the data are too limited to get detailed insight in the importance of a cis configuration around C9.

For both sulfated and non-sulfated Nod factors, an extensive fluorophore at the end of the acyl chain does not block bioactivity, if the acyl chain is long enough. The high bioactivity of NodR_{lv}-IV (BODIPY 581/591-C₁₆) shows that the two terminal carbon atoms are not required for perception by root hairs. Similarly, the carbon atoms beyond C12 are superfluous for Nod factor recognition by *Medicago truncatula* root hairs as concluded from the bioactivity of LCO-IV (BODIPY 558/568-C₁₂, S). These results are in agreement with the systematic study by Demont-Caulet et al. (1999), in which the importance of unsaturations and the length of the acyl chain was examined. A nodulation assay on *Medicago sativa* was used, showing that sulfated LCOs with an acyl chain of C8 are hardly active, whereas LCOs with an acyl chain of 12, 16 and 18 carbon atoms are, with C16 being most active. Although the assay is different, it is of note that these authors also propose specific recognition of the acyl chain.

A logical candidate for imposing the cis-bond configuration is a fatty acid binding pocket. We propose that such a putative lipid binding pocket is part of the Nod factor receptor. Based on the relation between bioactivity and acyl chain structure a consensus fatty acid binding pocket is suggested in figure 1 for the perception of NodR_{lv} factors. The most important features are the cis configuration around C11 and a relative big space in which the fluorophore will fit. Alternatively, the end of the acyl chain sticks out of the binding pocket. The consensus binding pocket for sulfated Nod factors could be similar in shape, but two carbon atoms shorter. The proposed requirements of the acyl chain structure with respect to bioactivity provide information necessary for the design of novel Nod factor derivatives. For example, these results predict that a sulfated LCO with a BODIPY 581/591-C₁₁ acyl chain would still have activity in the root hair deformation assay. Undoubtedly a more systematic study involving more (BODIPY) acyl chains would provide more detailed information, possibly proving our hypothesis that the lipid binding pocket of the Nod factor signaling receptor is kinked. And to examine the importance of the cis configuration in a direct way, it would be interesting to synthesize an LCO in which the cis-bond is replaced by a trans-bond at the same position. In summary, the results presented here provide the first evidence that a specific configuration of the Nod factor acyl chain is required for root hair deformation activity.

Where are Nod factors perceived?

Certainly, no straightforward answer existed to the question whether Nod factors are perceived extracellular or intracellular. Two studies indicate the possibility that Nod factors act intracellular in root hairs (Philip-Hollingsworth et al., 1997) or nodules (Timmers et al., 1998),

whereas another paper shows surface labeling of root hairs (Gadella Jr. et al., 1997b). Philip-Hollingsworth et al. studied the location of fluorescent Nod factors on white clover (*Trifolium repens*) and reported the accumulation of fluorescence inside root hairs within 30 minutes. These results are in marked contrast to the results described in this thesis. Four issues have to be kept in mind when interpreting the results of Philip-Hollingsworth et al. First, the NBD-labeled Nod factor was applied at a high concentration (1 μM). Second, unlike for BODIPY fluorophores, the fluorescence of the NBD probe is essentially quenched in aqueous environment (Haugland, 1996), which may result in an underestimation of Nod factors associated with the primary cell, of which two thirds is water (Cosgrove, 1997). Third, it is not analyzed whether the fluorescence represents the intact compound. Moreover, as the original Nod factor is the product after cleaving off the NBD label by root chitinases, degradation of the fluorescent derivative could lead to erratic interpretation of bioactivity tests (analyzed after at least two days of incubation). Fourth, the fluorescent label that has been used has a known affinity for membrane-water interfaces (Chattopadhyay and London, 1987; Huster et al., 2001), thereby probably modifying the physicochemical properties of the reducing end of a natural LCO and possibly altering the affinity for the cell wall and plasma membrane.

Being aware of these caveats and knowing the results described in this thesis (chapter 3, chapter 4 and chapter 5) there is strong evidence that Nod factor perception leading to root hair deformation takes place extracellular as will also be discussed below. First, when a low Nod factor concentration is applied exogenously, i.e. lower than or equal to 10 nM, the vast majority of fluorescence is associated with the cell wall. It is of note that the BODIPY acyl chain alone ends up in the root hair cytosol, showing that the chitin backbone is necessary for Nod factor binding to the cell wall. Second, no modification or degradation of the fluorescent Nod factor derivatives was observed within ten minutes after application. After 30-60 minutes only a minute fraction of NodR1v-II was present on roots of *Vicia sativa*, probably due to chitinase activity. These results indicate that the fluorescence accumulated at the surface of root hairs represents intact Nod factor.

Interestingly, a minute amount of fluorescence in the root hair cytoplasm could be observed, but only with the very sensitive FCM technique (chapter 4). Application of 0.1 nM free BODIPY labeled fatty acid (i.e. 100-fold lower than the concentration of Nod factor) gave similar FCM results. This indicates that the intracellular fluorescence observed upon Nod factor application probably reflects endomembrane labeling by a minor lipophilic degradation product, possibly a fatty acyl chain. Another possibility involving an active flip-flop mechanism of Nod factors is unlikely as the increase of fluorescence was immediate and could not be suppressed by competition with an excess of unlabeled Nod factor (data not shown). Administering high concentrations of labeled Nod factors resulted in cell wall and plasma membrane labeling, but no visible intracellular fluorescence that could reflect endocytosis. We therefore think that the

minor intracellular signal that could only be observed by FCM is reflecting a breakdown product.

In the study described in chapter 5, the sulfated derivative LCO-IV(BODIPY 558/568-C₁₂, S) was studied on both *Vicia sativa* (vetch) and *Medicago truncatula* (barrelclover) and the results were compared to binding of the non-sulfated derivative. In all combinations, the fluorescent derivatives were present in the cell wall when applied at 10 nM. Moreover, detailed molecular characterization by FCM shows that sulfated and non-sulfated LCOs have similar molecular mobility on compatible and non-compatible host-legumes. Thus, Nod factors derivatives are located at the same sites in the root hair cell wall on either host and non-host legumes. This indicates that decoration of the chitin backbone with a sulfate group is not sufficient to alter its binding characteristics to either *Vicia sativa* or *Medicago truncatula*.

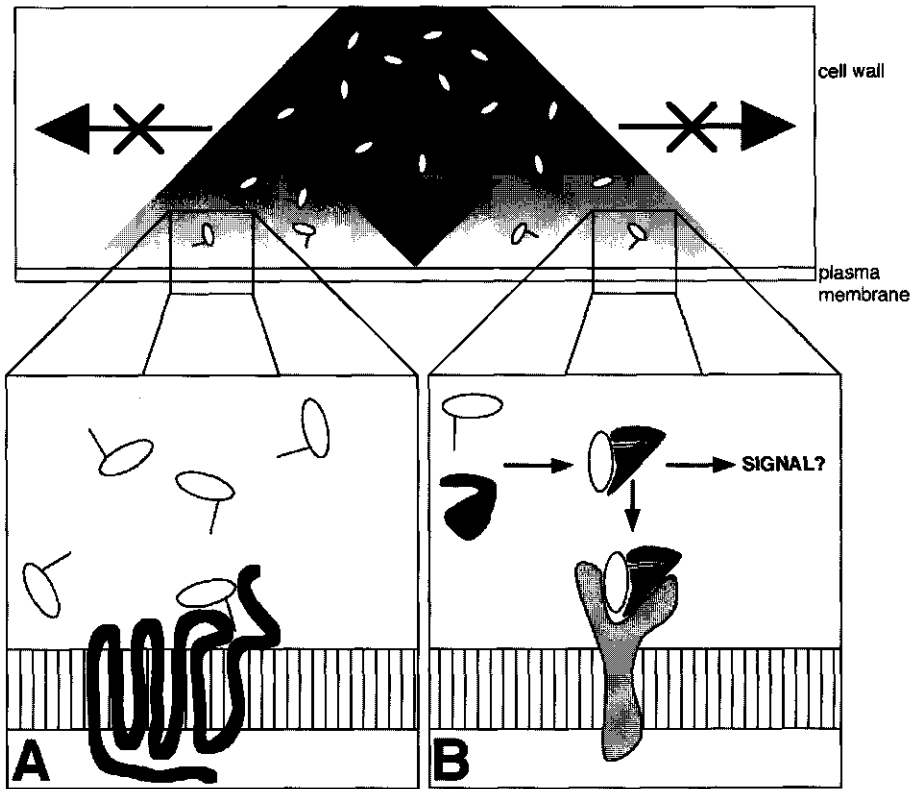


Figure 2: Possible modes of Nod factor perception. After binding and immobilization of Nod factors by the cell wall, Nod factors can be specifically recognized at the plasma membrane (A) or cell wall (B). In case of (A) only few Nod factors would reach a receptor (in this example a 7-transmembrane receptor activating a G-protein mediated pathway). If perception takes place in the cell wall (B), a secreted protein could bind a Nod factor, thereby activating a signaling pathway in the cell wall. Alternatively, the Nod factor-protein complex shuttles to an extracellular site of a transmembrane receptor, after which recognition of the complex activates a signaling cascade. Model B includes a hybrid binding site on the signaling receptor, partly recognizing the Nod factor and partly recognizing the binding protein.

Staining of the plasma membrane of root hairs at higher concentrations of Nod factors shows that the cell wall is permeable for Nod factors. Therefore, it can not be excluded that actual perception of Nod factors takes place at the plasma membrane, although the Nod factors are predominantly associated with the cell wall. This mode of perception (model A in figure 2) would implicate a role for the cell wall in grabbing Nod factors from the surface of the rhizobia followed by immobilization. Only a few Nod factor molecules finally end up at the membrane, which seems rather inefficient. However, the number of Nod factor molecules produced by a single *Rhizobium* bacterium (10^7 , see below) is consistent with this possibility. If we assume that the receptor contains a lipid binding pocket, which is concluded from the acyl chain recognition, the plasma membrane would not be the favorable location for the binding pocket. In this case, the continuous abundance of acyl chains (of membrane lipids) that are present at a very high concentration in the membrane compete extensively for the lipid binding pocket with the very low amount of Nod factor located in the plasma membrane. Hence, a mechanism in which the Nod factor acyl chain is responsible for membrane localization and association with the Nod factor receptor and the chitin backbone for specific recognition by a putative transmembrane Nod factor receptor is unlikely, both from theoretical considerations and given our experimental evidence. An alternative would be that the lipid binding pocket of the transmembrane receptor is located extracellularly. In this case no competition for the binding pocket between membrane lipids and Nod factors exists, yielding a more efficient activation mechanism.

The second possibility is that, besides binding and immobilization, also perception of Nod factors takes place in the cell wall (figure 2B). Still, within this option the Nod factor signal needs to be transduced across the plasma membrane. This could be achieved by a transmembrane protein recognizing a conformational change of a cell wall associated Nod factor binding protein upon Nod factor binding. Because we do not see a correlation between cell wall binding efficiency or mobility of Nod factors on the one hand and their capability to induce root hair deformation on the other hand, it is likely that in this case Nod factor binding and recognition is accomplished by two different molecules: a binding (immobilizing) molecule and a receptor molecule. The binding protein would be biologically relevant for providing an immobilized Nod factor source and the consequent positional information. The receptor molecule in this model specifically recognizes the sulfate group (or its absence) and certain features of the Nod factor acyl chain.

In this respect, it is interesting to note that the first Nod factor binding site (NFBS1) was characterized in *M.truncatula* root extracts that were most abundant in a high-density fraction, and not in the microsomal fraction (Bono et al., 1995). Moreover, a similar binding site was identified in tomato root extracts. Both the chitin moiety and the acyl chain were necessary for binding, but the absence of the sulfate group did not alter the binding characteristics. These data

fit nicely with the observed binding characteristics of the fluorescent LCOs *in vivo*. A high affinity binding site (NFBS2) was found in a plasma membrane-enriched fraction of *Medicago* cell suspension cultures. Although some recognition of the Nod factor reducing end was reported, no dependence of binding on the sulfate group was observed for both binding proteins (Gressent et al., 1999). Based on our results, we think that it is likely that our *in vivo* binding studies do reflect the same protein. Interestingly, both studies using completely different approaches point out that in addition to the Nod factor binding protein, another Nod factor recognizing factor is required to explain the different biological activity of non-sulfated and sulfated Nod factors.

Several groups have undertaken the analysis of mutants that are disturbed in Nod factor perception (Catoira et al., 2000; Wais et al., 2000; Walker et al., 2000). The idea is to obtain the Nod factor receptor by identifying the mutated genes. In the case that Nod factor perception takes place by a single receptor located at the plasma membrane (A, in figure 2), both the biochemical and genetic approach will be able to identify the Nod factor receptor. However, for the second option involving multiple components (B, in figure 2), the biochemical approach and the genetic approach will likely yield different proteins. Model B predicts that, for instance by a genetic approach, receptor like kinases could be identified having no affinity for Nod factors. Moreover, Nod factor binding proteins could be identified with a biochemical approach, and it could turn out that these have no apparent signal transducing activity. This mode of perception has some similarities with another signaling system in plants, involving the Cf9 receptor-like protein which is required to confer resistance against the *Cladosporium fulvum* disease (Torii, 2000). This Cf9 transmembrane protein does not have a significant intracellular domain for transducing signals, and binding of the ligand (Avr9) is independent of the presence of Cf9. These data indicate that, possibly similar to Nod factor perception, at least two proteins are involved in perception and subsequent signal transduction.

The characterization of ligand-receptor interactions in plants yields a complex picture due to interaction between multiple receptor-like proteins (Torii, 2000), suggesting, together with the knowledge of Nod factor perception so far, that also in case of Nod factor perception some surprises can be anticipated. To come to a complete picture of Nod factor perception we are convinced that we will need the combined effort of genetic, biochemical and *in situ* studies possibly each contributing an important part to a complex puzzle. This will also reveal the location at which Nod factors are perceived, whether either of the two models is correct and undoubtedly that both models were naively oversimplified.

Nod factor secretion and perception in nature

The experiments presented in this thesis are performed under well-defined artificial conditions. Therefore, it is of interest to translate the results to the natural situation in which the symbiosis is initiated. The lowest concentration at which Nod factors are fully active in the root hair

deformation test on *Vicia sativa* is 10^{-11} M. The Fåhrens slide is quite artificial in that it presents the Nod factors to the plant as a homogenous aqueous solution. The root hairs immediately bind and accumulate Nod factor in their cell walls, and deplete the Nod factors from the medium. Probably, a minimal threshold of accumulation has to be achieved to elicit a response. In other words, the concentration which is provided in the root hair deformation test is manifold lower than the concentration that actually ends up in the root hair cell wall. This is illustrated by the calculation of the actual Nod factor concentration in the cell wall as described in chapter 4, indicating that upon application of 10 nM Nod factor in the medium, the Nod factor concentration can be as high as 500 nM in the cell wall. Such a concentration would imply that in the root hair deformation assay under those conditions about 500,000 Nod factor molecules associate with a single root hair cell wall (chapter 4). In this respect it is of interest to consider the number of Nod factor molecules produced by a single wild-type induced *Rhizobium* bacteria which can be as high as 10 million (Orgambide et al., 1995). Assuming that the bacterium has a shape of a cylinder with a height of 2 μm and a diameter of 1 μm representing a volume of 1.6 femtoliter, the 10^7 Nod factors would imply a point source of Nod factors with a concentration of 10 mM. It is conceivable that the calculated number is an overestimation due to the optimal induction and cultivation of the bacteria and that only a small number of these Nod factors is available. Still, even a cautious estimate would lead to a relatively high number of molecules per bacterium.

From these simple calculations it seems that the bacterium produces many more Nod factor molecules than required for root hair deformation. We hypothesize that curling and infection thread initiation, necessary for infection, need a high local concentration rather than a low amount of Nod factor distributed over the entire root hair. On the one hand, these considerations argue in favor of model A (figure 2) where the cell wall acts as a buffer and only where a high amount of Nod factors is achieved, the plasmamembrane will be labeled. On the other hand, the observation that membrane bound Nod factors can easily transfer to a cell wall implicates a higher affinity for cell walls than for membranes. Also, it is likely that upon insertion in the membrane, the Nod factors can diffuse laterally like phospholipids in membranes, which would result in a quick dilution and consequent loss of the local generated signal.

A general role for the cell wall for the immobilization of ligands?

The studies described in chapter 4 and chapter 5 show an unexpected accumulation and immobilization of Nod factors in the root hair cell wall. Fluorescence correlation microscopy was used to obtain detailed information on diffusional behavior at a molecular level. Applying this technique to living root hairs has contributed greatly to interpreting the static images that are obtained by fluorescence imaging. The immobilization of Nod factors in the cell wall is interpreted as being important in the *Rhizobium*-legume symbiosis since the information on the location of a bacterium is of great importance to guide the root hair which curls around the

bacterium. Therefore, any soluble fast diffusing signal secreted by the bacteria that should provide the plant with spatial information on the location of the bacteria needs to be immobilized.

The retention of spatial information is not only important in *Rhizobium*-legume interactions, but also in other interactions of the plant with its environment. For example, when plants react to a pathogen by necrosis, it is of importance to spatially restrict the signal of the pathogen to induce necrosis solely in the cells that are in contact with the pathogen. Another example of spatially encoded information is provided by the relative well-characterized ligand-receptor interaction in plants which is the CLAVATA3-CLAVATA1 interaction. Also for the ligand CLAVATA3, which is probably secreted, it has been shown that spatial restriction of the protein is necessary for normal development. When this protein is ectopically expressed under control of the 35S promoter, thereby losing its natural spatially restricted pattern, organ initiation is obstructed (Doerner, 2000).

Based on the results presented in this thesis and the two other examples mentioned above, it is tempting to speculate that spatial restriction of signaling molecules is achieved by immobilization in the cell wall. So far, there is a lack of studies on ligands in plant cells, impeding a clear picture of perception of ligands by a plant cell and the role of the cell wall in particular. Future studies using labeled ligands *in vivo* are necessary to establish whether slow diffusion or immobilization of ligands by cell walls is a general phenomenon.

Also, it is of importance to explore approaches that can induce local signaling. In chapter 6, such a strategy is described. The use of photosensitive precursors is ideally suited to activate signaling with high spatial resolution. It has been shown that in *A.thaliana* root hairs the local influx of calcium by local photolysis of a caged calcium ionophore is enough to induce reorientation of the tip-growth (Bibikova et al., 1997). This result shows that in Nod factor signaling both extra- and intracellular mechanisms can exist to spatially restrict a signal and consequently drive root hair morphogenesis. In chapter 5, we analyzed the *Medicago truncatula* *hcl* mutant that is disturbed in curling and hence possibly disturbed in generating a local signal in response to Nod factors. Our results show that the *hcl* mutant is still able to immobilize and concentrate Nod factors suggesting that this part of the mechanism, possibly necessary for curling, is intact in this mutant. It is therefore likely that a yet unknown factor (possibly cytosolic) is disturbed in the *hcl* mutant, abolishing the required intracellular generation of locally activated signaling. To further investigate the significance of local intracellularly activated signaling for driving root hair morphogenesis and curling, it will be interesting to synthesize and use caged derivatives of signaling molecules and downstream components of the Nod factor signaling cascade. For example, the local uncaging of a photosensitive Nod factor will reveal the significance of spatially restricted Nod factor signaling. This powerful approach can also be applied to dissect which of the putative second messengers, e.g. phosphatidic acid (Den Hartog et al., 2001), is involved in transducing a local signal to the cytoskeleton.

REFERENCES

- Adams, S.R. and Tsien, R.Y. (1993) Controlling cell chemistry with caged compounds. *Annu. Rev. Physiol.*, **55**, 755-784.
- Arndt-Jovin, D.J., Latt, S.A., Striker, G. and Jovin, T.M. (1979) Fluorescence decay analysis in solution and in a microscope of DNAs and chromosomes stained with quinacrine. *J. Histochem. Cytochem.*, **27**, 87-95.
- Axelrod, D. (1989) Fluorescence polarization microscopy. *Meth. Cell Biol.*, **30**, 333-352.
- Bai, J. and Pagano, R.E. (1997) Measurement of spontaneous transfer and transbilayer movement of Bodipy-labeled lipids in lipid vesicles. *Biochemistry*, **36**, 8840-8848.
- Balaban, R.S., Kurtz, I., Cascio, H.E. and Smith, P.D. (1986) Microscopic spectral imaging using a video camera. *J. Microsc.*, **141**, 31-39.
- Barny, M.A. and Downie, J.A. (1993) Identification of the NodC protein in the inner but not the outer membrane of *Rhizobium leguminosarum*. *Mol. Plant-Microbe Interact.*, **6**, 669-672.
- Bastiaens, P.I.H. and Jovin, T.M. (1996) Microspectroscopic imaging tracks the intracellular processing of a signal transduction protein: fluorescent-labeled protein kinase C. *Proc. Natl. Acad. Sci. USA*, **93**, 8407-8412.
- Batzri, S. and Korn, E.D. (1973) Single bilayer liposomes prepared without sonication. *Biochim. Biophys. Acta*, **298**, 1015-1019.
- Beechem, J.M., Gratton, E., Ameloot, M., Knutson, J.R. and Brand, L. (1992) The global analysis of fluorescence intensity and anisotropy decay data: second-generation theory and programs. In *Topics in Fluorescence Spectroscopy*, (Lakowicz, J.R. (ed.)). Plenum Press, New York, Vol. 2, pp. 241-305.
- Berland, K.M., So, P.T.C. and Gratton, E. (1995) Two-photon fluorescence correlation spectroscopy: method and application to the intracellular environment. *Biophys. J.*, **68**, 694-701.
- Berland, K.M., So, P.T.C., Sen, Y., Mantulin, W.W. and Gratton, E. (1996) Scanning Two-Photon Fluctuation Correlation Spectroscopy: Particle Counting Measurements for Detection of Molecular Aggregation. *Biophys. J.*, **71**, 410-420.
- Bhuvanawari, T.V. and Solheim, B. (1985) Root hair deformation in the white clover/*Rhizobium trifolii* symbiosis. *Physiol. Plant.*, **63**, 25-34.
- Bibikova, T.N., Jacob, T., Dahse, I. and Gilroy, S. (1998) Localized changes in apoplastic and cytoplasmic pH are associated with root hair development in *Arabidopsis thaliana*. *Development*, **125**, 2925-2934.
- Bibikova, T.N., Zhigilei, A. and Gilroy, S. (1997) Root hair growth in *Arabidopsis thaliana* is directed by calcium and an endogenous polarity. *Planta*, **203**, 495-505.
- Bloemberg, G.V., Thomas-Oates, J.E., Lugtenberg, B.J.J. and Spink, H.P. (1994) Nodulation protein NodL of *Rhizobium leguminosarum* O-acetylates lipo-oligosaccharides, chitin fragments and N-acetylglucosamine in-vitro. *Mol. Microbiol.*, **11**, 793-804.
- Boller, T. and Mauch, F. (1988) Colorimetric assay for chitinase. *Methods Enzymol.*, **161**, 430-435.
- Bono, J.J., Rioud, J., Nicolaou, K.C., Bockovich, N.J., Estevez, V.A., Cullimore, J.V. and Ranjeva, R. (1995) Characterization of a binding site for chemically synthesized lipo- oligosaccharidic NodRm factors in particulate fractions prepared from roots. *Plant J.*, **7**, 253-260.

- Brauer, D., Otto, J. and Tu, S. (1995) Selective accumulation of the fluorescent pH indicator BCECF, in vacuoles of maize root-hair cells. *J. Plant Physiol.*, **145**, 57-61.
- Brauer, D., Uknalis, J., Triana, R. and Tu, S. (1996) Subcellular compartmentation of different lipophilic fluorescein derivatives in maize root epidermal cells. *Protoplasma*, **192**, 70-79.
- Bright, G.R. (1993) Fluorescence ratio imaging: issues and artifacts. In *Optical microscopy - Emerging methods and applications*, (Herman, B. and Lemasters, J.J. (eds.)). Academic Press, San Diego, pp. 87-114.
- Bright, G.R., Fisher, G.W., Rogowska, J. and Taylor, D.L. (1989) Fluorescence ratio imaging microscopy. *Meth. Cell Biol.*, **30**, 157-192.
- Brock, R., Hink, M.A. and Jovin, T.M. (1998) Fluorescence correlation microscopy (FCM) of cells in the presence of autofluorescence. *Biophys. J.*, **75**, 2547-2557.
- Brock, R. and Jovin, T.M. (1998) Fluorescence correlation microscopy (FCM) - FCS taken into the cell. *Cell Mol. Biol.*, **44**, 847-856.
- Brock, R., Vàmosi, G., Vereb, G. and Jovin, T.M. (1999) Rapid characterization of green fluorescent protein fusion proteins on the molecular and cellular level by fluorescence correlation microscopy. *Proc. Natl. Acad. Sci. USA*, **96**, 10123-10128.
- Brown, M.P. and Royer, C. (1997) Fluorescence spectroscopy as a tool to investigate protein interactions. *Curr. Opin. Biotechnol.*, **8**, 45-49.
- Bullen, A. and Saggau, P. (1999) High-speed, random-access fluorescence microscopy: II. Fast quantitative measurements with voltage-sensitive dyes. *Biophys. J.*, **76**, 2272-2287.
- Cabib, E. and Bowers, B. (1971) Chitin and yeast budding. *J. Biol. Chem.*, **246**, 152-159.
- Catoira, R., Galera, C., de Billy, F., Penmetsa, R.V., Journet, E.P., Maillet, F., Rosenberg, C., Cook, D., Gough, C. and Denarie, J. (2000) Four genes of medicago truncatula controlling components of a nod factor transduction pathway. *Plant Cell*, **12**, 1647-1666.
- Catoira, R., Timmers, A.C., Maillet, F., Galera, C., Penmetsa, R.V., Cook, D., Denarie, J. and Gough, C. (2001) The HCL gene of Medicago truncatula controls Rhizobium-induced root hair curling. *Development*, **128**, 1507-1518.
- Chattopadhyay, A. and London, E. (1987) Parallax method for direct measurement of membrane penetration depth utilizing fluorescence quenching by spin-labeled phospholipids. *Biochemistry*, **26**, 39-45.
- Clegg, R.M. (1995) Fluorescence resonanc energy transfer. *Curr. Biol.*, **6**, 103-110.
- Clegg, R.M. (1996) Fluorescence resonance energy transfer. In *Fluorescence imaging spectroscopy and microscopy*, (Wang, X.-F. and Herman, B. (eds.)). John Wiley & Sons, New York, pp. 179-252.
- Comfurius, P. and Zwaal, R.F. (1977) The enzymatic synthesis of phosphatidylserine and purification by CM-cellulose column chromatography. *Biochim. Biophys. Acta*, **488**, 36-42.
- Cosgrove, D.J. (1997) Assembly and enlargement of the primary cell wall in plants. *Annu. Rev. Cell. Dev. Biol.*, **13**, 171-201.
- Cullimore, J.V., Ranjeva, R. and Bono, J.J. (2001) Perception of lipo-chitoooligosaccharidic Nod factors in legumes. *Trends Plant Sci.*, **6**, 24-30.
- Demont-Caulet, N., Maillet, F., Tailler, D., Jacquinet, J.C., Prome, J.C., Nicolaou, K.C., Truchet, G., Beau, J.M. and Denarie, J. (1999) Nodule-inducing activity of synthetic Sinorhizobium meliloti nodulation

- factors and related lipo-chitooligosaccharides on alfalfa. Importance of the acyl chain structure. *Plant Physiol.*, **120**, 83-92.
- Den Hartog, M., Musgrave, A. and Munnik, T. (2001) Nod factor-induced phosphatidic acid and diacylglycerol pyrophosphate formation: a role for phospholipase C and D in root hair deformation. *Plant J.*, **25**, 55-65.
- Derman, M.P., Toker, A., Hartwig, J.H., Spokes, K., Falck, J.R., Chen, C.S., Cantley, L.C. and Cantley, L.G. (1997) The lipid products of phosphoinositide 3-kinase increase cell motility through protein kinase C. *J. Biol. Chem.*, **272**, 6465-6470.
- Devaux, P.F. (1992) Protein involvement in transmembrane lipid asymmetry. *Annu. Rev. Biophys. Biomol. Struct.*, **21**, 417-439.
- Dix, J.A. and Verkman, A.S. (1990) Mapping of fluorescence anisotropy in living cells by ratio imaging. *Biophys. J.*, **57**, 231-240.
- Doerner, P. (2000) Plant stem cells: The only constant thing is change. *Curr. Biol.*, **10**, R826-829.
- Domard, A. and Vasseur, V. (1991) Non-specificity of a colorimetric method for the estimation of N-acetyl-D-glucosamine. *Int. J. Biol. Macromol.*, **13**, 366-368.
- Downie, J.A. (1998) Functions of rhizobial nodulation genes. In *The Rhizobiaceae - Molecular Biology of model plant-associated bacteria*, (Spaink, H.P., Kondorosi, A. and Hooykaas, P.J.J. (eds.)). Kluwer, Dordrecht, The Netherlands, pp. 387-402.
- Downie, J.A. and Walker, S.A. (1999) Plant responses to nodulation factors. *Curr. Opin. Plant Biol.*, **2**, 483-489.
- Edward, J.T. (1970) Molecular volumes and the Stokes-Einstein equation. *J. Chem. Educ.*, **47**, 261-270.
- Ehrenberg, M. and Rigler, R. (1974) Rotational brownian motion and fluorescence intensity fluctuations. *Chem. Phys.*, **4**, 390-401.
- Ehrhardt, D.W., Atkinson, E.M. and Long, S.R. (1992) Depolarization of alfalfa root hair membrane potential by *rhizobium meliloti* nod factors. *Science*, **256**, 998-1000.
- Ehrhardt, D.W., Wais, R. and Long, S.R. (1996) Calcium spiking in plant root hairs responding to rhizobium nodulation signals. *Cell*, **85**, 673-681.
- Ellenberg, J., Lippincott-Schwartz, J. and Presley, J.F. (1999) Dual-colour imaging with GFP variants. *Trends Cell Biol.*, **9**, 52-56.
- Elsou, E.L. and Magde, D. (1974) Fluorescence correlation spectroscopy. I. Conceptual basis and theory. *Biopolymers*, **13**, 1-27.
- English, D., Cui, Y. and Siddiqui, R.A. (1996) Messenger functions of phosphatidic acid. *Chem. Phys. Lipids*, **80**, 117-132.
- Etzler, M.E., Kalsi, G., Ewing, N.N., Roberts, N.J., Day, R.B. and Murphy, J.B. (1999) A nod factor binding lectin with apyrase activity from legume roots. *Proc. Natl. Acad. Sci. USA*, **96**, 5856-5861.
- Felle, H.H., Kondorosi, E., Kondorosi, A. and Schultze, M. (1995) Nod signal-induced plasma membrane potential changes in alfalfa root hairs are differentially sensitive to structural modifications of the lipochitooligosaccharide. *Plant J.*, **7**, 939-947.
- Felle, H.H., Kondorosi, E., Kondorosi, A. and Schultze, M. (1996) Rapid alkalization in alfalfa root hairs in response to rhizobial lipochitooligosaccharide signals. *Plant J.*, **10**, 295-301.

-
- Felle, H.H., Kondorosi, E., Kondorosi, A. and Schultze, M. (1998) The role of ion fluxes in Nod factor signaling in *Medicago sativa*. *Plant J.*, **13**, 455-465.
- Folch, J., Lees, M. and Sloane-Stanley, G.H. (1957) A simple method for the isolation and purification of total lipids from animal tissue. *J. Biol. Chem.*, **226**, 497-509.
- Förster, T. (1948) Zwischenmolekulare Energiewanderung und Fluoreszenz. *Ann. Phys.*, **2**, 55-75.
- Fricker, M.D., Plieth, C., Knight, H., Blancaflor, E., Knight, M.R., White, N.S. and Gilroy, S. (1999) Fluorescence and luminescence techniques to probe ion activities in living plant cells. In *Fluorescent and luminescent probes for biological activity*, (Mason, W.T. (ed.)). Academic Press, London, pp. 569-596.
- Gadella Jr., T.W.J. (1999) Fluorescence Lifetime Imaging Microscopy (FLIM): Instrumentation and Applications. In *Fluorescent and Luminescent Probes for biological activity 2nd edition*, (Mason, W.T. (ed.)). Academic Press, London, pp. 467-479.
- Gadella Jr., T.W.J., Clegg, R.M. and Jovin, T.M. (1994) Fluorescence lifetime imaging microscopy: pixel-by-pixel analysis of phase-modulation data. *Bioimaging*, **2**, 139-159.
- Gadella Jr., T.W.J. and Jovin, T.M. (1995) Oligomerization of epidermal growth factor receptors on A431 cells studied by time-resolved fluorescence imaging microscopy. A stereochemical model for tyrosine kinase receptor activation. *J. Cell Biol.*, **129**, 1543-1558.
- Gadella Jr., T.W.J. and Jovin, T.M. (1997) Fast algorithms for the analysis of single and double exponential decay curves with a background term. Application to time-resolved imaging microscopy. *Bioimaging*, **5**, 19-39.
- Gadella Jr., T.W.J., Jovin, T.M. and Clegg, R.M. (1993) Fluorescence lifetime imaging microscopy (FLIM): Spatial resolution on the nanosecond time scale. *Biophys. Chem.*, **48**, 221-239.
- Gadella Jr., T.W.J., van der Krogt, G.M.N. and Bisseling, T. (1999) GFP-based FRET microscopy in single living plant cells. *Trends Plant Sci.*, **4**, 287-291.
- Gadella Jr., T.W.J., van Hoek, A. and Visser, A.J.W.G. (1997a) Construction and characterization of a frequency-domain fluorescence lifetime imaging microscopy system. *J. Fluorescence*, **7**, 35-43.
- Gadella Jr., T.W.J., Vereb, G., Hadri, A.E., Rohrig, H., Schmidt, J., John, M., Schell, J. and Bisseling, T. (1997b) Microspectroscopic imaging of nodulation factor-binding sites on living *Vicia sativa* roots using a novel bioactive fluorescent nodulation factor. *Biophys. J.*, **72**, 1986-1996.
- Gadella Jr., T.W.J. and Wirtz, K.W.A. (1994) Phospholipid binding and transfer by the nonspecific lipid-transfer protein (sterol carrier protein 2). *Eur. J. Biochem.*, **220**, 1019-1028.
- Gennerich, A. and Schild, D. (2000) Fluorescence correlation spectroscopy in small cytosolic compartments depends critically on the diffusion model used. *Biophys J.*, **79**, 3294-3306.
- Gerritsen, H.C., Sanders, R., Draaijer, A., Ince, C. and Levine, Y.K. (1997) Fluorescence lifetime imaging of oxygen in living cells. *J. Fluorescence*, **7**, 11-15.
- Gilroy, S. (1997) Fluorescence microscopy of living plant cells. *Ann. Rev. Plant Phys. Plant Mol. Biol.*, **48**, 165-190.

- Goedhart, J., Hink, M.A., Visser, A.J.W.G., Bisseling, T. and Gadella, T.W.J., Jr. (2000) *In vivo* fluorescence correlation microscopy (FCM) reveals accumulation and immobilization of Nod factors in root hair cell walls. *Plant J.*, **21**, 109-119.
- Goedhart, J., Rohrig, H., Hink, M.A., van Hoek, A., Visser, A.J.W.G., Bisseling, T. and Gadella, T.W.J., Jr. (1999) Nod factors integrate spontaneously in biomembranes and transfer rapidly between membranes and to root hairs, but transbilayer flip-flop does not occur. *Biochemistry*, **38**, 10898-10907.
- Gordon, G.W., Berry, G., Liang, X.H., Levine, B. and Herman, B. (1998) Quantitative fluorescence resonance energy transfer measurements using fluorescence microscopy. *Biophys. J.*, **74**, 2702-2713.
- Gressent, F., Drouillard, S., Mantegazza, N., Samain, E., Geremia, R.A., Canut, H., Niebel, A., Driguez, H., Ranjeva, R., Cullimore, J. and Bono, J.-J. (1999) Ligand specificity of a high-affinity binding site for lipo- chitooligosaccharidic nod factors in medicago cell suspension cultures. *Proc. Natl. Acad. Sci. USA*, **96**, 4704-4709.
- Gross, D. and Loew, L.M. (1989) Fluorescent indicators of membrane potential: microspectrofluorometry and imaging. *Meth. Cell Biol.*, **30**, 193-218.
- Gupta, M.C., Radhakrishnan, R. and Khorana, H.G. (1977) Glycerophospholipid synthesis: Improved general method and new analogs containing photoactivable groups. *Proc. Natl. Acad. Sci. USA*, **74**, 4315-4319.
- Haugland, R.P. (1996) *Handbook of fluorescent probes and research chemicals*. Molecular Probes Inc., Eugene.
- Heidstra, R. and Bisseling, T. (1996) Nod factor-induced host responses and mechanisms of Nod factor perception. *New Phytol.*, **133**, 25-43.
- Heidstra, R., Geurts, R., Franssen, H., Spaijk, H., van Kammen, A. and Bisseling, T. (1994) Root hair deformation activity of nodulation factors and their fate on *Vicia sativa*. *Plant Physiol.*, **105**, 787-797.
- Hink, M.A., Van Hoek, A. and Visser, A.J.W.G. (1999) Dynamics of phospholipid molecules in micelles: characterization with fluorescence correlation spectroscopy and time-resolved fluorescence anisotropy. *Langmuir*, **15**, 992-997.
- Hink, M.A. and Visser, A.J.W.G. (1998) Characterization of membrane mimetic systems with fluorescence correlation spectroscopy. In *Applied fluorescence in chemistry, biology and medicine*, (Rettig, W., Strehmel, B., Schrader, S. and Seitert, H. (eds.)). Springer Verlag, Berlin, pp. 101-118.
- Hirsch, A. (1992) Developmental biology of legume nodulation. *New Phytol.*, **122**, 211-237.
- Homan, R. and Pownall, H.J. (1988) Transbilayer diffusion of phospholipids: dependence on headgroup structure and acyl chain length. *Biochim. Biophys. Acta*, **938**, 155-166.
- Hovius, R., Vallotton, P., Wohland, T. and Vogel, H. (2000) Fluorescence techniques: shedding light on ligand-receptor interactions. *Trends Pharmacol. Sci.*, **21**, 266-273.
- Huster, D., Muller, P., Arnold, K. and Herrmann, A. (2001) Dynamics of Membrane Penetration of the Fluorescent 7-Nitrobenz-2-Oxa- 1,3-Diazol-4-yl (NBD) Group Attached to an Acyl Chain of Phosphatidylcholine. *Biophys. J.*, **80**, 822-831.
- Jameson, D.M., Gratton, E. and Hall, R.D. (1984) The measurement and analysis of heterogenous emissions by multifrequency phase and modulation fluorometry. *Appl. Spectrosc. Rev.*, **20**, 55-106.

- Johnson, I.D., Kang, H.C. and Haugland, R.P. (1991) Fluorescent membrane probes incorporating dipyrrometheneboron difluoride fluorophores. *Anal. Biochem.*, **198**, 228-237.
- Johnson, S.M., Bangham, A.D., Hill, M.W. and Korn, E.D. (1971) Single bilayer liposomes. *Biochim. Biophys. Acta*, **233**, 820-826.
- Jovin, T.M. and Arndt-Jovin, D.J. (1989a) FRET Microscopy: Digital imaging of fluorescence resonance energy transfer. Application in cell biology. In *Cell structure and function by microspectrofluorometry*, (Khen, E. and Hirschberg, J.G. (eds.)). Academic Press, New York, pp. 99-117.
- Jovin, T.M. and Arndt-Jovin, D.J. (1989b) Luminescence digital imaging microscopy. *Annu. Rev. Biophys. Biophys. Chem.*, **18**, 271-308.
- Jovin, T.M., Arndt-Jovin, D.J., Marriott, G., Clegg, R.M., Robert-Nicoud, M. and Schormann, T. (1990) Distance, wavelength and time: the versatile 3rd dimensions in light emission microscopy. In *Optical Microscopy for Biology*, (Herman, B. and Jacobson, K. (eds.)). Wiley-Liss, New York, pp. 575-602.
- Kaplan, J.H. (1990) Photochemical manipulation of divalent cation levels. *Annu. Rev. Physiol.*, **52**, 897-914.
- Kawamura, K., Shibata, T., Saget, O., Peel, D. and Bryant, P.J. (1999) A new family of growth factors produced by the fat body and active on *Drosophila* imaginal disc cells. *Development*, **126**, 211-219.
- Kawato, S., Kinoshita Jr., K. and Ikegami, A. (1977) Dynamic structures of lipid bilayers studied by nanosecond fluorescence techniques. *Biochemistry*, **16**, 2319-2324.
- Kean, E.L. (1968) Rapid, sensitive spectrophotometric method for quantitative determination of sulfatides. *J. Lipid Res.*, **9**, 319-327.
- Kim, Y.S., Yoon, G.M., Cho, H.S., Park, S.-H. and Pai, H.-S. (1998) CHRK1 receptor-like kinase contains a chitinase-related sequence in its extracellular domain, which has a specific binding activity for chitin molecules. *4th Korea-Germany Joint Symposium in Plant Biotechnology*, pp. 89-100.
- Kinjo, M. and Rigler, R. (1995) Ultrasensitive hybridization analysis using fluorescence correlation spectroscopy. *Nucl. Acids Res.*, **23**, 1795-1799.
- Kinoshita Jr., K., Kawato, S. and Ikegami, A. (1977) A theory of fluorescence polarization decay in membranes. *Biophys. J.*, **20**, 289-305.
- Lakowicz, J.R. and Berndt, K.W. (1991) Lifetime-selective fluorescence imaging using an rf phase-sensitive camera. *Rev. Sci. Instrum.*, **62**, 1727-1734.
- Lakowicz, J.R., Szmajcinski, H. and Johnson, M.L. (1992) Calcium imaging using fluorescence lifetimes and long-wavelength probes. *J. Fluorescence*, **2**, 47-62.
- Lerouge, F., Roche, P., Faucher, C., Maillet, F., Truchet, G., Promé, J.C. and Dénarié, J. (1990) Symbiotic host-specificity of *Rhizobium meliloti* is determined by a sulphated and acylated glucosamine oligosaccharide signal. *Nature*, **344**, 781-784.
- Long, S.R. (1996) *Rhizobium* symbiosis: Nod factors in perspective. *Plant Cell*, **8**, 1885-1898.
- Lopez-Lara, I.M., van den Berg, J.D., Thomas-Oates, J.E., Glushka, J., Lugtenberg, B.J. and Spaink, H.P. (1995) Structural identification of the lipo-chitin oligosaccharide nodulation signals of *Rhizobium loti*. *Mol. Microbiol.*, **15**, 627-638.
- Magde, D., Elson, E.L. and Webb, W.W. (1972) Thermodynamic fluctuations in a reacting system-measurement by fluorescence correlation spectroscopy. *Phys. Rev. Lett.*, **29**, 705-708.

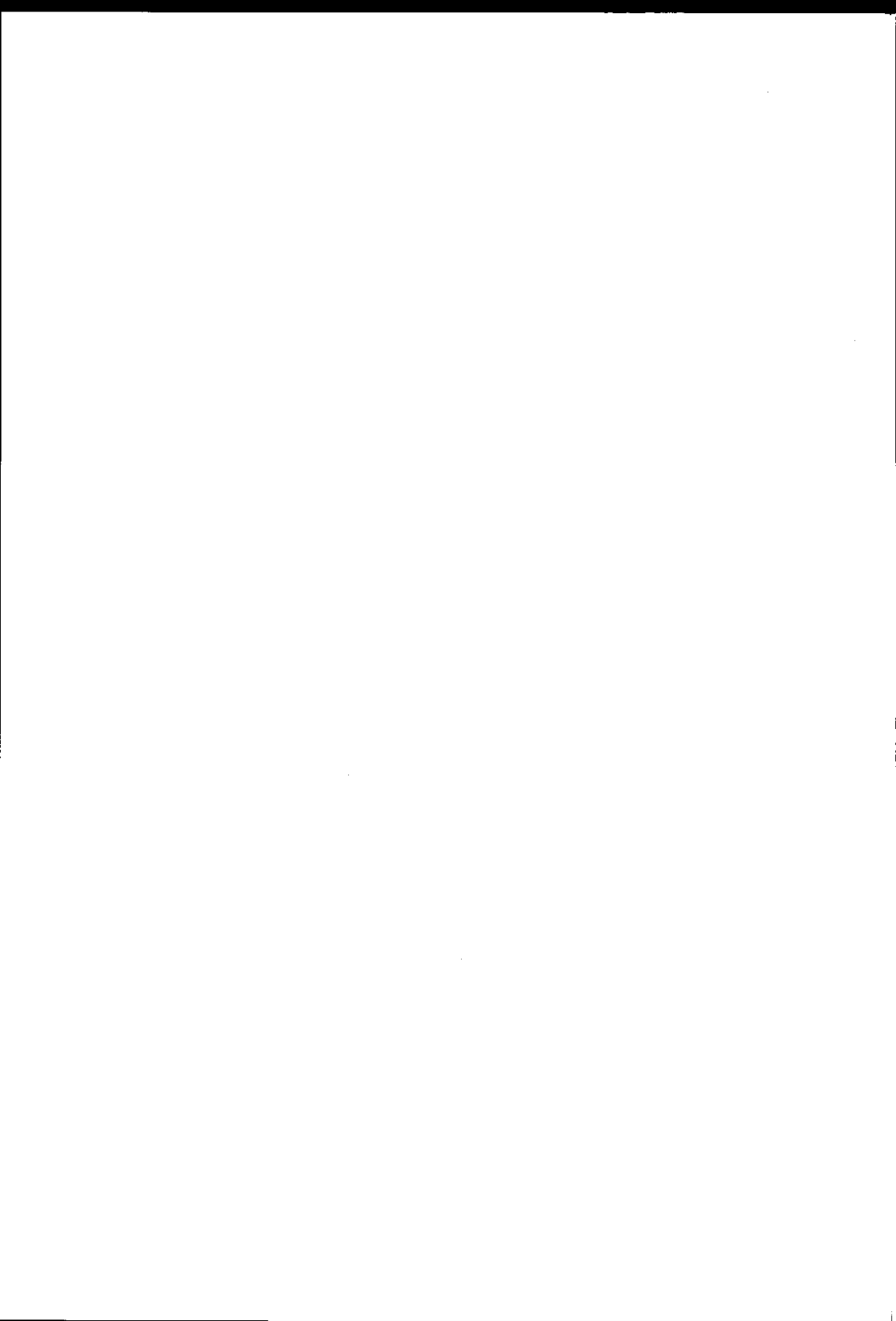
- Magde, D., Elson, E.L. and Webb, W.W. (1974) Fluorescence correlation spectroscopy. II. An experimental realization. *Biopolymers*, **13**, 29-61.
- Maiti, S., Haupts, U. and Webb, W.W. (1997) Fluorescence correlation spectroscopy: diagnostics for sparse molecules. *Proc. Natl. Acad. Sci. USA*, **94**, 11753-11757.
- Marquardt, D.W. (1963) An algorithm for least-squares estimation of non-linear parameters. *J. Soc. Ind. Appl. Math.*, **11**, 431-441.
- Martínez-Zaguilán, R., Gurulé, M.W. and Lynch, R.M. (1996) Simultaneous measurement of intracellular pH and Ca²⁺ in insulin-secreting cells by spectral imaging microscopy. *Am. J. Physiol.*, **270**, 1438-1446.
- Martínez-Zaguilán, R., Tompkins, L.S. and Lynch, R.M. (1994) Simultaneous analysis of multiple fluorescent probes in single cells by microspectroscopic imaging. *Proc. SPIE.*, **2137**, 17-28.
- McCray, J.A. and Trentham, D.R. (1989) Properties and uses of photoreactive caged compounds. *Annu. Rev. Biophys. Biophys. Chem.*, **18**, 239-270.
- Meseth, U., Wohland, T., Rigler, R. and Vogel, H. (1999) Resolution of fluorescence correlation measurements. *Biophys. J.*, **76**, 1619-1631.
- Miesenböck, G., De Angelis, D.A. and Rothman, J.E. (1998) Visualizing secretion and synaptic transmission with pH-sensitive green fluorescent proteins. *Nature*, **394**, 192-195.
- Miyawaki, A., Griesbeck, O., Heim, R. and Tsien, R.Y. (1999) Dynamic and quantitative Ca²⁺ measurements using improved cameleons. *Proc. Natl. Acad. Sci. USA*, **96**, 2135-2140.
- Miyawaki, A., Llopis, J., Heim, R., McCaffery, J.M., Adams, J.A., Ikura, M. and Tsien, R.Y. (1997) Fluorescent indicators for Ca²⁺ based on green fluorescent protein and calmodulin. *Nature*, **388**, 882-887.
- Moolenaar, W.H., Kruijer, W., Tilly, B.C., Verlaan, I., Bierman, A.J. and de Laat, S.W. (1986) Growth factor-like action of phosphatidic acid. *Nature*, **323**, 171-173.
- Munnik, T. (2001) Phosphatidic acid: an emerging plant lipid second messenger. *Trends Plant Sci.*, **6**, 227-233.
- Munnik, T., Arisz, S.A., de Vrije, T. and Musgrave, A. (1995) G protein activation stimulates phospholipase D signaling in plants. *Plant Cell*, **7**, 2197-2210.
- Murashige, T. and Skoog, F. (1962) A revised medium for rapid growth and bio-assays with tobacco tissue cultures. *Physiol. Plant.*, **15**, 473-497.
- Nerbonne, J.M., Richard, S., Nargeot, J. and Lester, H.A. (1984) New photoactivatable cyclic nucleotides produce intracellular jumps in cyclic AMP and cyclic GMP concentrations. *Nature*, **310**, 74-76.
- Nichols, J.W. and Pagano, R.E. (1981) Kinetics of soluble lipid monomer diffusion between vesicles. *Biochemistry*, **20**, 2783-2789.
- Nichols, J.W. and Pagano, R.E. (1982) Use of Resonance Energy Transfer To Study the Kinetics of Amphiphile Transfer Between Vesicles. *Biochemistry*, **21**, 1720-1726.
- Nicolaou, K.C., Bockovich, N.J., Carnague, D.R., Hummel, C.W. and Even, L.F. (1992) Total synthesis of NodRm-IV factors, the Rhizobium nodulation signals. *J. Am. Chem. Soc.*, **114**, 8701-8702.
- Niebel, A., Bono, J.-J., Ranjeva, R. and Cullimore, J.V. (1997) Identification of a high affinity binding site for lipooligosaccharidic NodRm factors in the microsomal fraction of Medicago cell suspension cultures. *Mol. Plant-Microbe Interact.*, **10**, 132-134.

-
- Oehlenschläger, F., Schwille, P. and Eigen, M. (1996) Detection of HIV-1 RNA by nucleic acid sequence-based amplification combined with fluorescence correlation spectroscopy. *Proc. Natl. Acad. Sci. USA*, **93**, 12811-12816.
- Oida, T., Sako, Y. and Kusumi, A. (1993) Fluorescence lifetime imaging microscopy (flimscopy). Methodology development and application to studies of endosome fusion in single cells. *Biophys. J.*, **64**, 676-685.
- Orgambide, G.G., Lee, J., Hollingsworth, R.I. and Dazzo, F.B. (1995) Structurally diverse chitolipooligosaccharide nod factors accumulate primarily in membranes of wild type *rhizobium leguminosorum* biovar *trifolii*. *Biochemistry*, **34**, 3832-3840.
- Pap, E.H., Drummen, G.P., Winter, V.J., Kooij, T.W., Rijken, P., Wirtz, K.W., Op den Kamp, J.A., Hage, W.J. and Post, J.A. (1999) Ratio-fluorescence microscopy of lipid oxidation in living cells using C11-BODIPY(581/591). *FEBS Lett.*, **453**, 278-282.
- Pawley, J.B. (ed.) (1995) *Handbook of biological confocal microscopy*. Plenum Press, New York.
- Periasamy, A., Wodnicki, P., Wang, X.F., Kwon, S., Gordon, G.W. and Herman, B. (1996) Time-resolved fluorescence lifetime imaging microscopy using a picosecond pulsed tunable dye laser system. *Rev. Sci. Instrum.*, **67**, 3722-3731.
- Philip-Hollingsworth, S., Dazzo, F.B. and Hollingsworth, R.I. (1997) Structural requirements of Rhizobium chitolipooligosaccharides for uptake and bioactivity in legume roots as revealed by synthetic analogs and fluorescent probes. *J. Lipid Res.*, **38**, 1229-1241.
- Pingret, J.L., Journet, E.P. and Barker, D.G. (1998) Rhizobium nod factor signaling. Evidence for a G protein-mediated transduction mechanism. *Plant Cell*, **10**, 659-672.
- Piston, W. (1999) Imaging living cells and tissues by two-photon excitation microscopy. *Trends Cell Biol.*, **9**, 66-69.
- Politz, J.C., Browne, E.S., Wolf, D.E. and Pederson, T. (1998) Intracellular diffusion and hybridization state of oligonucleotides measured by fluorescence correlation spectroscopy in living cells. *Proc. Nat. Acad. Sci. USA*, **95**, 6043-6048.
- Pollak, B.A. and Heim, R. (1999) Using GFP in FRET-based applications. *Trends Cell Biol.*, **9**, 57-60.
- Price, N.P.J., Relic, B., Talmont, F., Lewin, A., Promé, D., Pueppke, S.G., Maillet, F., Dénarié, J., Promé, J.-C. and Broughton, W.J. (1992) Broad-host-range *Rhizobium* species NGR234 secretes a family of carbamoylated, and fucosylated, nodulation signals that are O-acetylated or sulphated. *Mol. Microbiol.*, **6**, 3575-3584.
- Radin, N.S. (1984) Improved version of the Kean partition assay for cerebroside sulfate. *J. Lipid Res.*, **25**, 651-652.
- Rauer, B., Neumann, E., Widengren, J. and Rigler, R. (1996) Fluorescence correlation spectrometry of the interaction kinetics of tetramethylrhodamin α -bungarotoxin with *Torpedo californica* acetylcholine receptor. *Biophys. Chem.*, **58**, 3-12.
- Read, N.D., Allan, W.T.G., Knight, H., Malhot, R., Russell, A., Shacklock, P.S. and Trewavas, A.J. (1992) Imaging and measurement of cytosolic free calcium in plant and fungal cells. *J. Microsc.*, **166**, 57-86.

- Reissig, J.L., Strominger, J.L. and Leloir, L.F. (1955) A modified colorimetric method for the estimation of N-acetylamino sugars. *J. Biol. Chem.*, **217**, 959-966.
- Rigler, R. (1995) Fluorescence correlations, single molecule detection and large number screening. Applications in biotechnology. *J. Biotechnol.*, **41**, 177-186.
- Rigler, R., Foldes-Papp, Z., Meyer-Almes, F.-J., Sammet, C., Volcker, M. and Schnetz, A. (1998) Fluorescence cross-correlation: A new concept for polymerase chain reaction. *J. Biotechnol.*, **63**, 97-107.
- Rigler, R.J., Widengren, J. and Mets, Ü. (1992) Interaction and kinetics of single molecules as observed by fluorescence correlation spectroscopy. In *Fluorescence spectroscopy*, (Wolfbeis, O.S. (ed.)). Springer-Verlag, Berlin, pp. 13-24.
- Rivilla, R., Sutton, J.M. and Downie, J.A. (1995) Rhizobium leguminosarum NodT is related to a family of outer-membrane transport proteins that includes TolC, PrtF, CyaE and AprF. *Gene*, **161**, 27-31.
- Roche, P., Debelle, F., Mailet, F., Lerouge, P., Faucher, C., Truchet, G., Dénarié, J. and Promé, J.-C. (1991) Molecular basis of symbiotic host specificity in Rhizobium meliloti: nodH and nodPQ genes encode the sulfation of lipo-oligosaccharide signals. *Cell*, **67**, 1131-1143.
- Roseman, M.A. and Thompson, T.E. (1980) Mechanism of the spontaneous transfer of phospholipids. *Biochemistry*, **19**, 439-444.
- Sanders, R., Gerritsen, H.C., Draaier, A., Houpt, P.M. and Levine, Y.K. (1994) Fluorescence lifetime imaging of free calcium in single cells. *Bioimaging*, **2**, 131-138.
- Schlaman, H.R.M., Okker, R.J.H. and Lugtenberg, B.J.J. (1990) Subcellular localization of the Rhizobium leguminosarum nodI gene product. *J. Bacteriol.*, **172**, 5486-5489.
- Schwille, P., Bieschke, J. and Oehlenschläger, F. (1997a) Kinetic investigations by fluorescence correlation spectroscopy: the analytical and diagnostic potential of diffusion studies. *Biophys. Chem.*, **66**, 211-228.
- Schwille, P., Haupts, U., Maiti, S. and Webb, W.W. (1999) Molecular dynamics in living cells observed by fluorescence correlation spectroscopy with one- and two-photon excitation. *Biophys. J.*, **77**, 2251-2265.
- Schwille, P., Meyer-Almes, F.-J. and Rigler, R. (1997b) Dual-color fluorescence cross-correlation spectroscopy for multicomponent diffusional analysis in solution. *Biophys. J.*, **72**, 1878-1886.
- Selinger, Z. and Lapidot, Y. (1966) Synthesis of fatty acid anhydrides by reaction with dicyclohexylcarbodiimide. *J. Lipid Res.*, **7**, 174-175.
- Shechter, Y., Schlessinger, J., Jacobs, S., Chang, K.J. and Cuatrecasas, P. (1978) Fluorescent labeling of hormone receptors in viable cells: preparation and properties of highly fluorescent derivatives of epidermal growth factor and insulin. *Proc. Natl. Acad. Sci. USA*, **75**, 2135-2139.
- So, P.T.C., French, T. and Gratton, E. (1994) A frequency domain time-resolved microscope using a fast-scan CCD camera. *Proc. SPIE*, **2137**, 83-92.
- So, P.T.C., French, T., Yu, W.M., Berland, K.M., Dong, C.Y. and Gratton, E. (1995) Time-resolved fluorescence microscopy using two-photon excitation. *Bioimaging*, **3**, 49-63.
- Somerharju, P.J., Virtanen, J.A., Eklund, K.K., Vainio, P. and Kinnunen, P.K. (1985) 1-Palmitoyl-2-pyrenedecanoyl glycerophospholipids as membrane probes: evidence for regular distribution in liquid-crystalline phosphatidylcholine bilayers. *Biochemistry*, **24**, 2773-2781.

-
- Spaink, H.P., Sheeley, D.M., van Brussel, A.A., Glushka, J., York, W.S., Tak, T., Geiger, O., Kennedy, E.P., Reinhold, V.N. and Lugtenberg, B.J. (1991) A novel highly unsaturated fatty acid moiety of lipooligosaccharide signals determines host specificity of *Rhizobium*. *Nature*, **354**, 125-130.
- Spaink, H.P., Wijfjes, A.H.M. and Lugtenberg, B.J.J. (1995) *Rhizobium* NodI and NodJ proteins play a role in the efficiency of secretion of lipochitin oligosaccharides. *J. Bacteriol.*, **177**, 6276-6281.
- Staehelin, C., Granado, J., Muller, J., Wiemken, A., Mellor, R.B., Felix, G., Regenass, M., Broughton, W.J. and Boller, T. (1994a) Perception of *Rhizobium* nodulation factors by tomato cells and inactivation by root chitinases. *Proc. Natl. Acad. Sci. USA*, **91**, 2196-2200.
- Staehelin, C., Schultze, M., Kondorosi, E., Mellor, R.B., Boller, T. and Kondorosi, A. (1994b) Structural modifications in *Rhizobium meliloti* Nod factors influence their stability against hydrolysis by root chitinases. *Plant J.*, **5**, 319-330.
- Stauffer, T.P., Ahn, S. and Meyer, T. (1998) Receptor-induced transient reduction in plasma membrane PtdIns(4,5)P₂ concentration monitored in living cells. *Curr. Biol.*, **8**, 343-346.
- Struck, D.K., Hoekstra, D. and Pagano, R.E. (1981) Use of resonance energy transfer to monitor membrane fusion. *Biochemistry*, **20**, 4093-4099.
- Stryer, L. (1978) Fluorescence energy transfer as a spectroscopic ruler. *Ann. Rev. Biochem.*, **47**, 819-846.
- Sytsma, J., Vroom, J.M., de Grauw, C.J. and Gerritsen, H.C. (1998) Time gated fluorescence lifetime imaging and micro-volume spectroscopy using two-photon excitation. *J. Microsc.*, **191**, 39-51.
- Szmacinski, H. and Lakowicz, J.R. (1993) Optical measurements of pH using fluorescence lifetimes and phase-modulation fluorometry. *Anal. Chem.*, **65**, 1668-1674.
- Szmacinski, H., Lakowicz, J.R. and Johnson, M.L. (1994) Fluorescence lifetime imaging microscopy: homodyne technique using high-speed gated image intensifier. *Methods Enzymol.*, **240**, 723-748.
- Tadano-Aritomi, K. and Ishizuka, I. (1983) Determination of peracetylated sulfoglycolipids using the azure A method. *J. Lipid Res.*, **24**, 1368-1375.
- Timmers, A.C., Auriac, M.C., de Billy, F. and Truchet, G. (1998) Nod factor internalization and microtubular cytoskeleton changes occur concomitantly during nodule differentiation in alfalfa. *Development*, **125**, 339-349.
- Torii, K.U. (2000) Receptor kinase activation and signal transduction in plants: an emerging picture. *Curr. Opin. Plant Biol.*, **3**, 361-367.
- Truchet, G., Roche, P., Lerouge, P., Vasse, J., Camut, S., de Billy, F., Promé, J.-C. and Dénarié, J. (1991) Sulphated lipooligosaccharide signals of *Rhizobium meliloti* elicit root nodule organogenesis. *Nature*, **351**, 670-673.
- Tsien, R.Y. (1998) The green fluorescent protein. *Annu. Rev. Biochem.*, **67**, 509-544.
- Tsien, R.Y., Bacsai, J. and Adams, R. (1993) FRET for studying intracellular signalling. *Trends Cell Biol.*, **3**, 242-245.
- Van Brussel, A.A.N., Bakhuizen, R., van Spronsen, P., Spaink, H., Tak, T., Lugtenberg, B.J.J. and Kijne, J. (1992) Induction of pre-infection thread structures in the leguminous host plant by mitogenic lipooligosaccharides of *Rhizobium*. *Science*, **257**, 70-72.

- Van Brussel, A.A.N., Zaat, S.A.J., Canter Cremers, H.C.J., Wijffelman, C.A., Pees, E., Tak, T. and Lugtenberg, B.J.J. (1982) Small leguminosae as test plants for nodulation of *Rhizobium leguminosarum* and other rhizobia and agrobacteria harbouring a leguminosarum Sym-plasmid. *Plant. Sci. Lett.*, **27**, 317-325.
- Van den Berg, P.A.W., Van Hoek, A., Walentas, C.D., Perham, R.N. and Visser, A.J.W.G. (1998) Flavin fluorescence dynamics and photoinduced electron transfer in *Escherichia coli* glutathione reductase. *Biophys. J.*, **74**, 2046-2058.
- Van Hoek, A. and Visser, A.J.W.G. (1992) CW dye laser synchronously pumped by the third harmonic of a mode-locked cw Nd:YLF laser for tunable blue and green excitation and picosecond time-correlated photon counting detection. *Proc. SPIE-Int. Soc. Opt. Eng.*, **1640**, 325-329.
- Van Paridon, P.A., Gadella Jr., T.W.J., Somerharju, P.J. and Wirtz, K.W.A. (1988) Properties of the binding sites for the sn-1 and sn-2 acyl chains on the phosphatidylinositol transfer protein from bovine brain. *Biochemistry*, **27**, 6208-6214.
- Venkateswarlu, K., Oatey, P.B., Tavaré, J.M. and Cullen, P.J. (1998) Insulin-dependent translocation of ARNO to the plasma membrane of adipocytes requires phosphatidylinositol 3-kinase. *Curr Biol*, **8**, 463-466.
- Vereb, G., Jares Erijman, E., Selvin, P.R. and Jovin, T.M. (1998) Temporally and spectrally resolved imaging microscopy of lanthanide chelates. *Biophys. J.*, **74**, 2210-2222.
- Visser, T. (1998) Green fluorescent protein et FCS: deux outils pour la biologie cellulaire. *Biofutur*, **177**, 8.
- Wais, R.J., Galera, C., Oldroyd, G., Catoira, R., Penmetsa, R.V., Cook, D., Gough, C., Denarie, J. and Long, S.R. (2000) Genetic analysis of calcium spiking responses in nodulation mutants of *Medicago truncatula*. *Proc. Natl. Acad. Sci. USA*, **97**, 13407-13412.
- Walker, J.W., Reid, G.P., McCray, J.A. and Trentham, D.R. (1988) Photolabile 1-(2-nitrophenyl)ethyl phosphate esters of adenine nucleotide analogues. Synthesis and mechanism of photolysis. *J. Am. Chem. Soc.*, **110**, 7170-7177.
- Walker, J.W., Reid, G.P. and Trentham, D.R. (1989) Synthesis and properties of caged nucleotides. *Methods Enzymol.*, **172**, 288-301.
- Walker, J.W., Somlyo, A.V., Goldman, Y.E., Somlyo, A.P. and Trentham, D.R. (1987) Kinetics of smooth and skeletal muscle activation by laser pulse photolysis of caged inositol 1,4,5-trisphosphate. *Nature*, **327**, 249-252.
- Walker, S.A., Viprey, V. and Downie, J.A. (2000) Dissection of nodulation signaling using pea mutants defective for calcium spiking induced by nod factors and chitin oligomers. *Proc. Natl. Acad. Sci. USA*, **97**, 13413-13418.
- Wang, X.F., Periasamy, A. and Herman, B. (1992) Fluorescence lifetime imaging microscopy (FLIM): instrumentation and applications. *Crit. Rev. Anal. Chem.*, **23**, 369-395.
- Weiss, S. (1999) Fluorescence spectroscopy of single biomolecules. *Science*, **283**, 1676-1683.
- Whitaker, J.E., Haugland, R.P. and Prendergast, F. (1991) Spectral and photophysical studies of benzo[c]xanthene dyes: dual emission pH sensors. *Anal. Biochem.*, **194**, 330-344.
- Wu, P. and Brand, L. (1994) Resonance energy transfer: methods and applications. *Anal. Biochem.*, **218**, 1-13.



NEDERLANDSE SAMENVATTING

Om te kunnen groeien, hebben planten naast koolstofdioxide en water ook stikstof nodig als bouwstof. De koolstofdioxide halen planten uit de lucht, die voor 0.03 % uit koolstofdioxide bestaat. Hoewel onze atmosfeer voor bijna 80% uit stikstof bestaat, kunnen planten deze vorm van stikstof niet opnemen. Normaal gesproken zit er in de bodem bruikbare stikstof, of wordt dit door middel van bemesten aan de bodem toegevoegd. De plant onttrekt de stikstof via de wortels uit de bodem.

Er is echter een familie van planten die ook onder stikstofarme omstandigheden kan groeien. Dit zijn de vlinderbloemige planten. Voorbeelden van vlinderbloemigen zijn erwt, boon en soja. Ze kunnen samenwerken met *Rhizobium* bacteriën die voor de stikstofvoorziening zorgen. Dit biologisch fenomeen wordt symbiose genoemd. De bacteriën die gewoonlijk aanwezig zijn in de bodem, zitten tijdens de symbiose in knolletjes op de plantenwortel. Daar halen ze stikstof uit de lucht en zetten dit om zodat de plant het kan gebruiken. In ruil voor de stikstof geeft de plant bouwstoffen aan de bacteriën. Deze symbiose komt tot stand na de uitwisseling van signalen tussen de organismen, waarna de bacteriën via een infectiedraad de wortel binnegaan en vervolgens in de knolletjes op de plantenwortel gehuisvest worden. Wetenschappelijk gezien is dit proces erg interessant omdat er communicatie en samenwerking is tussen twee compleet verschillende organismen. Verder is het een interessant systeem omdat het wellicht mogelijk is, wanneer het proces in voldoende detail bekend is, om de mogelijkheid tot symbiose te introduceren in andere planten zodat deze ook op een stikstofarme bodem kunnen groeien.

De eerste stap die noodzakelijk is voor een succesvolle symbiose, is de uitwisseling van signalen. De plant begint deze "moleculaire dialoog" door flavonoïde-achtige verbindingen te produceren die herkend worden door het juiste type bacterie. In de bacterie wordt een signaaltransductiecascade geactiveerd, die leidt tot de synthese en uitscheiding van lipochitooligosacchariden. Deze signaalmoleculen worden ook wel Nod-factoren genoemd. De productie van Nod-factoren door de *Rhizobium* bacteriën is een vereiste stap voor een succesvolle symbiose en is noodzakelijk om de juiste bacteriesoort en plant tot elkaar te brengen. De algemene structuur van Nod-factoren omvat een chitine groep bestaande uit 3 tot 5 β -1,4-verbonden *N*-acetylglucosamine eenheden. Een vetzuurstaart van 16-20 koolstofatomen is verbonden aan de eindstandige niet-reducerende suiker. De exacte moleculaire structuur verschilt per *Rhizobium* soort. De vlinderbloemige plant herkent alleen bepaalde Nod-factor structuren. Dit zorgt voor specifieke samenwerking tussen bepaalde *Rhizobium* soorten en vlinderbloemigen.

Het signaalmolecuul kan ook in afwezigheid van de bacterie door de plant herkend worden. Als een oplossing met Nod-factor aan een plantenwortel wordt toegevoegd, is na enige tijd een verandering te zien in de wortelharen. Een wortelhaar is één cel die vanuit de wortel loodrecht op

de lengterichting van de wortel groeit. Op één wortel kunnen honderden tot duizenden wortelharen aanwezig zijn. Met het blote oog is dit als een harige structuur te zien. Als de plant de Nod-factor herkent, dan is na ongeveer twee uur een zwelling in de tip van de wortelharen te zien (met behulp van een microscoop). Vervolgens wordt vanuit deze zwelling een nieuwe uitgroei gevormd in een willekeurige richting. Deze specifieke Nod-factor respons van de wortelharen wordt "wortelhaar-deformatie" genoemd. De wortelharen kunnen zeer lage concentraties Nod-factor herkennen (nano- tot picomolair). Eén van de meest intrigerende vragen is, hoe de Nod-factor door de plant wordt herkend en waarom de signaalstof niet door andere planten herkend wordt.

Om de Nod-factoren ook bij zeer lage concentraties te kunnen bestuderen, worden ze zichtbaar gemaakt met behulp van fluorescentie. Door het aanstralen van een fluorescent molecuul, met een specifieke kleur licht, zal het in een aangeslagen toestand terechtkomen. Wanneer het molecuul weer spontaan naar de grondtoestand terugkeert, zal het licht met een lagere energie (hogere golflengte) uitzenden: fluoresceren. Het contrast wordt verkregen doordat andere aanwezige cellen c.q. moleculen niet fluoresceren. Dus het waargenomen fluorescentielicht is specifiek voor het molecuul dat een fluorescente groep heeft. In dit proefschrift worden diverse Nod-factoren beschreven die verschillende kleuren fluorescentie-licht uitzenden. De groen-, oranje- en rood-fluorescerende groepen zitten aan het eind van de vetzuurstaart.

In hoofdstuk 1 worden diverse geavanceerde fluorescentie microspectroscopie methoden beschreven. De combinatie van spectroscopie en microscopie heeft als voordeel dat een spectroscopische parameter bestudeert kan worden, terwijl tegelijkertijd ruimtelijke informatie (een plaatje) verkregen wordt. De vier technieken die beschreven worden, zijn fluorescentie ratio beeldvormings microscopie (FRIM), fluorescentie spectrale beeldvormings microscopie (FSPIM), fluorescentie levensduur beeldvormings microscopie (FLIM) en fluorescentie correlatie microscopie (FCM). Deze technieken kunnen worden gebruikt om de eigenschappen van fluorescente moleculen te meten in levende cellen.

Nod-factoren worden meestal geïsoleerd in kleine hoeveelheden uit een cultuur van *Rhizobium* bacteriën. Uit een liter medium met vele miljarden bacteriën wordt ongeveer een milligram Nod-factor verkregen. Hoewel dit genoeg is voor meer dan duizenden experimenten, is het nog zo weinig dat nauwkeurig afwegen zeer moeilijk is. Omdat het voor veel wetenschappelijke studies belangrijk is om te weten hoeveel Nod-factor je precies in handen hebt, is het noodzaak om een gevoelige methode te gebruiken om de hoeveelheid te bepalen. In hoofdstuk 2 worden twee nieuwe methoden beschreven die kleine hoeveelheden Nod-factoren kunnen kwantificeren. De eerste methode maakt gebruik van een Nod-factor afbrekend enzym dat suikereenheden (*N*-acetylglucosamine) van de Nod-factor afknipt. De suikereenheden kunnen worden gekwantificeerd door een chemische reactie waarbij een gekleurde stof ontstaat. De hoeveelheid Nod-factor die aanvankelijk aanwezig was, is evenredig met de hoeveelheid kleur

(lichtabsorptie). De tweede methode kan een specifiek type Nod-factor met een sulfaatgroep kwantificeren. De negatief geladen sulfaatgroep kan een ion-paar vormen met een blauw, positief geladen molecuul. Dit gekleurde complex wordt door een extractie geïsoleerd. De hoeveelheid blauwkleuring is direct evenredig met de hoeveelheid gesulfateerde Nod-factor.

In hoofdstuk 3 is met behulp van diverse spectroscopische technieken het moleculaire gedrag van fluorescente Nod-factoren bestudeert. Allereerst wordt onderzocht welke invloed de fluorescente groep heeft op de activiteit van de signaalstof. Een natuurlijke niet-fluorescente Nod-factor kan bij een concentratie van 10^{-11} M nog deformatie van wortelharen veroorzaken. De meest actieve fluorescente Nod-factor geeft bij 10^{-10} M nog wortelhaardeformatie. Alhoewel dus een tien keer hogere concentratie fluorescente Nod factor noodzakelijk is voor herkenning door de plant, is deze concentratie nog steeds zeer laag. Dit wijst erop dat de fluorescente groep de herkenning van de Nod-factor niet ernstig verstoort, en dat fluorescente Nod-factoren dezelfde eigenschappen hebben als natuurlijke Nod-factoren.

Nod-factoren hebben kenmerken die vergelijkbaar zijn met zeepmoleculen. Beide hebben een waterminnende kop en een waterafstotende vetzuurstaart. Van zeepmoleculen is het bekend dat ze in een waterige oplossing aanwezig zijn als bolvormige complexen bestaande uit 50-1000 moleculen. In deze complexen zijn de vetzuurstaarten gegroepeerd en afgeschermd van het water, terwijl de waterminnende koppen juist in contact zijn met het water. Deze complexen worden micellen genoemd. Membranen van cellen bestaan ook uit moleculen met een waterminnende kop en een waterafstotende vetzuurstaart. In dit geval wordt een vlakke structuur gevormd, bestaande uit twee lagen van moleculen. De waterafstotende staarten bevinden zich in het midden, en worden aan twee kanten van het water afgeschermd door de waterminnende koppen. Deze structuur heet een membraan bilaag.

Uit de in hoofdstuk 3 beschreven resultaten blijkt dat Nod-factoren door waterige oplossingen bewegen als individuele moleculen en dus geen micellen vormen bij een concentratie van 10^{-8} M. Maar in aanwezigheid van zeepmicellen en membranen associëren ze met deze structuren, waarbij de vetzuurstaart zich in de waterafstotende kern van de micel of de membraan bevindt. Ook is aangetoond dat Nod-factoren zeer snel van het ene membraan naar het andere membraan kunnen overspringen, of van een membraan naar een wortelhaar. Het is echter niet mogelijk om van de ene kant van een membraanbilaag via de waterafstotende kern naar de andere kant te "flip-floppen".

In hoofdstuk vier is onderzocht waar de fluorescente Nod-factoren heengaan nadat ze zijn toegevoegd aan het medium waarin de plantenwortel groeit. Meteen na toevoegen is er fluorescentie waar te nemen aan het oppervlak van de wortelhaar. Na het induceren van plasmolyse, waarbij de plasma-membraan gescheiden wordt van de celwand, is te zien dat de fluorescentie afkomstig is van de celwand. Drie uur na toevoeging zijn de wortelharen gedeformeerd. Dus de fluorescente Nod-factor wordt herkend door de plant.

Het is opvallend dat de Nod-factor niet aanwezig is in de nieuwe uitgroei van de wortelhaardeformatie. Dit betekent dat er nauwelijks of geen verplaatsing van de Nod-factoren

door de celwand plaatsvindt. Deze resultaten zijn bevestigd met Fluorescentie Correlatie Microscopie (FCM) waarmee de diffusiesnelheid en hoeveelheid Nod-factor zijn bepaald. De Nod-factor beweegt (diffundeert) 1000 keer langzamer in de celwand van een wortelhaar dan in het groeimedium. Tevens is er in de celwand vijftig keer meer fluorescente Nod-factor aanwezig dan in het medium. Deze resultaten laten zien dat de Nod-factor sterk bindt aan de celwand van de wortelharen. Dit zijn verbazende resultaten, omdat in hoofdstuk drie is aangetoond dat Nod-factoren graag in membranen aanwezig zijn. Blijkbaar is de binding aan de celwand sterker dan de binding aan de plasmamembraan van een wortelhaar. De verankering van Nod factoren door de celwand kan van belang zijn voor de wortelhaar. Een belangrijke stap voor het totstandkomen van de symbiose is het om de bacterie heen krullen van de wortelhaar. Om op de juiste plaats om de bacterie heen te krullen, heeft de wortelhaar informatie nodig waar de bacterie zich bevindt. Het kan zijn dat de plant het Nod factor signaal gebruikt om de bacterie te lokaliseren. De langzame diffusie zorgt ervoor dat de ruimtelijke informatie behouden blijft, wat onmogelijk zou zijn geweest als het signaal over het oppervlak van de wortelhaar zou bewegen.

In hoofdstuk vijf wordt de studie van Nod-factor binding en herkenning door wortelharen vervolgd. In dit geval worden zowel de in hoofdstuk 3 en 4 beschreven Nod-factoren gebruikt als nieuwe gesulfateerde Nod-factoren. De gesulfateerde Nod-factoren verschillen slechts in de aanwezigheid van een sulfaatgroep van de niet-gesulfateerde Nod-factoren. Alhoewel dit een kleine verandering lijkt, heeft het dramatische effecten op de herkenning door de plant. Alleen de niet-gesulfateerde Nod-factoren worden herkend door de plant wikke (*Vicia sativa*). De gesulfateerde Nod-factoren daarentegen worden slechts herkend door *Medicago truncatula*. Door verschillende combinaties van deze twee planten met de twee soorten Nod-factoren te maken, is het mogelijk om meer inzicht te krijgen in de specifieke herkenning van Nod-factoren door de plant. De best bruikbare, oranje-fluorescerende, gesulfateerde Nod-factor wordt door *Medicago* wortelharen nog herkend bij een concentratie van 10^{-10} M. Als de gesulfateerde Nod-factor wordt toegevoegd aan wikke reageren de wortelharen niet. Toch bindt de Nod-factor aan de buitenkant van de wortelhaar. Dit is ook in het omgekeerde geval zo, dus ook de niet-gesulfateerde Nod-factor die niet herkend wordt door *Medicago* bindt toch aan de wortelharen. Dus Nod-factoren binden aan wortelharen onafhankelijk of ze uiteindelijk wel of niet herkend worden. Tot dusver was het volledig onduidelijk waar Nod-factor herkenning door wortelharen plaatsvindt. De in dit proefschrift beschreven resultaten laten zien dat de celwand een belangrijke rol speelt in de Nod-factor herkenning. Verdere studies zullen moeten uitwijzen of Nod-factor herkenning daadwerkelijk plaatsvindt in de celwand.

Wanneer de wortelhaar een Nod-factor herkent, worden binnen in de wortelhaar verschillende moleculen aangemaakt om het signaal over te brengen. Deze moleculen zijn zogenaamde "boodschapper-moleculen", die de cel aanzetten tot een reactie. In bepaalde gevallen kan de cel tot een reactie worden gebracht door slechts het boodschapper-molecuul in de cel te introduceren. Eén van de boodschapper-moleculen die het Nod-factor signaal overbrengt is fosfatidezuur. In hoofdstuk 6 wordt een strategie beschreven om niet-actief fosfatidezuur in een

cel te brengen en vervolgens te activeren. Het doel is om te onderzoeken of de toename van fosfatidezuur voldoende is om de Nod-factor signaaloverdracht te activeren.

Het fosfatidezuur wordt uitgerust met een lichtgevoelige groep. Dit heeft tot gevolg dat het molecuul niet meer herkend wordt en dus niet actief is. De groep kan door blootstelling aan ultraviolet licht (UV) verwijderd worden. De resultaten laten zien dat deze strategie werkt en dat door blootstelling aan UV-licht actief fosfatidezuur in cellen gevormd wordt. Er is echter ook gebleken dat blootstelling van wortelharen aan UV-licht een schadelijk effect kan hebben. Dat kan waarschijnlijk opgelost worden door slechts een gedeelte van de cel te belichten met behulp van een gefocusseerde bron van UV-licht. Dit heeft als bijkomend voordeel dat in dat geval ook de invloed van lokale signalen bestudeert kan worden.

Samenvattend hebben de resultaten die beschreven zijn in dit proefschrift geleid tot nieuwe methoden om Nod-factoren te kwantificeren, tot een beter inzicht in de eigenschappen van het Nod-factor molecuul en ook tot meer inzicht in de herkenning van Nod-factoren door wortelharen.

DANKWOORD

Na vier jaar als Onderzoeker in Opleiding is het leuk om even stil te staan bij degenen die betrokken zijn geweest bij het onderzoek en/of opleiding. Als je op het grensvlak van biologie, scheikunde en fysica opereert, is het onontbeerlijk om ook vanuit elke hoek steun te krijgen. Allereerst wil ik Dorus bedanken voor zijn grote enthousiasme, wat zeer inspirerend en aanstekelijk werkt. Vooral de drang om (eigenschappen van) moleculen te visualiseren en kwantificeren leidt tot verrassende en heldere inzichten. Ton Bisseling wil ik bedanken voor de begeleiding vanuit het biologische perspectief. Dit heeft gezorgd voor een gerichte vraagstelling met focus op biologisch relevante experimenten. Ook de andere coördinatoren van het programma, Ton Visser, Alan Musgrave en Annemie Emons, wil ik bedanken voor hun bijdrage. Synthesis of fluorescent Nod factors was essential for the experiments described in this thesis. Therefore, I would like to thank Hörst Rohrig and Jean-Jacques Bono. Jean-Jacques, it has been a pleasure doing experiments together!

Hoewel ik me nog kan herinneren dat ik Mark de FCS heb gedemonstreerd, waren de rollen daarna al snel omgekeerd, en heb ik vele malen kunnen rekenen op zijn hulp bij metingen en interpretaties. De FCS experimenten aan wortelharen, die zijn begonnen als een "vrijdagmiddag-experiment", zijn een belangrijk onderdeel van dit proefschrift geworden. Arie van Hoek is essentieel geweest voor de tijd-opgeloste fluorescentie experimenten voor de Nod-factor karakterisatie. Als laatste van de drie van Biochemie wil ik Jan-Willem Borst bedanken voor de immer duidelijke antwoorden op alle vragen.

Martine den Hartog en Teun Munnik wil ik bedanken voor de stimulerende samenwerking en uitwisseling van ideeën. Ana and Martine are greatly acknowledged for keeping us busy in Amsterdam during the time our building was closed due to asbestos contamination. They gave an excellent private molecular biology course during this brief "sabbatical" and helped us to make GFP-lipid binding domain fusions. Joop is tijdens zijn afstudeervak de weg van de lipide-binding eiwitten verder ingeslagen en is vervolgens aangesteld als OiO op dit project. Joop, bedankt voor je inzet en humor, en tot wederziens aan de UvA.

I would like to thank Az-Eddine, Rossana and Gerard for transferring plates with seeds. Verder bedank ik alle collega's van Molbi die mij, als niet-moleculair bioloog, toch het gevoel hebben gegeven dat ik op de juiste plek zat.

Even onzichtbaar als belangrijk is de support van mensen achter het scherm. Paul en Jeroen, jullie bijdrage is van fantastische kwaliteit en ik hoop dat we nog vaak een discussie bij een glas bier, of als het moet per e-mail, kunnen voeren. Pap, mam en broeders bedankt voor jullie bijdrage in welke vorm dan ook. En, tenslotte, Monique, bedankt voor alle zorg en steun.

CURRICULUM VITAE

Joachim Goedhart werd geboren op 15 juni 1973 te Heemskerk. Na het behalen van het VWO diploma aan het Berlingh College te Beverwijk in juni 1991, werd in hetzelfde jaar begonnen met de studie moleculaire wetenschappen aan de Landbouwniversiteit in Wageningen. Als onderdeel van het doctoraal programma deed hij een eerste afstudeervak bij de vakgroep Moleculaire Fysica onder begeleiding van Drs. H.T.M. v. Lieshout en Dr. M. Hemminga, waarin met behulp van 2D-NMR de structuur van een oligonucleotide duplex werd onderzocht. Een tweede afstudeervak is uitgevoerd bij de vakgroep Biochemie onder begeleiding van Dr. T.W.J. Gadella Jr., waarin de eigenschappen van fluorescente phospholipiden in modelmembranen en cellen bestudeert zijn met behulp van fluorescentie spectroscopie en microscopie. Vervolgens is een drie-maands stage gedaan in de vakgroep Moleculaire Biologie (Dr. T. Jovin) aan het Max-Planck instituut voor biofysische chemie in Göttingen, Duitsland. Onder begeleiding van Dr. R. Brock is de EGF signaal transductie cascade bestudeert met behulp van biochemische technieken en met fluorescentie microscopie. Na het behalen van het doctoraalprogramma in juni 1996, is hij in november 1996 begonnen als toegevoegd onderzoeker op een project getiteld "Bestudering van cellulaire processen mbv een fluorescentie microscoop en uittesten van nieuwe apparatuur en onderzoeksmethoden", uitgevoerd in het MicroSpectroscopisch Centrum Wageningen.

Van augustus 1997 tot augustus 2001 was de auteur van dit proefschrift in dienst bij de stichting levenswetenschappen (SLW, tegenwoordig ALW) van de Nederlandse Organisatie voor Wetenschappelijk Onderzoek (NWO) als onderzoeker in opleiding. Het onderzoek is verricht in het laboratorium voor Biochemie (prof. C. Laane) en het laboratorium voor Moleculaire Biologie (prof. T. Bisseling) van Wageningen Universiteit onder begeleiding van Dr. T.W.J. Gadella Jr. De resultaten van dit onderzoek staan beschreven in dit proefschrift.

Vanaf augustus 2001 is hij werkzaam als post-doc op het project "Synthesis and application of novel caged-phospholipids for high resolution optical manipulation of lipid signaling events in single living cells" aan de vakgroep Moleculaire Cytologie van de Universiteit van Amsterdam, in dienst bij de divisie Chemische Wetenschappen van NWO.

LIST OF PUBLICATIONS

Articles in refereed journals

- Goedhart, J., M.A. Hink, A.J.W.G. Visser, T. Bisseling, and T.W.J. Gadella, Jr. 2000. In vivo fluorescence correlation microscopy (FCM) reveals accumulation and immobilization of Nod factors in root hair cell walls. *Plant J.* **21**: 109-119.
- Goedhart, J., H. Röhrig, M.A. Hink, A. van Hoek, A.J.W.G. Visser, T. Bisseling, and T.W.J. Gadella, Jr. 1999. Nod factors integrate spontaneously in biomembranes and transfer rapidly between membranes and to root hairs, but transbilayer flip-flop does not occur. *Biochemistry.* **38**: 10898-10907.

Book chapter

- Goedhart, J., and T.W.J. Gadella Jr. 2000. Advanced fluorescence microspectroscopic methods for the study of single living root hairs. *In* Root hairs: cell and Molecular Biology. R.W. Ridge and A.M.C. Emons (eds.) Springer-Verlag, Tokyo. 65-94.

Abstracts

- Gadella Jr., T.W.J., J. Goedhart, H. Röhrig, A. van Hoek, M.A. Hink, and A.J.W.G. Visser. 1999. Microspectroscopic imaging of Nod factor perception on single living *Vicia sativa* root hairs. *In* XVIth International Botanical Conference, St. Louis, USA.
- Gadella Jr., T.W.J., J. Goedhart, G.N.M. van der Krogt, R. Immink, R. Mirabella, and T. Bisseling. 1999. Microspectroscopic imaging of signaling in single living plant cells. *In* The XIth International Congress of histochemistry and cytochemistry, York, United Kingdom (p. 46).
- Gadella Jr., T.W.J., J. Goedhart, A. van Hoek, and A.J.W.G. Visser. 1996. Construction and applications of a frequency-domain fluorescence lifetime imaging microscope. *In* 2nd International Fluorescence Lifetime Imaging Meeting, Utrecht, The Netherlands.
- Gadella Jr., T.W.J., J. Goedhart, A. van Hoek, and A.J.W.G. Visser. 1996. Construction and applications of a frequency-domain fluorescence lifetime imaging microscope. *In* 12th International Biophysics Congress, Amsterdam, The Netherlands.
- Goedhart, J., and T.W.J. Gadella Jr. 2000. Fluorescent and caged phospholipid second messengers. *In* ANNO 2000: a lipid milestone, Utrecht, The Netherlands (p. 29).
- Goedhart, J., H. Röhrig, M.A. Hink, A.J.W.G. Visser, T. Bisseling, and T.W.J. Gadella, Jr. 1999. Mobility and distribution of fluorescent Nod factors on single living *Vicia sativa* root hairs. *In* 4th International Weber symposium on innovative fluorescence methodologies in biochemistry and medicine, Maui, Hawaii.

- Hink, M.A., J.W. Borst, G.N.M. van der Krogt, J. Goedhart, T.W.J. Gadella Jr., and A.J.W.G. Visser. 2000. Intracellular fluorescence correlation spectroscopy : towards monitoring signalling molecules in vivo. *Biophys. J.*, **78**: 442A.
- Hink, M.A., J. Goedhart, T.W.J. Gadella Jr., C. Laane, and A.J.W.G. Visser. 1999. Monitoring biomolecular interactions in living systems with fluorescence correlation microscopy. *Eur. J. Histochem.*, **43**: 27.
- Visser, A.J.W.G., J. Goedhart, A. van Hoek, and T.W.J. Gadella Jr. 1997. Biophysical Applications of a fluorescence lifetime imaging microscope. *Eur. Biophys. J.*, **26**: 121.

Submitted articles

- Goedhart, J., J.-J. Bono, and T.W.J. Gadella Jr. 2001. Rapid Colorimetric Quantification of Lipo-chitooligosaccharides from *Rhizobium loti* and *Rhizobium meliloti*. *Mol. Plant-Microbe Interact.*, submitted.
- Goedhart, J., J.-J. Bono, T. Bisseling, and T.W.J. Gadella Jr. 2001. Localization, immobilization and cell wall accumulation of sulfated and non-sulfated Nod factors is identical in root hairs of host and non-host legumes. *Plant J.*, submitted.